ACIBADEM MEHMET ALI AYDINLAR UNIVERSITY
INSTITUTE OF HEALTH SCIENCES

CORNEA TISSUE ENGINEERING USING HYDROGEL AND STEM CELL

SERAP FİDE

M.Sc. THESIS

DEPARTMENT OF MEDICAL BIOTECHNOLOGY

SUPERVISOR
Asst. Prof. Dr. Deniz Yücel

SECONDARY SUPERVISOR
Prof. Dr. Vasıf Nejat Hasırcı

ISTANBUL-2022

ACIBADEM MEHMET ALI AYDINLAR UNIVERSITY
INSTITUTE OF HEALTH SCIENCES

CORNEA TISSUE ENGINEERING USING HYDROGEL AND STEM CELL

SERAP FİDE

M.Sc. THESIS

DEPARTMENT OF MEDICAL BIOTECHNOLOGY

SUPERVISOR
Asst. Prof. Dr. Deniz Yücel

SECONDARY SUPERVISOR
Prof. Dr. Vasıf Nejat Hasırcı

ISTANBUL-2022

DECLARATION

I declare that this thesis work is my own work, I had no unethical behaviour at any stages from the planning to the writing of the thesis, I obtained all the information in this thesis in accordance with academic and ethical rules, I cited all the information and comments that were not obtained with this thesis work, and I provided resources in the list of references. I also declare that there was no violation of any patents and copyrights during the study and writing of this thesis.

28.06.2022

Serap Fide

PREFACE AND ACKNOWLEDGEMENT

I would like to express my deepest gratitude to my advisors Asst. Prof. Dr. Deniz YÜCEL and Prof. Dr. Vasıf Nejat HASIRCI for their continuous guidance, encouragement, support, and patience at all stages of my thesis. They helped me to look at my work from different perspectives with their knowledge, and whom I am proud to work with and always be a student of. I also sincerely appreciate the time and effort they put into improving my experience.

I would like to thank Asst. Prof. Dr. Ali Rıza Cenk ÇELEBİ for his guidance and support, who especially enlightened me with his deep knowledge in the field of cornea, and shared his vast knowledge and support. His motivation have been invaluable on both an academic and personal level, and I greatly appreciate that.

I would also like to thank Prof. Dr. Halime KENAR for her guidance in hydrogel experiments, helpful suggestions, and guidance, and always providing motivational support.

I would like to thank Prof. Dr. Halime KENAR and Asst. Prof. Dr. Görke GÜREL PEKÖZER, who participated in my thesis defence committee and provided constructive criticism at critical points.

I would like to thank Menekşe Ermiş ŞEN, PhD for giving me all her knowledge and experience in making methacrylate hyaluronic acid and hydrogel and contributing to my work with her valuable suggestions. I would also like to thank Funda CAN, who shared all her knowledge and experience at these stages with me and did not spare her support.

I would like to thank the members of METU BIOMATEN for their help and support in the ^{1}H-NMR test for methacrylate hyaluronic acid.

I would like to thank Selçuk BİRDOĞAN, the staff responsible for electron microscopy, for their assistance with the SEM images.

I would like to thank all my laboratory colleagues, especially Gözde KÖLE, for their support in my experiments since the beginning of my studies.

During this study, I was supported by TÜBİTAK-BİDEB 2210-C National MSc/MA Scholarship Program in the Priority Fields in Science and Technology program, and SBAG 118S587, and these grants are gratefully acknowledged. At the same time, I would like to thank the facilities offered by Acıbadem Mehmet Ali Aydınlar University and Acıbadem Biomaterials Center.

Lastly, I would like to express my deepest gratitude and thanks to my family Leyla FİDE, Harun FİDE, Yalçın FİDE and Seval FİDE, who always supported me and helped me overcome all the obstacles in my life.

I would like to thank my family, Çetin Yiğit AZAP, for all his support and motivation, as in all areas of my life, and who endured all my troubles with miraculous patience.

TABLE OF CONTENTS

DECLARATION iii

PREFACE AND ACKNOWLEDGEMENT iv

TABLE OF CONTENTS vi

LIST OF FIGURES xii

LIST OF TABLES xvi

ÖZET 17

ABSTRACT 18

1 INTRODUCTION AND AIM 19

2 BACKGROUND 22

2.1 Structure of Cornea 22
2.2 Corneal Diseases 25
2.3 Therapeutic Approaches for Corneal Diseases 26
2.4 Tissue Engineering 27
2.5 Cornea Tissue Engineering 28
2.5.1 Cell sources used in cornea tissue engineering 30
2.5.1.1 Stem cells 30
2.5.2 Scaffolds used in cornea tissue engineering 34
2.5.2.1 Hydrogels 37
2.5.2.2 Fibrous scaffolds via electrospinning 38
2.5.2.3 Polymers used in scaffold 39
2.5.2.3.1 Collagen 41
2.5.2.3.2 Methacrylated hyaluronic acid (MeHA) 42
2.5.2.3.3 Polylactic acid (PLA) 43
2.5.2.3.4 Poly(lactic-co-glycolic acid) (PLGA) 44

3 MATERIALS AND METHODS 45

3.1 Materials 45
3.2 Methods 46
3.2.1 Preparation of the hybrid scaffolds 46
3.2.1.1 Isolation of collagen from bovine achilles tendon 46
3.2.1.2 Fabrication of electrospun fibrous mesh 47
3.2.1.3 Synthesis of MeHA 49
3.2.1.4 Formation of MeHA hydrogels 51
3.2.1.5 Formation of collagen-MeHA interpenetrating networks (IPNs) 51

3.2.1.6 Construction of the hybrid scaffolds by combining hydrogels and electrospun fibrous mesh 51
3.2.2 Characterization of the hybrid scaffolds 52
3.2.2.1 Scanning electron microscopy 52
3.2.2.2 Mechanical analysis 53
3.2.2.3 Swelling test of the hydrogels 54
3.2.3 Characterization of WJ MSCs and their differentiation into keratocytes 54
3.2.3.1 Isolation and characterization of human WJ MSCs 54
3.2.3.1.1 Characterization of WJ MSCs with flow cytometry 55
3.2.3.1.2 Osteogenic differentiation for characterization of WJ MSCs 55
3.2.3.1.3 Chondrogenic differentiation for characterization of WJ MSCs 57
3.2.3.1.4 Growth kinetics of the isolated WJ MSCs 58
3.2.3.2 Differentiation of WJ MSCs into keratocytes 58
3.2.3.2.1 Induction of MSCs for keratocyte differentiation 58
3.2.3.2.2 Expression of specific keratocyte markers of MSCs upon keratocyte differentiation by immunostaining 59
3.2.4 Construction of corneal tissue substitute by combining wj mscs and hydrogel-based hybrid scaffolds 60
3.2.4.1 Viability and proliferation of cells in the corneal tissue substitute 61
3.2.4.2 Immunostaining analysis of WJ MSC-derived keratocytes in the corneal tissue substitute 62
3.2.5 Statistical analysis 62

4 RESULTS 63

4.1 Characterization of MeHA Hydrogels 63
4.1.1 Determination of acetylation degree upon MeHA synthesis (^{1}H-NMR) 63
4.1.2 The pH determination of MeHA solution 65
4.1.3 Morphology analysis by SEM 65
4.1.4 Swelling degree of hydrogels 66
4.2 Characterization of Electrospun Fibrous Meshes 67
4.2.1 Morphology analysis by SEM 67
4.2.2 Determination of fiber diameter and orientation 69
4.2.3 Mechanical analysis 71
4.3 Characterization of the Hybrid Scaffolds 72
4.3.1 Morphology analysis with SEM 72
4.3.2 Mechanical analysis 73
4.3.3 Transparency of the hybrid scaffolds 74
4.4 *In Vitro* Studies 75
4.4.1 Characterization of the isolated WJ MSCs 75
4.4.1.1 Flow cytometry analysis 75
4.4.1.2 Osteogenic differentiation of WJ MSCs 77
4.4.1.3 Chondrogenic differentiation of WJ MSCs 78
4.4.1.4 Growth kinetics of the isolated WJ MSCs 79
4.4.2 Differentiation of WJ MSCs into keratocyte cells 80
4.4.2.1 Protein expression analysis of MSCs by immunostaining upon keratocyte induction 80

4.4.3 Cell behaviour in the corneal tissue substitute 84
4.4.3.1 Viability of the cells in the hydrogels 85
4.4.3.2 Cell proliferation within the hybrid scaffolds 87
4.4.3.3 Cell morphology in the scaffolds 88
4.4.3.4 Immunostaining of MSC-derived keratocytes in the scaffolds 90

5 DISCUSSION 92

6 CONCLUSION 96

7 REFERENCES 97

8 APPENDIX 104

APPENDIX 1. Calibration Curves for Cell Number Determination of WJ MSCs 104
APPENDIX 2. Calibration Curves for ALP Activity 105

9 CURRICULUM VITAE 106

LIST OF ABBREVIATIONS \ SYMBOLS

3D	3 dimensions
ALDH1A1	Aldehyde dehydrogenase 1 family, member a1
ALP	Alkaline phosphatase
AM	Amniotic membrane
bFGF	Basic fibroblast growth factor
BM MSCs	Bone marrow-derived mesenchymal stem cell
BSA	Bovine serum albumin
CEC	Corneal endothelial cell
CLSCs	Cord lining stem cells
CO_2	Carbon dioxide
Col/MeHA	Collagen- methacrylated hyaluronic acid
CTE	Cornea tissue engineering
D_2O	Heavy water
DAPI	4,6-diamidino-2-phenylindole dihydrochloride
dH_2O	Distilled water
DMEM	Dulbecco's modified eagle medium
DMF	N,N-dimethylformamide
DMSO	Dimethyl sulfoxide
DNA	Deoxyribonucleic acid
DPBS	Dulbecco's phosphate buffered saline
DS	Degree of swelling
ECM	Extracellular matrix
ESCs	Embryonic stem cells
FBS	Fetal bovine serum
FGF	Fibroblast growth factor
FITC	Fluorescein Isothiocyanate
GAGs	Glycosaminoglycans
GelMA	Methacrylated gelatin
Gly-X-Y	Glycine-proline-hydroxyproline
HA	Hyaluronic acid

hASCs	Human adipose stem cells
hCESCs	Human corneal epithelial stem cells
hCFs	Human corneal fibroblasts
HCl	Hydrochloric acid
hCSCs	Human corneal stromal cells
hCSSCs	Human corneal stromal stem cells
hESCs	Human embryonic stem cells
HK	Human keratocytes
H-NMR	Proton nuclear magnetic resonance
IBMX	3-isobutyl-1-methylxanthine
IPSCs	Induced pluripotent stem cells
ITS	Insulin-transferrin-selenite
LEC-like	Limbal epithelial cell-like
LSCs	Corneal limbal epithelial stem cells
LUM	Lumican
MeHA	Methacrylated hyaluronic acid
MEM	Minimum essential medium
MSCs	Mesenchymal stem cells
NaCl	Sodium chloride
NaOH	Sodium hydroxide
PBS	Phosphate buffered saline
PBST	Phosphate-buffered saline with triton-x
PCL	Poly (ε –caprolactone)
PEG	Poly (ethylene glycol)
Pen/Strep	Penicillin/streptomycin
PFA	Paraformaldehyde
PGA	Poly(glycolic acid)
PHEMA	Polyhydroxyethyl methacrylated
PLDLA	Poly (L,D lactic acid)
PLGA	Poly (lactide-co-glycolide)
PLLA	Poly-L-lactic acid
PMMA	Polymethylmethacrylate

PNIPAM	Poly-n-isopropylacrylamide
PVA	Poly (vinyl alcohol)
RNA	Ribonucleic acid
RPEC	Retinal pigment epithelial cells
SEM	Scanning electron microscopy
SF	Silk and fibroin
TGF-β	Transforming growth factor-β
WJ MSC	Wharton's Jelly mesenchymal stem cells

LIST OF FIGURES

Figure 1. Schematic drawing of the structure of the eye. 22
Figure 2. Schematic presentation of the structure and layers of the cornea. 23
Figure 3. The principle of tissue engineering. 28
Figure 4. Schematic representation of umbilical cord. 34
Figure 5. Schematic representation of electrospinning set-up. 39
Figure 6. Chemical structure of hyaluronic acid. 42
Figure 7. Chemical methacrylation of HA to obtain MeHA. 43
Figure 8. Chemical structure of PLA. 43
Figure 9. Chemical structure of PLGA. 44
Figure 10. Schematic presentation of the collagen isolation procedure. 47
Figure 11. Synthesis of methacrylated hyaluronic acid by binding of methacrylated groups to the hydroxyl groups of hyaluronic acid. 50
Figure 12. Schematic presentation of the synthesis of MeHA. 50
Figure 13. Schematic presentation of the design of the developed cornea tissue equivalent and preparation of its three layers to for cell-free hydrogel-fiber hybrid constructs. 52
Figure 14. A representative stress/strain curve to obtain Young's modulus of materials. 53
Figure 15. Schematic presentation of the design of the developed cornea tissue equivalent. 61
Figure 16. ^{1}H-NMR spectra of (a) hyaluronic acid and (b) MeHA (1% MeHA and 1% Irgacure in PBS), prepared in D_2O at room temperature. (c) The expanded region of MeHA NMR spectrum between 1.5 and 2 ppm was presented showing the methacrylation of hyaluronic acid. 64
Figure 17. The pH value determination of MeHA solution (1% MeHA and 1% Irgacure in PBS). 65
Figure 18. SEM images of MeHA hydrogels prepared with 1% MeHA and 0.5% Irgacure. MeHA hydrogels (a,b) prepared in PBS, and (c,d) in dH_2O. Magnifications: (a,c) X1000, (b) X2000, (d) X500; scale bars: (a,c,d) 100µm, (b) 50µm. 66

Figure 19. SEM images of PCL-collagen fibers prepared under two different conditions: (a-c) applied voltage 17 kV, distance 17 cm, flow rate 2.5 µL/min; (d-f) applied voltage 15 kV, distance 24 cm, flow rate 1.5 µL/min. Magnifications: (a,d) X20000, (b,e) X50000, (c,f) X100000; scale bars: (a,d) 5 µm, (b,e) 3 µm, (c,f) 1 µm. ……68
Figure 20. SEM images of PLA-PLGA fibers prepared under two different conditions: (a-b) applied potential 11.5kV, distance 15 cm, flow rate 0.1 mL/h; (c-d) applied potential 11.5 kV, distance 15 cm, flow rate 0.4 mL/h. Magnifications: (a,b) X2000, (c,d) X5000; scale bars: (a,b) 50 µm, (b,c) 30 µm. 69
Figure 21. SEM images of PLA-PLGA fibers prepared with optimized parameters: applied potential 11.5 kV, distance15 cm, flow rate 0.8 mL/h. Magnifications: (a) X150, (b) X1200, (c) X3500; scale bars: (a) 1 mm, (b) 100 µm, (c) 40 µm. 69
Figure 22. The distribution of (a) fiber diameter and (b) fiber orientation of the electrospun random fibrous mesh fabricated under optimized conditions..... 71
Figure 23. SEM images of the multilayered cell-free corneal scaffold. (a) Longitudinal section of the scaffold, (b) thin MeHA hydrogel layer, (c) random fibrous mesh, (d) thick MeHA hydrogel layer. Magnifications: (a,d) X500, (b) X650, (c) X1200; Scale bars: (a,d) 300 µm, (b) 200 µm, (c) 100 µm. 73
Figure 24. Stereomicroscope images taken to evaluate transparency of the layers of the scaffold and the final hybrid scaffold. (a) PLA-PLGA fibrous mesh, (b) MeHA hydrogel, (c) the final hybrid construct composed of thin layer MeHA hydrogel, fibrous mesh and thick layer MeHA hydrogel. Magnifications: (a) X0.63, (b) X1, (c) X1.25 ……74
Figure 25. Flow cytometry histograms for different cell surface antigen expression of WJ MSCs isolated from human umbilical cord matrix and histograms of isotype controls. ……76
Figure 26. ALP activity of the undifferentiated WJ MSCs (control) and the differentiated cells after 7 and 14 days of osteogenic induction. (#: $p>0.05$, * $p<0.005$) ……78
Figure 27. Light microscope images of WJ MSCs after Alcian blue staining; (a) control, and (b) cells subjected to chondrogenic induction for 14 days; (c) control, and (d) cells subjected to chondrogenic induction for 21 days. Scale bars: 100 µm..... 79

Figure 28. Growth profile of the isolated WJ MSCs. 80
Figure 29. Immunostaining analysis of (a-c) ALDH1A1 (red) and (d-f) LUM (green) expressions of the undifferentiated WJ MSCs at the end of 7 day culture. Magnifications: (a,d) X10, (b,e) X20, (c,f) X40; scale bars: (a,d) 100 µm, (b,e) 50 µm, (c,f) 20 µm. ……81
Figure 30. Immunostaining analysis of (a-c) ALDH1A1 (red) and (d-f) LUM (green) expressions of the keratocyte differentiated WJ MSCs at the end of 7 day induction. Magnifications: (a,d) X10, (b,e) X20, (c,f) X40; scale bars: (a,d) 100 µm, (b,e) 50 µm, (c,f) 20 µm. ……82
Figure 31. Immunostaining analysis of (a-c) ALDH1A1 (red) and (d-f) LUM (green) expressions of the undifferentiated WJ MSCs at the end of 14 day culture. Magnifications: (a,d) X10, (b,e) X20, (c,f) X40; scale bars: (a,d) 100 µm, (b,e) 50 µm, (c,f) 20 µm. ……83
Figure 32. Immunostaining analysis of (a-c) ALDH1A1 (red) and (d-f) LUM (green) expressions of the keratocyte differentiated WJ MSCs at the end of 14 day induction. Magnifications: (a,d) X10, (b,e) X20, (c,f) X40; scale bars: (a,d) 100 µm, (b,e) 50 µm, (c,f) 20 µm. ……84
Figure 33. LSCM image of cell-free scaffold after Live-Dead assay application at the end of 7day induction. Magnification X5, scale bar: 200 µm. 85
Figure 34. LSCM image of WJ MSCs within the hybrid scaffold after Live-Dead assay application at the end of 1 day culture. The alive cells stained with calcein AM (green) and the dead cells stained with ethidium homodimer-1 (red). (a) The z-stack images (total thickness of the taken image: 112 µm), (b) image taken from longitudinal section (c) 2D image at a certain focal plane. (a-c) Magnification X10, scale bar: 100 µm.. 86
Figure 35. Live-Dead analysis of WJ MSCs in the scaffold at the end of 7-day induction. The cells stained with calcein AM (green) for live and ethidium homodimer-1 (red) for dead cells. (a) The z-stack images (total thickness of the taken image: 167 µm), (b) image taken from longitudinal section (c) 2D image at a certain focal plane. (a-b) Magnification X5, scale bar: 200 µm. 87
Figure 36. Proliferation of WJ MSCs cultured on TCPs and the final constructs on day 1 and day 7. (# p>0.05, * p>0.05) 88

Figure 37. SEM images of the cell-loaded corneal tissue substitute. (a) Thin MeHA hydrogel layer, (b) top two layers of scaffold including thin MeHA hydrogel and electrospun random fibrous mesh, (c) electrospun random fibrous mesh, (d) cell-loaded thick MeHA hydrogel, (e) longitudinal section of hybrid scaffold, (f) cell within the thick hydrogel. Magnifications: (a,f) X1000, (b,d) X2000, (c) X3500; (e) X650; Scale bars: (a) 100 µm, (b,d) 50 µm, (c) 40 µm, (d) 200 µm, (e) 10 µm..... 89
Figure 38. Immunostaining analysis of samples. (a-c) cell-free scaffolds used as control; (d-f) the expression of ALDH1A1 (red) of cells on the tissue substitute at the end of 7 day induction. Magnifications: (a,d) X10, (b,e) X20, (c,f) X40; Scale bars: (a,d) 50 µm, (b,e) 20 µm, (c,f) 100 µm. 90
Figure 39. Immunostaining analysis of samples. (a-c) cell-free scaffolds used as control; (d-f) the expression of LUM (green) of cells on the tissue substitute at the end of 7 day induction. Magnifications: (a,d) X10, (b,e) X20, (c,f) X40; Scale bars: (a,d) 50 µm, (b,e) 20 µm, (c,f) 100 µm. 91
Figure 40. The calibration curve obtained by WST-1 assay using WJ MSCs. 104
Figure 41. The calibration curve obtained by MTS assay using WJ MSCs. 104
Figure 42. The calibration curve for ALP activity prepared by p-nitrophenol at different concentrations. 105

LIST OF TABLES

Table 1. The positive and negative markers for the characterization of mesenchymal stem cells (86). 33
Table 2. The scaffolds and cells used in the examples of cornea tissue engineering. 36
Table 3. Optimization of electrospinning parameters. 49
Table 4. Composition of the expansion medium and the osteogenic induction medium. ……56
Table 5. Composition of the expansion medium and the chondrogenic induction medium. ……57
Table 6. Composition of the expansion medium and the keratocyte induction medium. ……59
Table 7. Weight and swelling degree of hydrogel samples over time. 67
Table 8. The expression of surface antigens of WJ MSCs (P3) based on isotypes. .. 77

ÖZET

Hidrojel ve Kök Hücre Temelli Kornea Doku Mühendisliği

Yapısal bir bariyer görevi gören ve gözü enfeksiyonlara karşı koruyan kornea, fiziksel, kimyasal, termal yaralanmalar gibi bazı faktörlerden zarar görebilmektedir. Doku mühendisliği, kornea hasarlarının tedavisi için umut verici bir yaklaşımdır. Bu çalışmada doku mühendisliği yaklaşımı ile *in vitro* koşullarda kök hücre içeren, hidrojel bazlı, 3 boyutlu hibrit kornea doku eşleniği geliştirilmesi amaçlandı. Hibrit yapı iskelesi, ince MeHA hidrojeli, elektroeğirme ile elde edilen düzensiz lifli ağ ve kalın MeHA hidrojelinin birleştirilmesiyle elde edildi. İskelelerin morfolojileri, şişme dereceleri, mekanik özellikleri ve şeffaflıkları açısından karakterize edildi. İnsan Wharton's Jelly mezenkimal kök hücreleri (WJ MKHleri) kullanılarak kalın MeHA hidrojeline ekildi. WJ MKH'lerin, keratositlere farklılaşmak üzere indüklendi ve farklılaşma immün boyama ile keratosite özgü spesifik markerlerin ekspresyonu ile gösterildi. İndüklenen WJ MKHlerinin hibrit doku iskeleleri içindeki canlılığı, çoğalması ve morfolojisi araştırıldı. Hücrelerin çoğunun yapı içerisinde canlı olduğu görüldü. MKHlerin indüklenmesinin ardından çoğalmadığı, ancak ekim sayılarını korudukları ortaya kondu. SEM morfoloji sonuçları, uygun entegrasyon ile üç katmanlı hibrit doku iskelesinin başarılı bir şekilde üretildiğini ve hücrelerin hidrojel gözenekleri içine yerleştiğini gösterdi. İmmün boyama sonuçları hücrelerin doku iskelesi içinde indüksiyon sonucunda keratositlere farklılaştığını spesifik markerlerın ekspresyonu ile ortaya koydu. Geliştirilen kornea doku eşleniği *in vivo* çalışmalarda test edilebilecek ve kornea hasarları ve hastalıkları için umut verici bir tedavi yaklaşımı olabilecek niteliktedir.

Anahtar Sözcükler: Kornea doku mühendisliği, Wharton's Jelly mezenkimal kök hücreleri, hidrojel, elektroeğrilmiş lifli yapı, hibrit doku iskelesi.

ABSTRACT

Cornea Tissue Engineering Using Hydrogel and Stem Cell

Cornea, which acts as a structural barrier and protects eye against infections, can be damaged by some factors like physical, chemical, and thermal injuries. Tissue engineering is a promising approach for the treatment of cornea damages. In this study, it was aimed to develop a stem cell loaded, hydrogel based, 3D, hybrid corneal tissue substitute under *in vitro* conditions via tissue engineering approach. The hybrid scaffold was constructed by combining thin MeHA hydrogel, electrospun random fibrous mesh, and thick MeHA hydrogel. The scaffolds were characterized in terms of morphology, swelling degree, mechanical properties, and transparency. Human Wharton's Jelly mesenchymal stem cells (WJ MSCs) was used and loaded into thick MeHA hydrogel. WJ MSCs were induced to differentiate into keratocytes, and then differentiation was shown with immunostaining by the expression of specific keratocyte markers. The viability, proliferation, and morphology of induced-WJ MSCs within the hybrid scaffolds were investigated. It was observed that most of cells were alive within the construct. It was revealed that MSCs were not proliferated after induction, but they conserved their loading number. SEM morphology results showed that three layered hybrid scaffold was produced successfully with proper integration, and the cells were located within the pores of hydrogel. At the end of keratocyte induction, immunostaining results revealed that the cells demonstrated the expression of keratocyte specific markers, which indicated their differentiate into keratocytes within the scaffold. The developed corneal tissue substitute could be tested under *in vivo* studies and could be a promising treatment approach for corneal damages and diseases.

Keywords: Cornea tissue engineering, Wharton's Jelly mesenchymal stem cells, hydrogel, electrospun fibrous mesh, hybrid scaffold.

1 INTRODUCTION AND AIM

According to the data of 2010, it is estimated that more than 10 million people suffer from blindness because of corneal damages due to the lack of appropriate treatment for corneal diseases or corneal injuries, and it is known that approximately 60 000 patients undergo corneal transplantation every year (1). Cornea tissue engineering (CTE), which was developed as an alternative method to corneal transplantation due to the donor shortage experienced all over the world, has been a frequently studied area in the past decade (2).

Tissue engineering is an interdisciplinary field that aims to develop a biological substitute that can replace dysfunctional and damaged tissue by applying engineering and life science principles (3). The tissue-engineered constructs preferably consist of the patient's own cells and biomaterials called as scaffolds that mimic the extracellular matrix of the native tissue. The physical and chemical properties of biomaterials play an important role in providing the necessary support for cell adhesion and proliferation.

The CTE approach requires a scaffold to temporarily function as corneal ECM (4). Therefore, the design created in CTE is expected to show transparency and mechanical strength similar to cornea tissue (5). At the same time, scaffolds should provide suitable environment for corneal cells. The necessity of mimicking the natural corneal extracellular matrix environment with the best scaffold material has been confirmed by various studies (6-14).

The cornea, a transparent part of the eyeball, acts as a structural barrier and protects eye against infections (15). The most important function of the cornea is to contribute most to the refractive power of the eye, and thus to focus the external image on the retina with minimum dispersion (16, 17). The cornea is a convex tissue and consists of 5 layers (18). The outermost corneal epithelium is a stratified squamous epithelial tissue originating from limbal stem cells (19). Bowman's membrane, which supports the basal cells in the epithelial tissue, consists of collagen fibers in an irregular organization. The stroma layer in the middle is composed of connective tissue

containing collagen and proteoglycans, and is the thickest layer in the cornea (3). The organization of collagen fibers in a certain order gives transparency to the cornea. Descemet's membrane, a thick basement membrane, supports single-layer flat endothelial cells in the innermost layer. These cells are responsible for the fluid balance in the stroma layer so that the cornea remains transparent.

Similar to natural tissue, hydrogels are widely used as a biomaterial in corneal tissue engineering due to their large water content (20). Hydrogel scaffolds lack the fibrous structure that acts as a load-bearing component in natural tissue, resulting in reduced mechanical performance. The use of crosslinking methods, the use of synthetic and/or natural polymers together and optimizing their ratios are among the most frequently used methods to improve mechanical performance of the scaffolds (21).

Electrospinning is used to create fibrous scaffolds supported with fibers at nano or micro scale for CTE (22). The biomaterials obtained by this method provide a suitable environment for cell attachment and proliferation in biomimetic tissue engineering due to their fibrous structure similar to the extracellular matrix in natural tissues with high surface/volume ratio and good porosity.

Keratocytes (10), epithelial cells (23), endothelial cells (12) and various stem cells such as limbal stem cells, human umbilical cord stem cells, dental pulp stem cells, adipose-derived stem cells and etc. are used as cell source in CTE (24-27).

In a small number of preclinical studies, scaffolds that mimic all layers of the cornea have been tried to be created, but none of them are clinically applicable and studies continue (22). The most important point to be considered in the biomaterials to be developed for corneal tissue is that they should be transparent and mechanically flexible (5). There are still difficulties in producing a corneal tissue substitute that will fully meet its biological and mechanical properties. In order to fill the gap in this area, it is important to obtain a high-performance corneal equivalent that can better mimic the microstructure of the layers of the natural corneal tissue.

Corneal transplantation is applied in irreversible and progressive corneal damages and diseases. It is a promising approach to develop an alternative corneal substitute by utilizing tissue engineering principles in order to meet the increasing need for donors and to minimize immunological reactions with a artificial corneal tissue that will preferably consist of the patient's own cells. In this study, it was aimed to develop a stem cell loaded, hydrogel based, 3D, hybrid corneal tissue substitute under *in vitro* conditions via tissue engineering approach. The hybrid scaffold was planned to be constructed by combining thin methacrylated hyaluronic acid (MeHA) hydrogel, electrospun random fibrous mesh, and thick MeHA hydrogel to imitate corneal epithelium, Bowman's membrane, and corneal stroma, respectively. The use of human Wharton's Jelly mesenchymal stem cells derived from umbilical cord matrix was planned to differentiate into keratocytes. It was thought that the corneal tissue substitute developed *in vitro*, consisting of mesenchymal stem cells and a biodegradable cell carrier, might have potential in regenerative treatment approaches.

In this study, it was aimed to develop a corneal tissue substitute consisting of hydrogel-based hybrid scaffold loaded with keratocyte-like cells differentiated from WJ MSCs. The corneal tissue substitute design was inspired by the histological properties and functions of the natural corneal tissue. In this concept, the construct was planned to be formed by three layers, thin MeHA hydrogel, electrospun random fibrous mesh, and cell-loaded thick MeHA hydrogel to imitate corneal epithelium, Bowman's membrane and corneal stroma, respectively. It was planned to use WJ MSCs, which are promising in the field of tissue engineering due to their ability to differentiate into various cell types. It was thought that the developed corneal tissue substitute might have a potential in regenerative approaches for the treatment of cornea damages.

2 BACKGROUND

2.1 Structure of Cornea

Cornea is a transparent tissue located on the anterior window of the eyeball (Figure 1) (15). It is approximately 535 µm thick in the centre and 550-600 µm thick at the periphery. The most important function of the cornea is to contribute most to the refractive power of the eye, and thus, to focus the external image on the retina with minimum dispersion (16). Cornea is an avascular tissue, and therefore, the required oxygen and glucose to fulfil the cornea's metabolic functions are provided from the aqueous humour of the anterior chamber and from the tear film formed on its outer surface (28). Tears contain antibacterial and UV protective agents (proteins like tear albumin, lactoferrin, enzymes like lysozyme, lipids, metabolites, and electrolytes) to protect corneal epithelium.

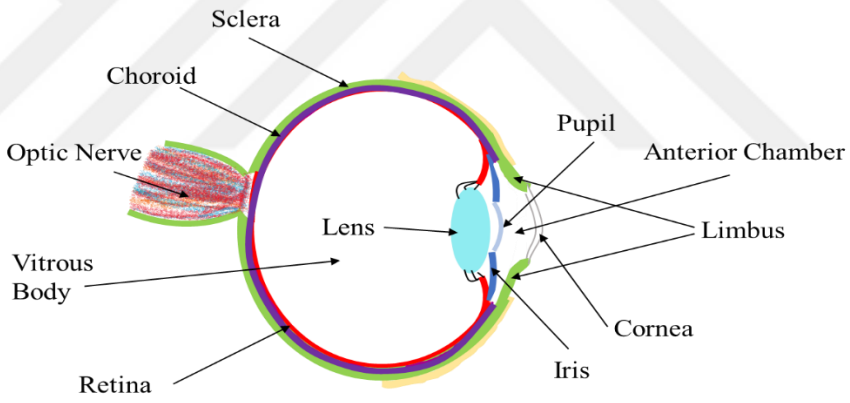

Figure 1. Schematic drawing of the structure of the eye.

The cornea is a convex tissue, and consists of five layers as corneal epithelium at the surface, Bowman's membrane (anterior basement membrane), corneal stroma, Descemet's membrane (posterior basement membrane) and corneal endothelium (Figure 2) (15). The size of the cornea is 11-12 mm horizontally and 9-11 mm vertically (18). The thinnest central region is 535 µm in thickness, and it thickens gradually towards the periphery in the range of 550 to 600 µm in thickness (29). This change in corneal tissue thickness is mainly due to the increase in the amount of collagen in the stroma (30). Cornea consists of three types of cells that are epithelial

cells, keratocytes, and endothelial cells, and its extracellular matrix (ECM) consists mainly of collagen and glycosaminoglycans (15).

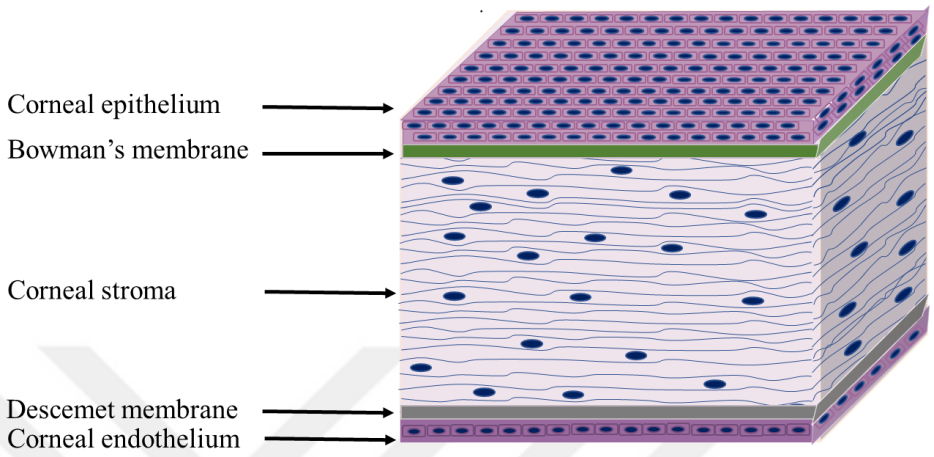

Figure 2. Schematic presentation of the structure and layers of the cornea.

The corneal epithelium, the exterior layer of the cornea, is a 50-90 µm thick nonkeratinized, stratified squamous epithelial tissue which is composed of 5 to 7 layer epithelial cells (31). The basal columnar cells originate from limbal stem cells and can regenerate within 24 hours (19). Stem cells divide asymmetrically to differentiate into basal central corneal epithelial cells. After these cells differentiate into wing or suprabasal cells, they migrate to the surface of the cornea as becoming superficial corneal epithelial cells (32). Although corneal epithelium does not contain blood vessels under normal conditions, many neutrophils and lymphocytes settle to the stroma in case of inflammation by migrating from the vessels in corneoscleral limbus, the region between the cornea and sclera. The corneal epithelium is fed by tears, aqueous humour and limbal capillaries (33, 34).

Epithelial basal cells attach onto the Bowman's membrane that is approximately 8-10 µm thick (15). It is composed of mainly type IV collagen, laminin, perlacan (a heparan sulfate proteoglycan) and nidogen (a sulfated glycoprotein) as well as fibronectin (35). Bowman's membrane is a homogeneous layer and contains randomly organized collagen fibers that have a diameter of 18 nm (15). Since the Bowman's

membrane does not have a self-renewal feature, when there is a damage, an opaque wound that can impair vision occurs.

Stroma is the thickest layer of cornea with approximately 450 μm in thickness (15). It constitutes 90% of the cornea tissue. Corneal stroma is made of connective tissue containing collagen and proteoglycan. The orthogonal lamellar organization of collagen fibers in the corneal stroma frame is important to provide light transmittance through the cornea and for its mechanical properties. Corneal stroma contains keratocytes, which are responsible for the regulation of extracellular matrix (ECM) components of the corneal stroma through collagen and proteoglycan synthesis (22, 36). Keratocytes are derived from neural crest cells which migrate to settle in the mesenchyme and remain as modified fibrocytes in the stroma throughout life (37). From there they migrate to settle in the mesenchyme and remain as modified fibroblast in the stroma throughout life. Stromal keratocytes are rarely dispersed in the stroma and their numbers range from 200 million to 1.5 billion (32). Keratocytes are actively involved in the production of glycosaminoglycans. There are 3 types of glycosaminoglycans in the stroma: keratan sulfate (50%), chondroitin sulfate C (25%) and chondroitin sulfate A (25%). Keratocytes have role in stroma organization and maintenance of the cornea transparency by crystalline proteins' expression and proteoglycans' production (38-40). During wound healing process keratocytes convert their phenotypes into fibroblasts and myofibroblasts leading to reduced stroma transparency. At the injury site fibroblasts start to secrete biglycan, fibronectin and collagen type I and type III. Then, this fibroblastic transformation is associated with reduced cornea transparency by decrease in the expression of transketolase (TKT) (32, 39, 40). The fibroblasts gradually acquire the keratocyte phenotype upon tissue repair and the cornea becomes transparent (32, 36).

The phenotype of keratocytes can be determined by specific cell marker expressions like CD34, a hematopoietic marker; aldehyde dehydrogenase (ALDH) classes 1 and 3, SLRP keratocan and keratan sulfate (38). Also, it expresses lumican, β-actin, tachykinin precursor 1, tachykinin receptor 1, collagen types I-III-V and VI.

Descemet membrane, a 10-15 μm thick basement membrane, supports monolayer of endothelial cells in the innermost layer. This membrane mainly consists of type I collagen and, also contains type VI collagen (39).

The corneal endothelium, the innermost layer of cornea, consists of monolayer of flat epithelial cells with a thickness of 5 μm (38). Corneal endothelial cells have polygonal shape and are in direct contact with the aqueous anterior chamber (41, 42). They are responsible for feeding of the corneal stroma and maintaining the transparency by moisturizing the cornea since excessive hydration of the stroma leads to the opacity. There is an active pump mechanism in the endothelium. It prevents swelling of corneal stroma by eliminating excess liquid with the activity of Na^+ / K^+ pumps and Mg^+ ionic pumps (43). Thus, endothelial cells act as a stabilizing pump that regulates the amount of fluid in the cornea, and thus take role in maintaining cornea transparency. Endothelial cells may change to fibroblast-like cells under excessive stress and trauma (44). When there is a loss of corneal endothelium, they cannot proliferate, but they expand and fill the lost regions.

2.2 Corneal Diseases

The cornea acts as an external barrier and protects the inner parts of the eye against germs, dust and harmful substances (45). It shares this task with the eyelids, eye socket, tear and sclera (16). Cornea is the entry point of the rays into the eye, it provides refraction of the light and filters some of the UV light (46). Even though it acts as a protective barrier, abrasion, physical, chemical, thermal and photokeratitis-induced factors can cause various damages at different level to the cornea (16, 45, 47). Corneal dystrophies (48), dry eye (47), keratitis (49), and allergies (50) are the main corneal diseases.

Allergy may develop due to pollen or various drugs, contact lenses, and cosmetics used, and it shows symptoms such as redness, itching, burning, stinging, tearing and watering (50). Keratitis can be occurred due to corneal infections by bacteria, viruses or fungi, and displays symptoms of pain, watering, burring and blurred vision (49). The transparent corneal tissue can become blurred, thin or even perforated due to keratitis. When the tears that feed the cornea cannot be produced continuously, dry

eyes may occur with a feeling of stinging symptoms due to dry weather, connective tissue diseases, the use of various drugs and long-term use of lenses (47). The other disease may be corneal ulceration caused by a bacterial infection invading the cornea due to injury or trauma and may result in vision loss on advancing period of the disease (51). Corneal dystrophies begin with decreased corneal endothelial cell number and impaired pumping function over time, and result in thick and opaque cornea, eventually vision decreases (48). When the edema reaches the outer surface of the cornea, it can also form small blisters and pain. Keratoconus occurs when the structural integrity of the cornea may be impaired as the corneal tissue becomes thinner and loses its normal curvature and takes the shape of a cone (52). Although the exact cause is not known, this disease may be inherited and may cause moderate to severe astigmatism and blurred vision.

2.3 Therapeutic Approaches for Corneal Diseases

According to 2010 data, it is estimated that more than 10 million people are experiencing blindness due to corneal diseases and known that approximately 60 000 patients undergo corneal transplants each year (53).

There are several different clinical treatments available for mild or severe corneal damage (54). Pharmacological treatment methods such as autologous serum administration, antibiotics and anti-inflammatory drug administration are applied in less complex cases in which some parts of the cornea are affected. For instance, pharmacological treatments can be applied in mild epithelial degeneration and dehydration problems. These problems can be treated with autologous serum and/or antibiotic practices.

As an alternative method, gene therapy is applied in various diseases such as corneal scar, corneal vascularization and inflammation to eliminate the problems inherited and acquired diseases of the cornea (55). The accessibility, transparency, immune privilege and stability of the cornea make the gene therapy appropriate approach for corneal injuries.

In more complex cases where multiple layers of the cornea are affected, the damaged area and or the entire cornea must be replaced (56). For permanent or severely deformed corneal injuries, since the net vision cannot be repaired by alternative methods, keratoplasty, corneal transplant, is preferred. In this widely used treatment method, healthy corneal tissue taken from a donor is implanted to the diseased corneal tissue (57). For this process, recipient and donor tissues must be compatible with each other. Although the success rate of corneal transplantation is higher than other treatments, donor limitation and tissue rejection are the main difficulties (2). Therefore, artificial corneal implant has been developed for the treatment of damaged cornea.

Replacing the damaged cornea with artificial cornea (keratoprosthesis) is called prostho-keratoplasty (58). Although the use of keratoprosthesis was first used with hard materials such as glass and quartz in the 19th century, it was observed that it would be more appropriate to make the material to be used for corneal conjugation from polymer. It is intended to allow adequate oxygen permeability and nutrient permeability to protect the cellular components of the formed tissue and to interact with adjacent tissues. The biomaterials used for this purpose have been changed over time. More biocompatible synthetic polymers have been used to better mimic the corneal extracellular matrix (ECM). Considering the initial studies, it is seen that poly (methyl methacrylate) (PMMA) (59) and poly (2-hydroxyethyl methacrylate) (PHEMA) (60) were the most frequently used polymer in this field. Combination of biomaterials with cells to obtain corneal tissue substitutes by tissue engineering is an alternative treatment approach which has been frequently studied for cornea repair in the past decade.

2.4 Tissue Engineering

Tissue engineering is an interdisciplinary field that aims to develop a biological substitute by applying the principles of engineering and life sciences (3). Tissue engineering approach that aims to repair and improve damaged or lost tissue structures and/or functions due to injury, accident or different pathological conditions. It includes combination of targeted tissue specific cells and scaffolds, and optionally integration

of biological agents (Figure 3). Tissue-engineered constructs consist of biomaterials called scaffolds that mimic the extracellular matrix (ECM), and cells that are preferably the patient's own cells. Physical and chemical properties of the scaffolds play an important role in providing the necessary support for cell attachment, proliferation, organization and even differentiation.

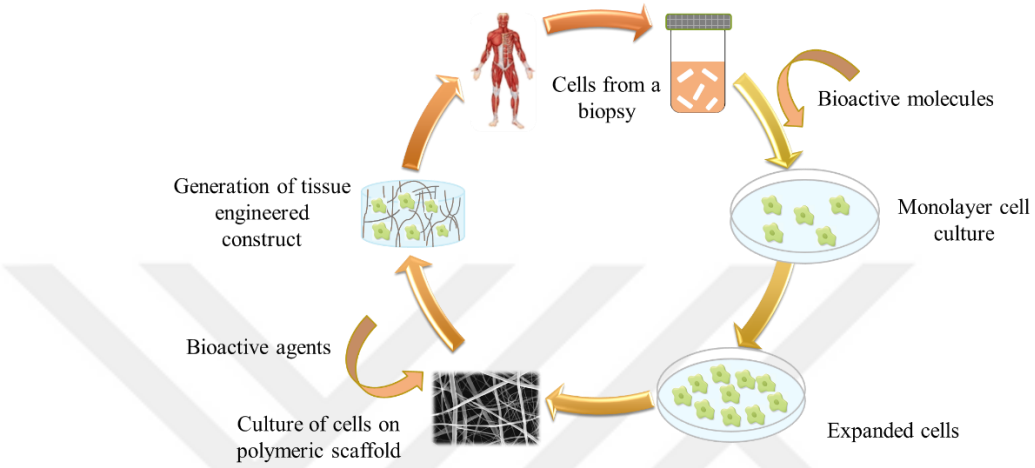

Figure 3. The principle of tissue engineering.

The histological properties of the target tissue should be known very well to imitate its ECM and cellular composition in order to develop an ideal tissue equivalent (3). For that purpose, mature cells or stem cells can be preferably isolated from the patient to prevent immunological response. Tissue-inducing biological agents, such as growth factors and tissue specific molecules can be integrated into scaffolds (61). The scaffold should be biocompatible so that it does not evoke any immune reaction or a minimal immune reaction (62). Due to fact that the cells can produce their own ECM, scaffolds should preferably be biodegradable and should not have any toxic end-products. It should have appropriate mechanical properties depend on the target tissue. Moreover, it should have a suitable porosity to enable cell penetration, cell-cell interaction and exchange of necessary nutrients for the cells (58).

2.5 Cornea Tissue Engineering

Various methods have been applied for the treatment of the damaged cornea to date (54-58, 63). Pharmacological treatment methods specific to cornea injuries are

suitable for relieving symptoms without providing permanent solutions to cornea injuries. Gene therapy methods cannot be actively used in every region. Although the success rate of the keratoplasty is higher than other methods, donor tissue availability and tissue rejection limits the application of this method (2). Due to these problems, developing cornea tissue equivalents via tissue engineering is a promising alternative approach for cornea transplantation.

Considering the functionality of the cornea, there are four main design requirements in cornea substitutes' design as providing protection, allowing light transmittance, having an ideal optical interface and being biocompatible (5). It is important to mimic the histological features of the native cornea as closely as possible (8, 64, 65). In this intend, the construct to be created should have an ideal flexibility. The ultimate corneal tissue substitute should have an appropriate transparency. It should also undertake the protection function provided by the natural cornea.

The extracellular matrix (ECM) composed of extracellular molecules secreted by cells provides structural and biochemical support for the cells that are housed (66). It induces cell-matrix interactions, cell adhesion, migration, proliferation, and also differentiation. ECM also provides mechanical support to the cells. The main molecules form the ECM are collagen fibers, elastin fibers, proteoglycans and glycosaminoglycans (GAGs). Cells interact with ECM via cell membrane receptors, integrins, and signals from ECM are transmitted to the inside of the cell.

The main components of proteoglycans are unbranched polysaccharide structures (GAGs) consisting of repeating disaccharides of an amino sugar and an uronic acid (3). Heparan sulfate, chondroitin sulfate and keratan sulfate are the most important components of GAGs, which consist of different types of disaccharides. Heparan sulfate is involved in the cell signalling by secreting growth factors. Hyaluronic acid is formed by repeating gluconic acid and N-acetyl glucosamine. It is a free ECM part that does not have a proteoglycan component and is found in large quantities in early embryos.

Collagen is a chain structure consisting of proline, glycine and aspartic acid (67). Before being secreted, three chains come together to bend to form collagen fibrils, forming a triple helix structure. There are different types of collagens consisting of different chains. Collagen type I is the most common type of collagen in most tissues.

Collagen helixes are covalently crosslinked, affecting the changing mechanical properties of tissues with age. Elastin is the protein that provides elasticity and acts on the cell signalling. Laminin, on the other hand, is a glycoprotein consisting of three crosslinked disulfide-bonded polypeptides found in basal lamina. Fibronectin, containing integrin binding regions, is involved in directing the organization of the ECM. It contributes to cell binding with its RGD sequence which binds to integrins on the cell surface.

2.5.1 Cell sources used in cornea tissue engineering

Adult keratocytes and stem cells are used to obtain an *in vitro* corneal tissue substitutes in cornea tissue engineering (22). Adult keratocytes (10, 11), epithelial cells (23) and endothelial cells (12) in natural cornea tissue are mostly used. Embryonic stem cells can be preferred because they have high self-renewal capacity and high differentiation potential. However, since there are ethical issues about embryonic stem cells and there is a risk of teratoma formation, adult stem cells would be an alternative cell source.

Because of their ability to quickly differentiate into the desired cell type, limbal stem cells (68), corneal stromal stem cells (20), mesenchymal stem cells derived from human umbilical cord (26), dental pulp (27), postnatal periodontal ligament tissue (69) and adipose tissue (70) are used in cornea tissue engineering.

2.5.1.1 Stem cells

Stem cells are undifferentiated cells that have high ability to undergo mitosis and renew themselves (71). These cells have potential to differentiate into different specialized tissue cells when they are induced with certain biological signals. Stem cells are classified according to their origin, as embryonic, germinal, or somatic (fetal or adult). Advances in stem cell biology make these cells potential sources to be used in the field of regenerative medicine and tissue engineering.

Stem cells are defined by the following identities that differ these cells from other cells in the body (72, 73).

1) They have an ability to divide and renew themselves over long period of time.

2) They are not specialized.

3) They give rise to various specialized cell types via differentiation by appropriate induction.

4) Stem cells should be able to functionally regenerate the damaged tissue after transplantation to the recipient.

Stem cells are classified as totipotent, pluripotent and multipotent according to their differentiation potential (74). Totipotent stem cells are the stem cells that make up the whole embryo and the extra-embryonic tissues with their unlimited differentiation capacity. All blastomeres up to 8 cells in the early embryo period are totipotent (71). Pluripotent stem cells can form all cell types in the body. The pluripotent stem cells can differentiate into many different types of cells originating from endoderm, ectoderm and mesoderm. Multipotent stem cells are programmed to differentiate into certain tissues. For example, adult stem cells typically produce cell types of tissue in which they are located.

Embryonic stem cells (ESCs) which are derived from blastocyst stage of an embryo, have pluripotent properties (75). ESCs are obtained from the inner cell mass of blastocyst. ESCs simultaneously form embryoid bodies in suspension culture *in vitro*. They can differentiate into various cell types that are derived from endoderm, mesoderm, and ectoderm layers. ESCs express high levels of telomerase activity; therefore, they have unlimited proliferation capacity. This property of ESCs leads to risk of teratoma formation. The other limitation of ESCs is ethical concern since they are obtained from embryo. In addition, the choice of appropriate differentiation protocols to obtain functional mature cells is still important problem about ESCs.

As a solution to the ethical debates regarding the use of embryonic stem cells, induced pluripotent stem cells (IPSCs) have been used as a new alternative method (76). IPSCs are obtained from somatic cells like fibroblasts which are reprogrammed to form ESC-like cells with ESC properties such as high proliferation and differentiation capacity (77). Like ESCs, IPSCs can differentiate into all cell types derived from endoderm, mesoderm, and ectoderm. Therefore, IPSCs appear as an alternative cell source to provide regeneration by differentiating into tissues such as retinal pigment epithelium and corneal epithelium (78). Since they are obtained from

somatic cells there is no ethical problems of IPSCs like isolating the cells that we encounter especially in ESCs from embryo. However, like ESCs because of high telomerase activity they carry the risk of teratoma formation in undifferentiated state. They should be carefully utilized in cell therapy and regenerative medicine; however, IPSCs have a great potential to be used in *in vitro* disease modelling.

Another cell type with high proliferation capacity is the stem cell found in the cornea (15). Corneal epithelial stem cells are located in the corneoscleral limbus, the transition zone between the cornea and the sclera. For this reason, it is also called limbal (epithelial) stem cell. Limbal stem cells located on the basement membrane, have high proliferation capacity, and they undergo symmetric and asymmetric cell division (79). While two identical stem cells are obtained with symmetric division, one stem cell and one differentiated are obtained with asymmetric division. It has an important repair and renewal mechanism for the corneal epithelium. It is known that the corneal tissue is constantly being renewed by stem cells and these stem cells play an important role in the persistence of corneal transparency (80).

Mesenchymal stem cells (MSC) are stem cells that can differentiate into various mesodermal cell types and induce angiogenesis in both *in vitro* and *in vivo* (81). MSCs are frequently preferred in the field of tissue engineering in recent years due to their self-renewal capacity, differentiation potential, enhancing blood vessel formation, preventing cell death, and immune regulating function. MSCs are especially important for clinical applications because of their reduced teratoma formation risk and reduced immune rejection. MSCs are commonly isolated from bone marrow stroma and have a tendency to differentiate into osteocyte, chondrocyte and adipocyte (82, 83). MSCs adhere to tissue culture plastics under standard *in vitro* culture conditions and express specific surface antigens like CD105 (endoglin), CD73 (5′-nucleotidase) and CD90 (Thy-1) that are expected positive markers (≥95%), while they do not express hematopoietic stem cells markers like CD34 (sialomucin) and CD45 (PTPRC) (≤2%) (Table 1) (84). In addition, MSCs express CD44 (LHR or MC56) surface antigen which is important for cell attachment to hyaluronan (85).

Table 1. The positive and negative markers for the characterization of mesenchymal stem cells (86).

POSITIVE (≥95%)	**NEGATIVE (≤2%)**
CD105	CD45
CD73	CD34
CD90	CD14 or CD11b
	CD79α or CD19
	HLA-DR

Besides bone marrow, MSCs are present in almost all adult tissues such as adipose tissue (87), umbilical cord blood and matrix (88), peripheral blood (89), and dental pulp (90). Despite its many advantages, BMSCs are obtained by invasive method from limited amount of tissues compared to other MSC sources. This is the most important point which directs scientists to the other MSC sources.

Umbilical cord matrix (Wharton's Jelly) excluding two arteries and one vein is a mucous connective tissue (Figure 4) which consists of collagen, hyaluronan, proteoglycan and mucopolysaccharides (15, 84, 91). ECM components of Wharton's Jelly are associated with factors required for cell growth, proliferation and differentiation, such as insulin growth factor, transforming growth factor (TGF-β) and fibroblast growth factor (FGF) (92). In addition, it takes part in remodeling of ECM. Umbilical cord stem cells are stem cells that are found in cord blood or umbilical cord matrix (Wharton's Jelly) (93). MSCs in the umbilical cord matrix (Wharton's Jelly) can be easily isolated by explant culture (94) or enzymatic digestion (95). Since umbilical cord is a discarded tissue after birth, the access to tissue is easy and it is not an invasive procedure. Cells obtained from Wharton's Jelly express high levels of mesenchymal stem cell markers which are CD105, CD73, CD90 and CD44, and have superior differentiation ability (93). In addition, MSCs derived from Wharton's Jelly have low immunogenicity. They can be isolated and cultured *in vitro* quickly, and abundant stem cells can be isolated and retain their stemness for a longer time than MSCs from other sources. Cells obtained from umbilical cord have high proliferation and differentiation properties due to their neonatal origin. Besides their tendency to differentiate osteocytes, chondrocytes and adipocytes (93, 96-98), these MSCs can be

differentiated into corneal epithelial, stromal keratocytes and endothelial cells (99, 100). Although it is known to have promising effects on corneal damage by differentiating into keratocytes, there are limited number of studies in the literature about the use of Wharton's Jelly mesenchymal stem cells (WJ MSCs) in cornea tissue engineering.

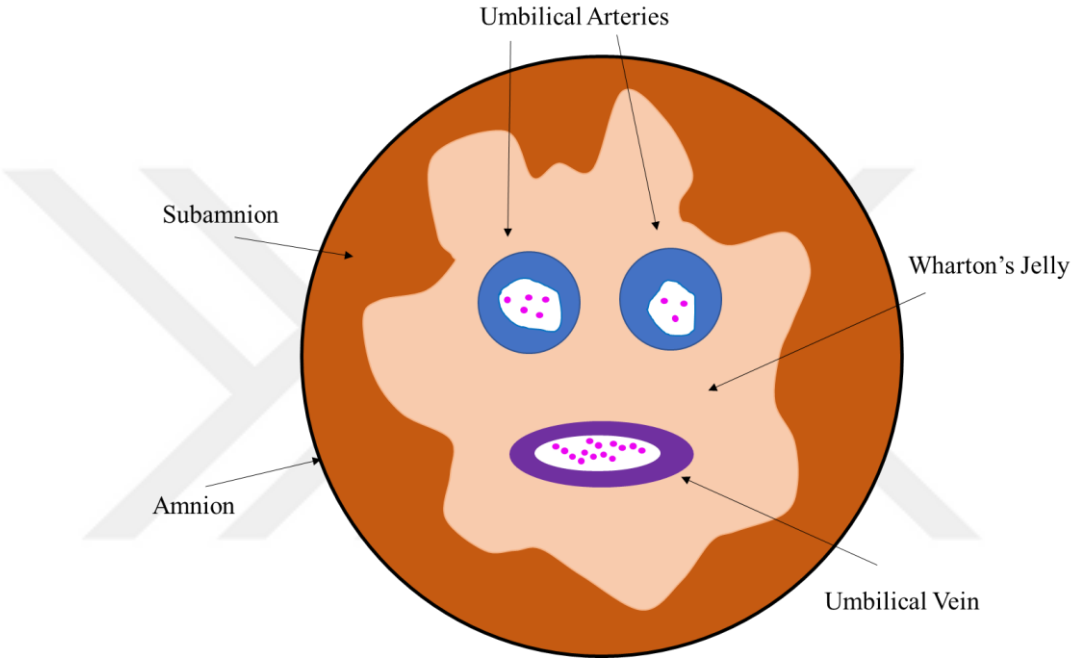

Figure 4. Schematic representation of umbilical cord.

2.5.2 Scaffolds used in cornea tissue engineering

Tissue scaffolds composed of biomaterials mimicking the ECM of target tissue are combined with cells in tissue engineering to replace the losses in human tissues and to reduce the healing process time (3). The physical and chemical properties of scaffolds that can be natural and/or synthetic materials can be adjusted to fulfil or support the functions of living tissues in the human body. The scaffolds play an important role in supporting for cell adhesion, proliferation, migration, and also providing appropriate environment for nutrient diffusion. An ideal tissue scaffold to be used in corneal tissue engineering should be able to imitate the architecture and

content of natural corneal tissue as much as possible (22). The examples of scaffolds and cells used in cornea tissue engineering studies were shown in Table 2.

Similar to native corneal tissue, hydrogels are widely used as a biomaterial in corneal tissue engineering due to their large water content (21, 24, 101-109). Scaffolds can be made of hydrogels which are designed to be porous and bioresorbable to induce cell attachment, proliferation, migration, and differentiation. Various natural materials such as collagen (110), fibrin (111), silk (112), and synthetic materials such as poly(vinyl alcohol) (PVA) (102), poly(ethylene glycol) (PEG) (113), poly(acrylic acid) (114) and poly(N-isopropyl acrylamide) (114) have been used to fabricate hydrogel scaffolds. However, these hydrogel scaffolds lack the fibrous structure that acts as a load-bearing component in native tissue, therefore, it results in reduced mechanical performance. For that reason, in corneal tissue engineering applications, using constructs composed of synthetic and/or natural polymers, and optimizing their composition and crosslinking degree are among the frequently used strategies to enhance chemical and mechanical properties of hydrogel based scaffolds (21). In addition, the hydrogels can be combined with other forms of scaffolds such as fibrous meshes, sponges, films or 3D printed constructs.

Polymeric fibrous meshes obtained by electrospinning are also used in cornea tissue engineering (8, 22, 25, 115-117). The fibrous meshes with a fiber diameter at nano or submicron level provide a suitable environment for cell attachment and proliferation in biomimetic tissue engineering, since their fibrous structure similar to the native ECM with high surface/volume ratio and good porosity. Foams or sponges are also used in cornea tissue engineering applications with the advantage of their porous structures (8, 12, 14, 105, 118). In foam applications, which are preferred to be seeded together with the cell, the pores are connected to each other which allows cell growth, migration and proliferation (8). 3D bioprinting method is also used in corneal tissue engineering applications to mimic the 3D biological architecture of the cornea by layer-by-layer deposition of bioink (119-123). In this method, the hydrogel chosen for the target tissue, cells and even growth factors was used as bioink.

Table 2. The scaffolds and cells used in the examples of cornea tissue engineering.

Cornea tissue layer	**Biomaterial**	**Cell type**	**Preclinical studies**	**Ref.**
Epithelium	PVA-Collagen hydrogel	Human and rabbit CECs	Animal model: rabbit	(102)
Epithelium	PVA-AM hydrogel	Rabbit CECs	Animal model: rabbit	(103)
Epithelium	HA hydrogel	hCESCs	*Ex vivo*	(104)
Epithelium	Collagen hydrogel	LSCs	*Ex vivo*	(24)
Epithelium	PCL nanofibrous mesh	LSCs	*In vitro*	(115)
Epithelium	PLGA nanofibrous mesh	Conjunctival epithelial cell	Animal model: rabbit	(116)
Epithelium	PLA nanofibrous mesh	BM-MSCs, Ad-MSCs and/or LSCs	Animal model: rabbit	(25)
Epithelium and stroma	P(L/DL)LA-PHBV micropatterned films and foam	RPECs and 3T3 fibroblasts	*In vitro*	(14)
Stroma and Bowman's membrane	Collagen-based double-layered scaffold: foam and fibrous mesh	HKs and RPECs	*In vitro*	(8)
Stroma	P(L/DL)LA-PHBV film	HK and RPECs	*In vitro*	(13)
Stroma	Multi-layered silk film	hCSSCs and hCFs	*In vitro*	(124)
Stroma	Collagen-based micropatterned film	HKs and RPECs	*In vitro*	(125)
Stroma	Collagen foam and film	Stromal fibroblasts	*In vitro*	(118)
Stroma	Collagen foam and hydrogel	Stromal fibroblasts	*In vitro*	(105)
Stroma	PLDLA multi-nanofibrous mesh	hCSCs	*In vitro*	(117)
Endothelium	Chitosan– PEG hydrogel film	CECs	*Ex vivo*	(113)

Endothelium	Hydroxyethyl chitosan, gelatin, and chondroitin sulfate membrane	CECs	Animal model: rats	(126)
Endothelium	Gelatin hydrogel	CECs	*In vitro*	(106)
Full-thickness cornea	Fibrin-agarose hydrogels	Animal-derived CECs	*In vitro*	(107)
Full-thickness cornea	Collagen-chitosan hydrogels	Without cells	Animal model: pig	(108)
Full-thickness cornea	Gelatin fibrous mesh and alginate hydrogel	Without cells	*In vitro*	(21)
Full-thickness cornea	Patterned silk fibroin film and collagen hydrogel	HKs	*In vitro*	(109)
Full-thickness cornea	Collagen/glycosaminoglycan-based foam	HKs, epithelial and CECs	*In vitro*	(12)
Full-thickness cornea	3D printed PLA	LEC-like cells and CEC-like cells derived from hESCs	Animal model: pig and rabbit	(121)

*HA: Hyaluronic acid; PCL: Polycaprolactone; PLGA: Poly(lactic-co-glycolic acid); PLA: Poly (lactic acid); PLDLA: Poly (L,D lactic acid); PEG: poly(ethylene glycol); PVA: poly(vinyl alcohol); AM: Amniotic membrane; HK: Human keratocytes; hASCs : Human adipose stem cells; RPEC: retinal pigment epithelial cells; LEC-like: Limbal epithelial cell-like; CEC-like: Corneal endothelial cell-like; hESCs: Human embryonic stem cells; hCSSCs: Human corneal stromal stem cells; hCFs: human corneal fibroblasts; hCSCs: Human corneal stromal cells; CECs: Corneal endothelial cells; hCESCs: Human corneal epithelial stem cells; LSCs: corneal limbal epithelial stem cells

2.5.2.1 Hydrogels

Similar to native tissue, hydrogels are widely used as a biomaterial in corneal tissue engineering due to their large water content (21). Various natural materials such as collagen (24), fibrin (127) and silk (128) have been used to fabricate hydrogel scaffolds. In order to obtain a full layer of corneal substitute, it was reported that the collagen-chitosan hydrogel was used on a porcine model (108). A dendrimer cross-linked collagen hydrogel (129) and fibrin agarose hydrogel (107) were prepared and

studied as an *in vitro* study. In addition, the cross-linked recombinant human collagen type 3 hydrogels were used on human in Phase 1 clinical trials (57). However, these hydrogel-based scaffolds lack the fibrous structure that acts as a load-bearing component in native tissue; therefore, it leads to reduced mechanical performance. In order to improve the biochemical and mechanical properties of the corneal substitutes, the hybrid scaffolds are formed in terms of chemical composition by combining synthetic and/or natural polymers or in terms of physical composition by using different forms of scaffolds together in a single construct. For instance, in one of the study polycaprolactone (PCL) fiber-reinforced alginate hydrogels were produced (21). It was reported that hydrogels reinforced with PCL fibers significantly increased the mechanical properties of hydrogels, but the resulting composite hydrogels were not suitable for corneal tissue engineering application due to their opacity (130). In order to ensure sufficient transparency, the percentages of polymers were changed, and the plasma discharge method was applied (131). In this context, it is still a challenge to produce appropriate 3D corneal substitutes housing targeted cell types and having ideal mechanical properties and transparency.

2.5.2.2 Fibrous scaffolds via electrospinning

Electrospinning is a commonly used method to fabricate fibrous scaffolds in tissue engineering. In cornea tissue engineering as a biomimetic approach the electrospun fibrous meshes were used with their high surface/volume ratio and porosity to support cell penetration, cell proliferation and differentiation (83). Electrospinning is a versatile fabrication method that is based on the principle of pushing the polymer solution with a certain flow rate and applying high voltage between the syringe needle and the collector (Figure 5). While the polymer solution in the syringe was pushed at a certain flow rate, a droplet of polymer solution at the tip of syringe needle becomes cone shape called Taylor cone upon increase in applied potential. Then by the ejection of the polymer droplet under electric field and evaporation of the solvent, nano- or micro-scale fibers form a mesh structure on the metal collector (132). The parameters such as polymer concentration, solvent type, syringe needle tip, distance between the needle and the collector (a rotating mandrel, a metal sheet or parallel bars), applied

potential, flow rate of the polymer solution should be optimized to obtain uniform and non-fused fibers.

To date, lots of polymers have been electrospun to obtain nano- or micro-scale fibers prepared for use in corneal tissue engineering. Besides natural polymers such as collagen (8), gelatin (21), hyaluronic acid (HA) (133), chitosan (133), and silk fibroins (SF) (134), synthetic polymers such as polycaprolactone (PCL) (115), poly-L-lactic acid (PLLA) (135), PLDLA (117) and poly (lactide-co-glycolide) (PLGA) (116) have also been fabricated to be used in corneal tissue engineering.

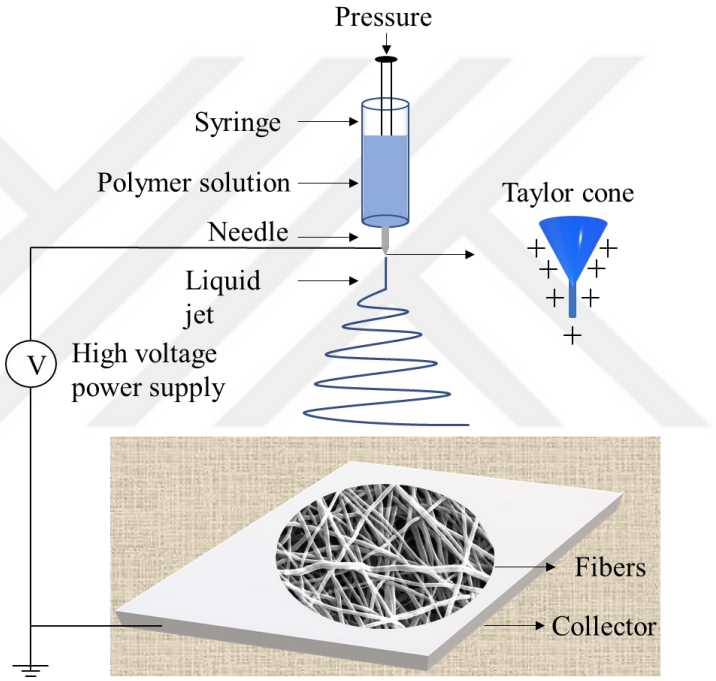

Figure 5. Schematic representation of electrospinning set-up.

2.5.2.3 Polymers used in scaffold

The natural origin polymers are widely used in tissue engineering applications due to their various properties such as biocompatibility, biodegradability, biofunctionality, non-toxicity and non-carcinogenicity, and pH stability. Natural polymers are classified into three main groups: proteins, polysaccharides, and polynucleotides. Proteins are polypeptide compounds that are formed as a result of amino acids being linked by peptide bonds. Silk, keratin, collagen, gelatin, fibrinogen, elastin, actin, and myosin

are examples of protein-derived natural polymers. Polysaccharides, on the other hand, are structures formed by mono- and disaccharides with glycosidic bonds in the polycarbohydrate structure. Cellulose, starch, dextran, chitin, chitosan, alginate are examples of natural polymers originating from polysaccharides. There are three important types of glycosaminoglycans in the connective tissue as heparin, chondrotin-6-sulphate, and hyaluronic acid. Hyaluronic acid is the material that keeps the tissues young and alive and prevents cell destruction. Polynucleotides, another type of natural polymer, are ribonucleic acid and deoxyribonucleic acid. The primary reason for the preference of natural polymers used in the scaffolds is to imitate natural tissue, with their similar properties even under *in vitro* conditions. They degrade with enzymes in the natural environment and do not have toxicity problems. However, they might evoke an immune response when derived from different individual or species. In addition, the most important disadvantage of natural polymers is their complex structure; therefore, their manipulation is difficult, and they are not stable at high temperatures.

The synthetic polymers are also used in tissue engineering due to their improved mechanical properties and stability at high temperature. A large number of polymers are biocompatible, biodegradable and do not cause an immunological response. In addition, they can be easily tailored by changing processing conditions and components in the desired direction to obtain the desired tissue property in tissue engineering applications (13, 14, 25, 83, 116). Poly (lactic acid) (PLA) (25), poly (L,D lactic acid) (PLDLA) (13, 14), and poly(lactide-co-glycolic acid) (PLGA) (116) are among the most widely used synthetic polymers in tissue engineering, including corneal tissue engineering.

The functional role of the cornea requires four major design criteria as protection, transparency, an ideal optical interface, and biocompatibility. Many synthetic polymers, such as polyhydroxyethyl methacrylate (PHEMA) (136) and polymethylmethacrylate (PMMA) (7), have shown excellent biocompatibility in the past studies and are excellent sources for corneal transplantation. Poly-glycolide (PGA) and PLGA are generally used in corneal tissue engineering (137). PLGA is a

copolymer of PLA and PGA has been approved by the FDA for clinical use. Poly-N-isopropylacrylamide (PNIPAM) supports the growth of cells(138).

The commonly used natural polymer is collagen, a kind of structural protein, makes up 71% of the dry weight of the natural corneal stroma (57). Collagen supports cell survival and induces cell proliferation and differentiation as a component of the extracellular matrix (139). For this reason, collagen hydrogels, collagen sponges, collagen films and reinforced collagen skeletons have been used to date (140). As an alternative approach, collagen-like peptides, gelatin hydrogels, synthetic polymers, fish scale derived bio-cornea, silk fibroin and decellularized cornea have been also used.

2.5.2.3.1 Collagen

Collagen is the most abundant protein by weight in humans and animals (141, 142). It is an important protein found in different connective tissues such as skin, bone, cartilage and tendon, and constitutes approximately 1/3 of the total protein. Collagen molecules consist of three polypeptide chains in a helical structure. Polypeptide subunits, α-chains form the triple helix of the collagen molecule (143). Two α-chains convert to a peptide chain dimer known as β-peptide chain, while three α chains convert to peptide chain trimer known as γ-peptide chain (tropocollagen molecule) (141). Each peptide chain is approximately 300 nm long, 1.5 nm in diameter, with a molar mass of about 100 kDa, and contains exactly 1050 amino acid residues wrapped around each other in a characteristic triple helix (144). It has a high molecular weight of 300-350 kDa. The amino acid sequence in collagen is a repeating tripeptide unit (Gly-X-Y) (145). Gly refers glycine, X is for proline and Y is for hydroxyproline. Collagen helices are cross-linked covalently and affect the change in mechanical properties of tissues with age. There are many types of collagens such as collagen type I, II, III, IV, etc. that can consist of similar or different chains in the triple helix (3).

2.5.2.3.2 Methacrylated hyaluronic acid (MeHA)

The most common glycosaminoglycan, one of the natural polysaccharides found in vertebrate tissues, is known as hyaluronic acid (HA) or hyaluronan (146). It is a glycosaminoglycan whose monosaccharide units are linked by alternating β-1,3 and β-1,4 glycosidic bonds and consists of repeating N-acetyl-d-glucosamine and d-glucuronic acid units (Figure 6). The fact that it contains various functional groups such as amide, carboxyl and hydroxyl in its structure makes it easy to modify (147). Its properties, such as being biocompatible, biodegradable, non-immunogenic and non-toxic, have made HA a potential natural material to be used in tissue engineering (148).

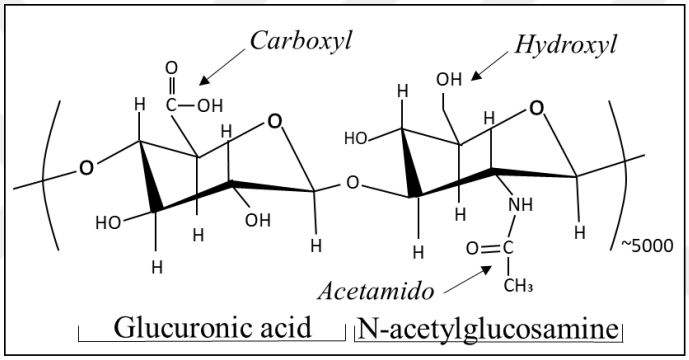

Figure 6**.** Chemical structure of hyaluronic acid.

HA is broken down in the body by the enzyme hyaluronidase (149). Therefore, for tissue engineering applications the degradation rate can be reduced by cross-linking of HA chains. Photopolymerization is the most effective method used in crosslinking, and chemical methacrylation of HA is used to obtain photopolymerizable conjugate (150). Addition of methacrylic anhydride to form methacrylated hyaluronic acid (MeHA) results in a UV photocrosslinkable hydrogel as shown in Figure 7 (150). In this context, the degree of crosslinking is very important. It has been shown that the crosslinking density, which will affect the mechanical properties of the scaffolds, induces cell adhesion, morphology, proliferation and even differentiation (151).

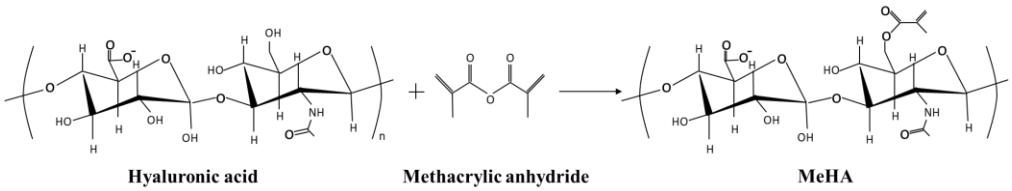

Figure 7. Chemical methacrylation of HA to obtain MeHA.

2.5.2.3.3 Polylactic acid (PLA)

Polylactic acid (PLA) is a thermoplastic synthetic polymer with high strength and modulus (152). The monomeric unit of the PLA backbone is represented by the formula CH_3–CH(OH)–COOH (Figure 8) (153).

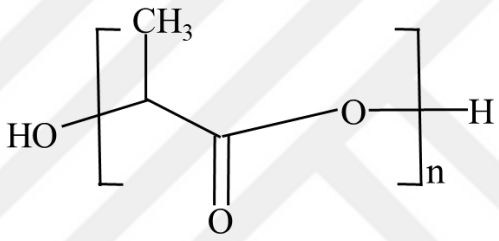

Figure 8. Chemical structure of PLA.

It is commonly obtained industrially by the polymerization of lactic acid or the ring-opening polymerization (ROP) of lactide monomer. The Young's modulus ranges from semi-crystalline to high-crystalline polymer with 2.7-16 GPa (154). It is also used in the field of biomedical, packaging and textile fibers due to its transparency, low toxicity, easy processing, biocompatibility, biodegradability and environmentally friendly properties (155, 156). It is also used in tissue engineering as scaffolds for tissue replacement and regeneration (25). It provides good printability with its high surface energy (121). Therefore, it allows it to be widely used in 3D printing. However, there are also disadvantages that limit its use with high brittleness and poor crystallization properties (152).

2.5.2.3.4 Poly(lactic-co-glycolic acid) (PLGA)

Poly(lactic-co-glycolic acid) (PLGA) is a copolymer with biodegradability and biocompatibility properties (157). PLGA is synthesized by ring-opening copolymerization of cyclic dimers (1,4-dioxane-2,5-diones) of two different monomers, glycolic acid and lactic acid (Figure 9).

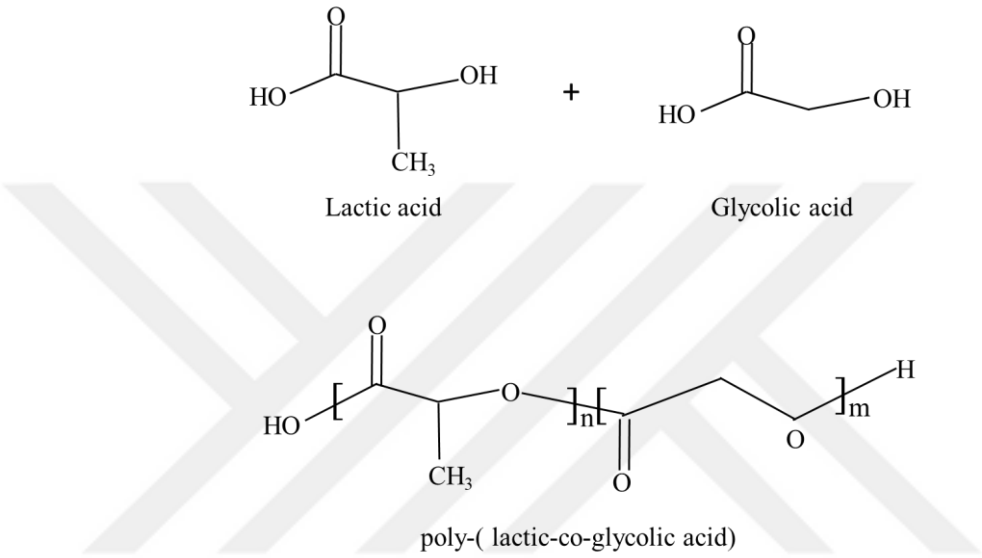

Figure 9. Chemical structure of PLGA.

PLGA degrades by hydrolysis of ester bonds in the presence of water (158). Lactic acid and glycolic acid are metabolized in the body. Therefore, there is a minimal systemic toxicity associated with the use of PLGA for biomaterial applications, and acidic degradation of PLGA has been reported to lower the local pH sufficiently (159). It is preferred in tissue engineering applications due to its good mechanical behavior, low toxicity, porosity, biodegradability and biocompatibility (160, 161).

3 MATERIALS AND METHODS

3.1 Materials

Poly (lactic-co-glycolic acid) (PLGA) (50:50, Mw: 153 000 g/mol) was obtained from Purac, Corbion Company (Netherlands). Type I atelocollagen from bovine achilles tendon was obtained from Bugamed Biotechnology (Eskisehir, Turkey). SnakeSkin dialysis tubing 10 000 MWCO was purchased from Thermo Fisher Scientific (USA). Hyaluronic acid, methacrylic anhydride, NaOH, acetic acid, Irgacure 2959, glutaraldehyde, cacodylic acid, NaCl, dexamethasone, ascorbate-2-phosphate, DAPI, trypsin-EDTA, silver-nitrate, sodium thiosulfate, FITC-Phalloidin, WST-1, proline, sodium pyruvate, trypan blue, DMSO, insulin-transferrin-selenite (ITS), TGFβ3, BSA, Triton-X-100 were obtained from Sigma-Aldrich (USA). Paraformaldehyde, N,N-dimethylformamide (DMF), HCl were obtained from Merck Company (USA). β-glycerol phosphate disodium salt 5-hydrate and ascorbic acid were purchased from Biochemica (UK). ALP kit was purchased from Randox. LIVE/DEAD™ Viability/Cytotoxicity Kit was purchased from ThermoFisher Scientific (USA) and ABP Bioscience (USA). Dulbecco's Modified Eagle Medium:F12 (DMEM:F12), advanced MEM (minimum essential medium), penicillin/streptomycin (Pen/Strep), basic fibroblast growth factor (bFGF) and fetal bovine serum (FBS) were purchased from Gibco. All antibodies for flow cytometry were purchased from BD Biosciences. Alpha-Smooth muscle actin (α-SMA) was obtained from Syc-Tek. Aldehyde dehydrogenase 1 family, member A1 (ALDH1A1) monoclonal antibody, lumican (LUM) recombinant rabbit monoclonal antibody, goat Alexa Fluor 555 anti-mouse secondary antibody and goat Alexa Fluor 488 anti-mouse IgG (H+L) superclonal™ recombinant secondary antibody were purchased from Invitrogen (USA).

3.2 Methods

3.2.1 Preparation of the hybrid scaffolds

3.2.1.1 Isolation of collagen from bovine achilles tendon

Collagen isolation procedure with its steps was presented in Figure 10. Firstly, bovine achilles tendon was mechanically cleaned by the removal of fascia (connective) tissue, and immediately afterwards washed with distilled water. Tissues were cut into small pieces to enhance the penetration of the enzyme into the tendon. The tissues were kept in 5 volumes of 0.5 M acetic acid solution (5:1) at 4°C by shaking at 90 rpm for at least 16 h until swollen. The tissues were mechanically disrupted in the blender. Afterwards, the fluid part of the tissue homogenate was taken and centrifuged at 10000 g at 4°C for 15 min. Then, the supernatant was immediately passed through filter paper. The filtrate was added onto 1.8 M NaCl solution (1:1, v:v) and kept at 4°C overnight. The precipitated collagen was taken and centrifuged at 10000 g at 4°C for 30 min. Collagen pellet was resuspended and diluted with 0.5 M acetic acid and mixed at 350 rpm with magnetic stirrer. Collagen solution was placed in dialysis tubing (10 000 MWCO) and dialyzed in 0.1 M acetic acid at 4 °C for 3 days. At the end of the period, acetic acid solution was replaced with distilled water and kept at 4°C overnight. The distilled water was refreshed, and the system was stirred with the magnetic stirrer for 8 h, and the dialysis process was terminated. Then, the collagen solution was taken into petri dishes and frozen at -80°C overnight. The samples were dried with freeze-dryer (Labconco) for 24 h and the lyophilized collagen was obtained for later use.

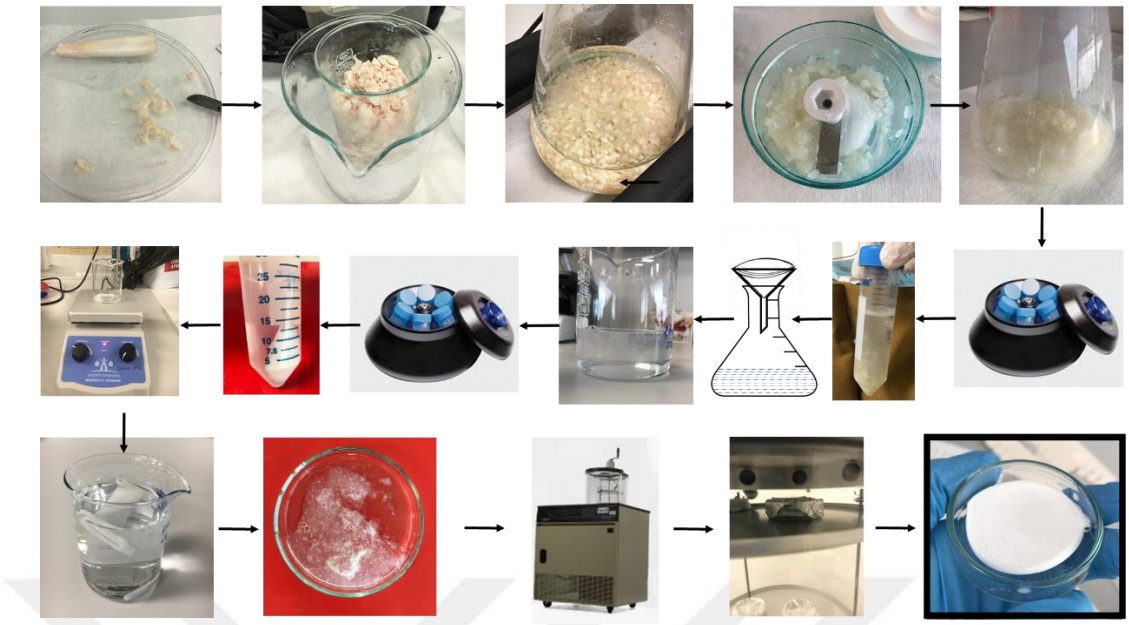

Figure 10. Schematic presentation of the collagen isolation procedure.

3.2.1.2 Fabrication of electrospun fibrous mesh

Fibrous meshes planned to mimic the Bowman's membrane were obtained by electrospinning method that is based on the principle of fiber drawing with the help of electrostatic forces. By this method, meshes consisting of fibers in nano/micro-diameter can be produced by charging polymer solutions with high electric current. The electrospinning system (Innovenso, NE100) was consisted of power supply providing high voltage, syringe pump (New Era Pump Systems) with syringe containing polymer solution and a metal, grounded collector. As the potential was applied, electrical charges begin to act on the drop of polymer. When the electrical forces reach a magnitude to overcome the surface tension, the charged polymer solution at the tip of the syringe needle was ejected and polymeric fibrous mesh was deposited on the flat, metal collector. Electrospinning parameters were optimized by changing the distance of the collector from the needle, applied voltage, flow rate and solvent type in order to ensure that the collected fibers on the plate were of the desired thickness and without beads (Table 3).

The isolated collagen solution of 5% (w/v) in 0.5 M acetic acid, and PCL-collagen solution (11:1, w:w) of 12% (w/v) in formic acid- acetic acid (7:3, v:v) were prepared

for electrospinning. The polymer solutions were placed into a 10 mL syringe capped with 18 and 23-Ga needle. During the optimization process, the distance between two poles (13-16 cm), flow rate (5-27 μL/min) and applied potential (4-13 kV) were changed. Although many parameters were tried, the fibers could not be collected on the plate that might be due to incomplete dissolution of the isolated collagen in solution. Therefore, afterwards atelocollagen type I from bovine Achilles tendon purchased from Bugamed was used and blended with PCL in order to make electrospinning process better as well as to improve mechanical properties of the mesh. Electrospinning parameters' optimization was also done using PCL-collagen blend solution (12%, w/v) with 23 Ga needle by changing the distance between the two poles (11-25 cm), the flow rate (1.5-2.5 μL/min) and the applied potential (13-20 kV). Despite the electrospinning process improved and fiber form was obtained, the fibers were fused, and the process was not reproducible. It was thought that the problem might be due to collagen; therefore, instead of collagen synthetic polymeric blend PLA-PLGA was used in the electrospinning. Tough PLA (Mw: 182 000 g/mol) was chosen because of its transparent property considering its importance in cornea tissue engineering. The blend solution of PLA-PLGA (1:1, w:w) was prepared in chloroform at 5% (w/v) concentration. During the optimization process, the distance between the two poles (11-26 cm), the flow rate (1-2 ml/h) and the applied potential (10-20 kV) were tested using a 23Ga needle. Although wide range of parameters were tried, fiber formation was not observed on the collector. For this reason, it was planned to increase the amount of PLA as well as polymer concentration to make the solution more viscous for electrospinning. Polymer solution of PLA-PLGA (2:1, w:w) at the concentration of 20% (w/v) was prepared in chloroform, and optimization studies were conducted using a 23Ga needle by adjusting the distance between the two poles (15-21 cm), flow rate (0.1-0.8 mL/h) and applied potential (11-20 kV). For the further studies, using PLA-PLGA (2:1, w:w, 20%, w/v) the determined optimized parameters as 0.8 mL/h flow rate, 11.5 kV applied voltage and 15 cm distance between the two poles were used. The transparency of the electrospun fibrous mesh was checked with the appearance of letters using stereomicroscope.

Table 3. Optimization of electrospinning parameters.

Polymer compositions	**Solvent type**	**Applied voltage (kV)**	**Distance between the two poles (cm)**	**Flow rate (µL/min)**
Collagen (5%, w/v)	acetic acid	4, 9, 11, 12, 13	13, 14, 15, 16	5, 6, 10, 15, 20, 25, 27
PCL-Collagen (11:1, w:w) (12%, w/v)	formic acid : acetic acid (7:3, v:v)	13, 14, 14.5, 15, 16, 17, 18, 18.5, 19, 20, 24	11, 12, 13, 14, 15, 16, 17, 19, 23, 24, 25, 26	1.5, 2.5
PLA-PLGA (1:1, w:w) (5%, w/v)	chloroform	10, 12, 13, 15, 16, 17, 18, 20	12, 13, 14, 15, 16, 17, 19, 23, 24, 25, 26	16.6, 25, 33.3
PLA-PLGA (2:1, w:w) (20%, w/v)	chloroform	11, 11.5, 12, 14.5, 15, 18, 19, 20	15, 18, 21	13.3, 6.6, 1.6

3.2.1.3 Synthesis of MeHA

MeHA was synthesized by binding of methacrylated groups to the hydroxyl groups of hyaluronic acid according to the method adapted from Eke G. et al. (2017) (Figure 11) (150). The steps of the protocol were presented in Figure 12. Firstly, 3 volume of dimethylformamide (DMF) was added onto 2 volume of hyaluronic acid (0.5%, w/v, in distilled water). A solution of methacrylic anhydride (1%, w/v) was added dropwise by stirring at +4°C. The pH of the prepared solution was adjusted to pH 8-9 with NaOH (0.5 M) and incubated by stirring at +4°C overnight. Afterwards, the solution was taken into the dialysis tube and dialyzed against distilled water for a week. The dialysate was frozen at -80°C and lyophilized for long term use.

The degree of methacrylation of MeHA was determined by proton nuclear magnetic resonance (^{1}H-NMR). ^{1}H-NMR spectra of MeHA samples in D_2O (C=30 mg/mL) were obtained on a Bruker DPX 400 spectrometer operating with 16 scans at ^{1}H resonance frequency of 400 MHz at room temperature. The degree of methacrylation of hyaluronic acid was determined by calculating the number of methacryloyl groups per HA disaccharide repeat unit. It was calculated from the ratio of the relative peak integrations of the protons of the methacrylate groups in MeHA (peak at 1.80 ppm) to methyl protons (peak at 1.88 ppm) according to the equation:

$$\text{DM}\ (\%)\ = \frac{\text{Peak integration of methacrylate protons}}{\text{Total peak integrations of methacrylate and methyl protons}}\ \text{x}\ 100$$

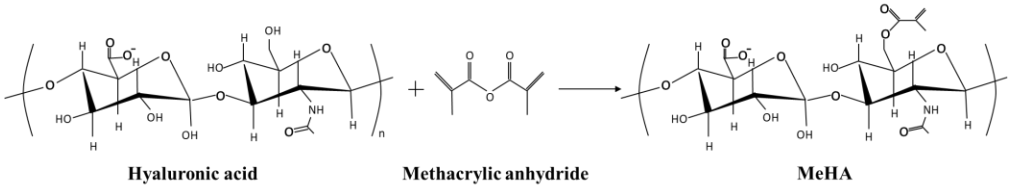

Figure 11. Synthesis of methacrylated hyaluronic acid by binding of methacrylated groups to the hydroxyl groups of hyaluronic acid.

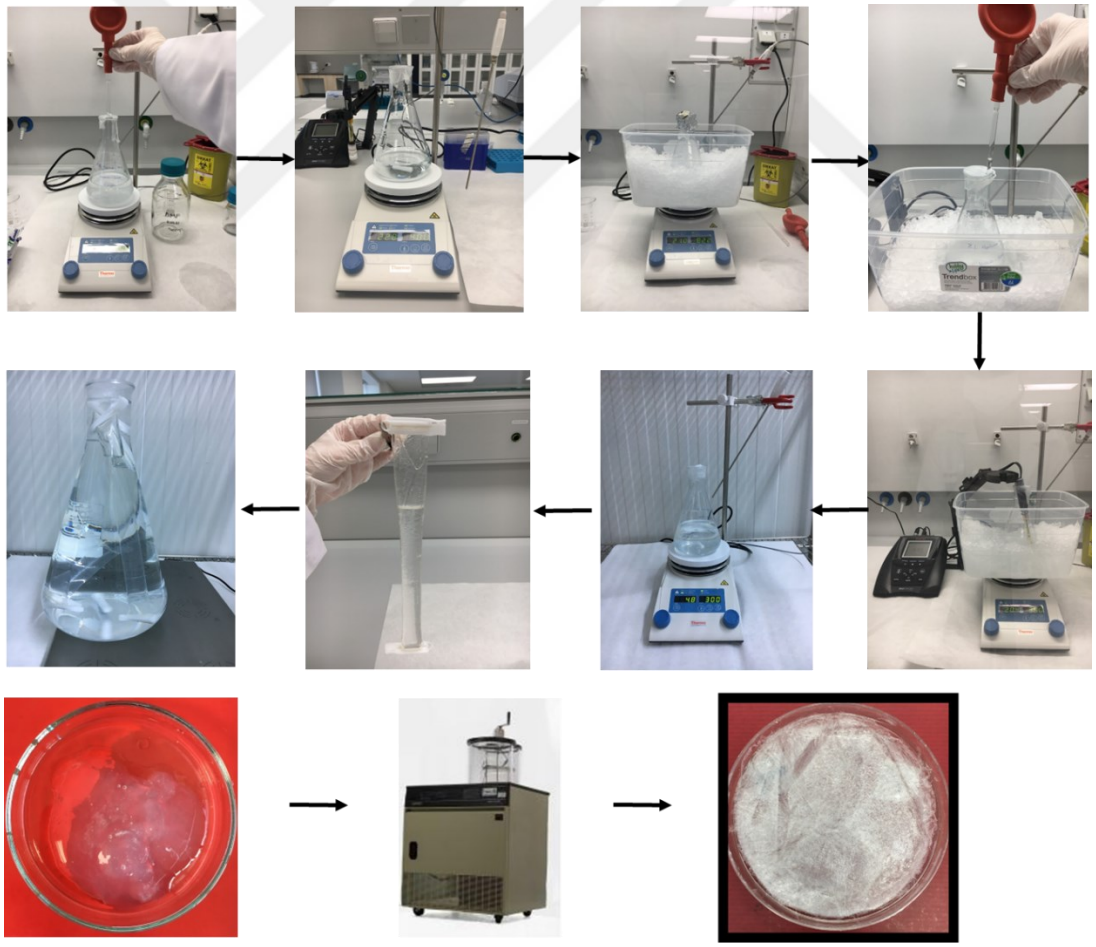

Figure 12. Schematic presentation of the synthesis of MeHA.

3.2.1.4 Formation of MeHA hydrogels

MeHA hydrogels were prepared by dissolving the lyophilized MeHA (1%, w/v) in PBS (10mM, pH7.4). 2-hydroxy-1(4(hydroxyethoxy)phenyl)-2-methyl-1-propanone (Irgacure 2959; 0.5%, w/v) was added into the solution and stirred at 40°C. After obtaining a homogeneous solution, the pH of the solution was checked and it was poured into a tissue culture well plate. Then, by applying UV irradiation at 365 nm for 13 min, gelation was occurred by crosslinking and MeHA hydrogels were obtained.

3.2.1.5 Formation of collagen-MeHA interpenetrating networks (IPNs)

The isolated collagen type I from bovine achilles tendon was planned to be used for the formation of hydrogels. However, it was observed that the isolated telocollagen didn't dissolve in the same way every time. Therefore, the atelocollagen type I from bovine achilles tendon purchased from Bugamed was used and dissolved in 0.02M acetic acid at a concentration of 15.7 mg/mL. The collagen solution was mixed with MeHA solution, and in the hydrogel solution the collagen concentration became 0.4% by weight in the final solution and MeHA concentration was 1% (w/v). Then, 1.5% photoinitiator solution (Irgacure 2959) was added to the solution and stirred for 5 min. After stirring the solution at 48°C overnight, the prepared solutions poured into a tissue culture well plate and irradiated with UV at 365 nm for 13 min onto directly solution to form hydrogel. However, gelation was not occurred with collagen–MeHA, therefore, only MeHA hydrogels were used in the further studies.

3.2.1.6 Construction of the hybrid scaffolds by combining hydrogels and electrospun fibrous mesh

It was aimed to develop a natural corneal ECM-like 3D, multi-layered construct composed of thin MeHA hydrogel, PLA-PLGA electrospun fibrous mesh and thick MeHA hydrogel to mimic three layers of cornea as epithelium, Bowman layer and stroma, respectively, as shown in Figure 13.

Firstly, the thin MeHA hydrogel was formed as explained in Section 3.2.1.4. Then the electrospun random fibrous mesh produced under optimized conditions (Section 3.2.1.2) was placed onto the thin MeHA hydrogel. Then, two layered construct was turned upside down, the thick MeHA hydrogel was formed onto the fibrous mesh by applying the protocol in Section 3.2.1.4. The transparency of the hybrid construct was checked with the appearance of letters using stereomicroscope.

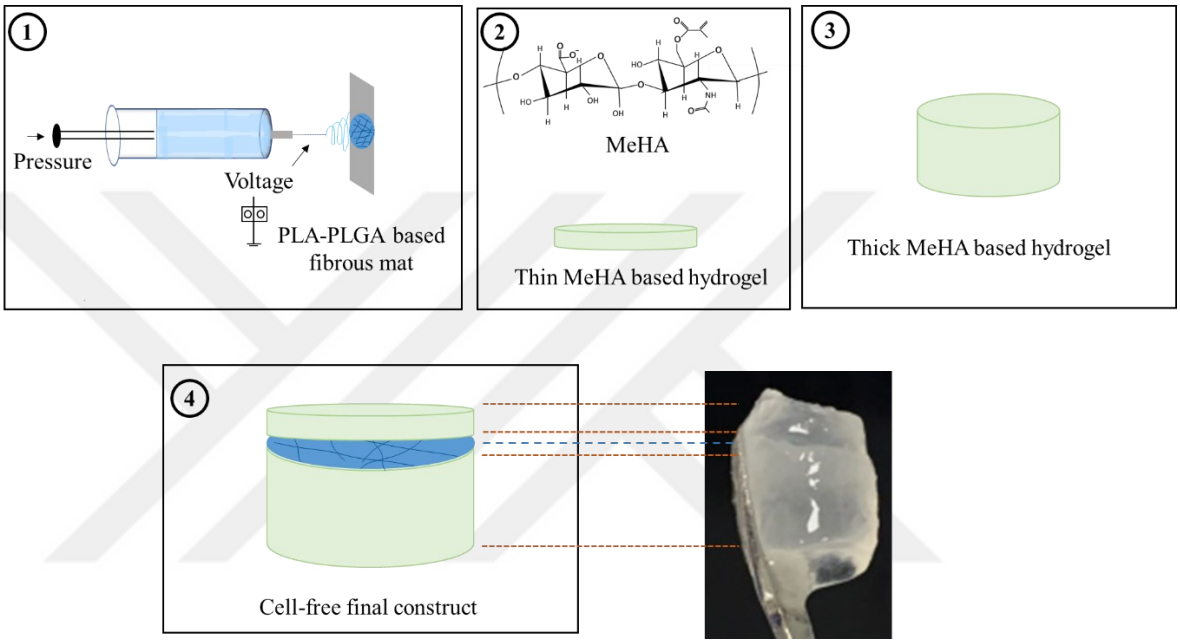

Figure 13. Schematic presentation of the design of the developed cornea tissue equivalent and preparation of its three layers to for cell-free hydrogel-fiber hybrid constructs.

3.2.2 Characterization of the hybrid scaffolds

3.2.2.1 Scanning electron microscopy

The morphology of the hybrid scaffold parts including the electrospun random fibrous meshes and the hydrogels were examined with Scanning Electron Microscopy (SEM). The samples were coated with gold under vacuum by sputter coater (Leica EM

ACE600). SEM analysis was done by Thermo Quatrro ESEM at Acıbadem Mehmet Ali Aydınlar University, Electron Microscopy Laboratory.

3.2.2.2 Mechanical analysis

The mechanical properties of the electrospun fibrous meshes were determined with Mechanical Testing Machine (Shimadzu AGS-X Series Universal Test Machine, Japan). The fibrous meshes were cut as 1 cm in width, 4 cm in length, 0.01 mm thickness and were fixed to the holders of the tensile attachment. The samples (n=4) were studied with tensile test under 1 mm/min test speed. The stress-strain curve was obtained and Young's modulus of the samples were calculated from the slope of the elastic region of the curve (Figure 14).

The mechanical properties of hydrogel part of the scaffold were determined by the compression test. The hybrid scaffold (thin layer MeHA hydrogel, fibrous mesh and thick layer MeHA hydrogel) samples prepared with dimensions of 4 mm in diameter and 7 mm in length. An initial compression contact of 0.01 N was applied prior to the tests. The samples (n=5) were studied with compression test under 1 mm/min test speed. Young's modulus of the samples was calculated from the slope of the elastic region of the stress-strain curve (Figure 14).

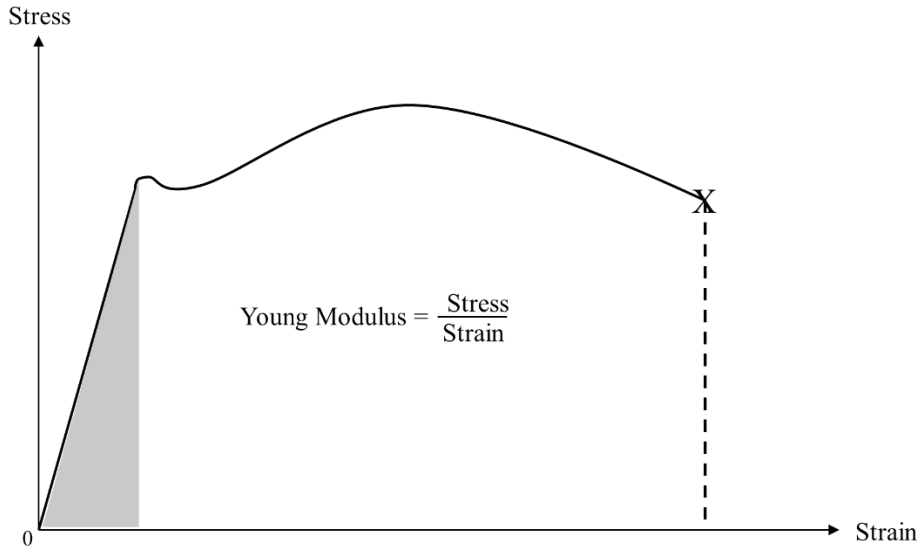

Figure 14. A representative stress/strain curve to obtain Young's modulus of materials.

3.2.2.3 Swelling test of the hydrogels

To determine the degree of swelling (DS) of the MeHA hydrogels, the hydrogels were incubated in the medium (DMEM low glucose) for 48 h at 37°C. The degree of swelling was calculated according to the following equation using the weights of the dry hydrogels (w_d) and the weights of the wet hydrogels (w_s) measured at certain time intervals. DS was calculated according to the following equation.

$$DS\ (\%) = \frac{w_s - w_d}{w_s} \text{ x } 100$$

3.2.3 Characterization of WJ MSCs and their differentiation into keratocytes

3.2.3.1 Isolation and characterization of human WJ MSCs

In this study, WJ MSCs were used as a cell source to be used in the development of cornea tissue equivalent by differentiating them into keratocytes. Human WJ MSCs which were previously isolated by explant culture from the umbilical cord matrix for a study of Asst. Prof. Dr. Deniz Yücel Acıbadem Mehmet Ali Aydınlar University were used in this thesis study (Acıbadem Mehmet Ali Aydınlar University, Istanbul, ATADEK-2020/02). Firstly, umbilical cord samples were washed with PBS and two arteries and a vein were removed from the tissue. The matrix of part of the tissue was cut into small pieces and explant culture was done in the expansion medium composed of DMEM: F12 (1:1) supplemented with 10% FBS, penicillin/streptomycin (Pen/Strep, 100 unit/mL, /100 µg/mL) and bFGF (1ng/mL) at 37°C in a humidified CO_2 incubator. The cells migrated from tissue onto the tissue culture plate and proliferated. When they reached 80% confluency, the cells were subcultured. The cells were detached from the flask with 0.05% Try-EDTA, centrifuged at 2200 rpm for 5 min, and then resuspended cell pellet was seeded to a larger surface area. The cell stocks at different passage were stored in the expansion medium containing 10% DMSO in liquid nitrogen vapor until use.

3.2.3.1.1 Characterization of WJ MSCs with flow cytometry

The expression of specific cell surface antigens of WJ MSCs (at passage 3) were analysed by flow cytometer. The antibodies against MSCs' markers such as CD105, CD73, CD90, and CD44, hematopoietic stem cell markers such as CD34 and CD45, and immunogenic antigens such as HLA-ABC and HLA-DR were used with the isotype controls. The used antibodies were CD105-FITC, CD90- PerCp, CD73-PerCp, CD44-PE, HLA-ABC-PE, HLA-DR-PerCp, CD34-PE and CD45-FITC, and the isotype controls were IgG2α-PerCp, IgG1-FITC, IgG1-PerCp and IgG1-PE. For flow cytometry analysis, MSCs were detached by trypsinization and centrifuged, then the cell pellet was resuspended in 1% BSA (in PBS) and centrifuged at 1500 rpm for 5 min at $+4^0$C. Then the pellet was resuspended and incubated with fluorochrome conjugated monoclonal antibodies for an hour at +4°C. The cells were washed with 1% BSA (in PBS) and then centrifuged at 1500 rpm for 5 minutes at +4°C. This step was applied twice. The cells were fixed with 1% PFA (in PBS) at room temperature for 10 min and centrifuged at 1500 rpm for 5 min at +4°C. The cells were rinsed with PBS and analysed with flow cytometer (FACS Verse, BD Bioscience). The positive and negative expression of cell surface antigens were determined by taking into consideration the results of the isotype controls which were used to see the signals from non-specific binding of antibodies.

3.2.3.1.2 Osteogenic differentiation for characterization of WJ MSCs

For osteogenic differentiation, the isolated WJ MSCs at P3 were seeded as $5x10^3$ cells/well into 24 well plates and cultured in the expansion medium overnight (Table 4). After 1 day of incubation, the cells were cultured in the osteogenic induction medium (Table 4) containing stimulants such as dexamethasone, ascorbic acid and β-glycerophosphate for 14 days in CO_2 incubator at 37°C, and the medium was changed three times a week. The undifferentiated WJ MSC, as a control, was incubated for a same time in the expansion medium. Osteogenic differentiation of WJ MSCs was assessed by alkaline phosphatase (ALP) activity.

Table 4. Composition of the expansion medium and the osteogenic induction medium.

Expansion medium	**Osteogenic induction medium**
DMEM: F12 (1:1)	DMEM low glucose
FBS (10%)	FBS (10%)
Pen/Strep (100 units/mL-100 µg/mL)	Pen/Strep (100 units/mL-100 µg/mL)
bFGF (1 ng/mL)	Dexamethasone (100 nM)
	Ascorbic acid (50 µg/mL)
	β-glycerophosphate (10 mM)

The osteogenic differentiation indicator, ALP activity was done on 7th and 14th days of the osteogenic induction. ALP assay is based on the formation of a yellow product p-nitrophenol by dephosphorylation of substrate p-nitrophenyl phosphate in the presence of ALP enzyme. At the end of indicated periods, the cells were rinsed with PBS and lysed with 0.1% (v/v) Triton X-100 (in 0.1 M, pH 9.0 Tris-HCl buffer). The lysates were frozen at -20°C for 10 min and then thawed at 37°C for 10 min. This freeze/thaw process was repeated three times, and then the samples were sonicated (Omni-Ruptur 4000 Sonicator) 30 s with 30 s breaks for 10 min. Then, the samples were centrifuged at 5000 rpm for 10 min at +4°C. Supernatants of 50 µL was mixed with 50 µL of 0.1% (v/v) Triton X-100 (in 0.1 M, pH 9.0 Tris-HCl buffer), and 20 µL of ALP substrate was added. The solution of 0.1% (v/v) Triton X-100 in the absence of lysate (in the absence of ALP) was used as a blank. Absorbance of the yellow product was measured spectrophotometrically at 405 nm for 16 min with 2 min intervals. ALP activity was expressed as nmol of substrate converted to product/min of cell lysate using the calibration curve for the enzymatic product (Appendix 2-Figure 42).

3.2.3.1.3 Chondrogenic differentiation for characterization of WJ MSCs

Besides osteogenic differentiation, the isolated WJ MSCs were induced to differentiate into chondrogenic cells to confirm that they were MSCs. WJ MSCs at P3 were seeded at $5x10^3$ cells/well into 24 well plates in the expansion medium in a 5% CO_2 incubator at 37°C until they reached 80% confluency (Table 5). To induce chondrogenic differentiation, the cells were incubated in the chondrogenic induction medium (Table 5) containing stimulants ITS, dexamethasone, proline, ascorbate-2-phosphate, TGFβ1 for 21 days while changing the induction medium three times a week. The undifferentiated WJ MSCs cultured in the expansion medium was used as a control. Chondrogenic differentiation was assessed by Alcian blue staining that is commonly used method for cartilage tissue by staining the glycosaminoglycans and proteoglycans. On 21st day of culture, the cells were fixed in 4% PFA and stained with 1% (w/v) Alcian Blue (pH 2.5, in 3% acetic acid) solution for 30 min. After washing with distilled water for 2 min, the samples were examined under light microscope.

Table 5. Composition of the expansion medium and the chondrogenic induction medium.

Expansion medium	**Induction medium**
DMEM: F12 (1:1)	DMEM low glucose
FBS (10%)	FBS (10%)
Pen/Strep (100 units/mL-100 µg/mL)	Pen/Strep (100 units/mL-100 µg/mL)
bFGF (1 ng/mL)	ITS (1%)
	Dexamethasone (10 nM)
	Proline (40 µg/mL)
	Ascorbate-2-phosphate (1 µM)
	TGFβ1 (5 ng/mL)

3.2.3.1.4 Growth kinetics of the isolated WJ MSCs

Isolated WJ MSCs (Passage 4) were seeded into 24 well plate at a density of $5x10^3$ cells/well and cultured in the expansion medium at 37ºC in a CO_2 incubator. At the end of 24, 48, 72, 96, 144, 192 and 240 h of incubation, number of cells (n=3) was determined by Cell Proliferation Reagent Water-Soluble Tetrazolium Salt (WST-1) Assay in which tetrazolium salt was converted to formazan by the viable cells. WST-1 working solution was prepared at a ratio of 20:1 in the expansion medium. The cells were incubated in WST-1 working solution in a CO_2 incubator at 37ºC for 2 h. The colored product, formazan, was transferred to a 96-well plate and absorbance was measured at 440 nm with the Elisa Reader. Measured OD values were converted to the cell number using the calibration curve (Appendix 1- Figure 40). Then, logarithmic cell number vs time graph was obtained to calculate the cell doubling time according to the following equation;

$$G = \frac{\Delta t}{3.3\ x\ (\frac{\log b}{\log B})}$$

G: Generation time (doubling time)

Δt: time interval between beginning of the exponential phase and end of the exponential phase

log b: logarithmic cell number at the end of the beginning cell number

log B: logarithmic cell number at the beginning of the beginning cell number

3.2.3.2 Differentiation of WJ MSCs into keratocytes

3.2.3.2.1 Induction of MSCs for keratocyte differentiation

When the isolated WJ MSCs at P3-4 reached 90% confluency, they were trypsinized and seeded at a density of $5x10^4$ cells/well into 24 well plates. After 24 h of incubation in the expansion medium in a 5% CO_2 incubator at 37°C, the medium was replaced with keratocyte induction medium (Table 6). The undifferentiated WJ MSC cultured in the expansion was used as a control. The media were refreshed three times a week thereafter. At the end of 7^{th} and 14^{th} days of induction, comparing with

the undifferentiated cell the differentiation of the cells were evaluated by immunocytochemistry analysis.

Table 6. Composition of the expansion medium and the keratocyte induction medium.

Expansion medium	**Induction medium**
DMEM: F12 (1:1)	Advanced DMEM
FBS (10%)	Pen/Strep (100 units/mL-100 µg/mL)
Pen/Strep (100 units/mL-100 µg/mL)	Ascorbate-2-phosphate (1 mM)
bFGF (1 ng/mL)	bFGF (10 ng/mL)
	TGFβ3 (1 ng/mL)

3.2.3.2.2 Expression of specific keratocyte markers of MSCs upon keratocyte differentiation by immunostaining

Immunostaining with antibodies recognizing the specific keratocyte antigens was applied to the WJ MSCs induced to differentiate into keratocytes as mentioned in Section 3.2.3.2.1. For that purpose, the cells were fixed with 4% PFA at the end of the day 7 and 14. After washing with PBS, the cells were incubated with 100 mM glycine (in PBS) for 15 min at room temperature for the saturation of PFA groups and washed with PBS. Cell membrane was permeabilized with 0.1% Triton X-100 in PBS (PBST) for 10 min at room temperature. Following PBS washing, the cells were kept in 1% BSA (in PBST) at 37ºC for 30 min to mask nonspecific bindings. The cells were incubated in primary antibody solution (prepared in 0.1% BSA) overnight at 4ºC in a solution. The primary antibodies were anti-human ALDH1A1 (mouse; clone 5G9E6C9; dilution factor, 1:60) and anti-human lumican (rabbit; clone JE11-45, dilution factor, 1:150). After washing with PBS, the cells were incubated with secondary antibodies in PBST for an hour at 37ºC. Goat anti-rabbit immunoglobulin conjugated to Alexa-Fluor 488 (dilution factor, 1:100) and goat anti-mouse immunoglobulin conjugated to Alexa-Fluor 555 (dilution factor) were used as the secondary antibodies. Following washing with PBS, the cells' nuclei were stained with

DAPI (1:5000, in PBS) for 10 min at room temperature. Then, the samples were washed with PBS and examined with the laser scanning confocal microscope (LSCM, LSM700, Zeiss).

3.2.4 Construction of corneal tissue substitute by combining wj mscs and hydrogel-based hybrid scaffolds

It was aimed to develop a multilayered cornea tissue equivalent composed of cell-free thin MeHA hydrogel, PLA-PLGA electrospun fibrous mesh and cells loaded thick MeHA hydrogel to mimic three layers of cornea as epithelium, Bowman layer and stroma, respectively, as shown in Figure 15. WJ MSCs were loaded into the thick MeHA hydrogel during formation of the construct, and then these stem cells were induced to differentiate into keratocytes within the 3D construct.

MeHA hydrogels prepared for *in vitro* studies were prepared with 1% MeHA (w/v) and 1% Irgacure (w/v). After obtaining a homogeneous solution, the pH of the solution was checked to be used in *in vitro* studies. As explained in Section 3.2.1.6, firstly the thin MeHA hydrogel was formed and the electrospun random fibrous mesh was placed onto the thin MeHA hydrogel. Then, two layered construct was turned upside down. On the other hand, the isolated WJ MSCs (P3-4) that reached 90% confluency were detached from the tissue culture plates by trypsinization and counted. The cells at a density of $4x10^5$ cells/construct were mixed with MeHA hydrogel solution that was prepared as mentioned in Section 3.2.1.6. The hydrogel solution containing cells was poured onto the fibrous mesh and by UV irradiation at 365 nm for 13 min, gelation was occurred and cell-load thick MeHA hydrogels were formed onto the two layers. Consequently, the cell-loaded construct composed of three layers was produced and incubated in the expansion medium for 24 h in a 5% CO_2 incubator at 37°C. A day after, the expansion medium was replaced with keratocyte induction medium as explained in Section 3.2.3.2.1. Cell-containing constructs were cultured in the keratocyte induction medium composed of advanced DMEM supplemented with Pen/Strep (100 units/mL-100 µg/mL), 1 mM ascorbate-2-phosphate, 10 ng/mL bFGF and 1 ng/mL TGFβ3 for 7 days at 37ºC and 5% CO_2 incubator. The medium was refreshed three times a week. At the end of 7^{th} day of induction, the cell viability,

proliferation and their behaviour within the corneal tissue substitute were analysed by Live/Dead assay, MTS assay and immunostaining.

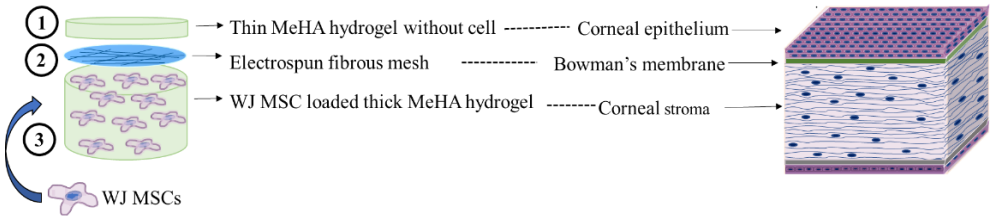

Figure 15. Schematic presentation of the design of the developed cornea tissue equivalent.

3.2.4.1 Viability and proliferation of cells in the corneal tissue substitute

The viability and proliferation analysis were performed with Live/Dead and MTS assays at 1st day of culture before starting keratocyte induction and on the 7th day of keratocyte induction. For Live/Dead assay, the medium of the samples was removed, and the cells were incubated with calcein AM and ethidium homodimer-1 staining solution that was prepared in DPBS for 30 min, the samples were examined with LSCM (LSM 700, Zeiss).

Proliferation of the cells in the corneal tissue substitutes was determined by Cell Titer 96* AQueous One Solution Cell Proliferation Assay (MTS Assay). The MTS assay, which is a colorimetric test, is based on the conversion of a tetrazolium salt into a coloured formazan product via mitochondrial activity of the cells. MTS analysis was performed on 1st day of culture and 7th day of keratocyte induction of the cells in the tissue substitute. The cells cultured on the tissue culture polystyrene were used as a positive control. At the end of indicated periods, the number of cells in each sample was determined in triplicate by MTS analysis. The cell-free scaffolds were used as blanks. 10% MTS/PES working solution in the expansion medium prepared with low glucose DMEM was added onto the cell-seeded scaffolds and control TCP wells. After 2 h incubation of the samples at 37^{o}C in a CO_2 incubator, the absorbance of formazan, the product of the MTS assay, was measured at 490 nm with the Elisa Plate Reader, and then the cell number was determined using the calibration curve (Appendix 1-Figure 41).

3.2.4.2 Immunostaining analysis of WJ MSC-derived keratocytes in the corneal tissue substitute

Immunostaining analysis was done to evaluate keratocyte differentiation of WJ MSCs loaded in the thick MeHA hydrogel layer of the corneal tissue substitute. At 7th day of keratocyte induction, the samples were fixed with 4% PFA for 2 h at room temperature and washed with PBS. According to the protocol given in Section 3.2.3.2.2, the fixed samples were incubated with 100 mM glycine (in PBS) for 15 min at room temperature. After washing with PBS, the samples were incubated with 0.1% Triton X-100 in PBS (PBST) for 10 min at room temperature. Following PBS washing, the constructs were kept in 1% BSA (in PBST) at 37^{o}C for 30 min. The samples were incubated in primary antibody solution (prepared in 0.1% BSA) overnight at 4^{o}C in a solution. The primary antibodies were anti-human ALDH1A1 (mouse; clone 5G9E6C9; dilution factor, 1:60) and anti-human lumican (rabbit; clone JE11-45, dilution factor, 1:150). After washing with PBS, the samples were incubated with secondary antibodies in PBST for an hour at 37^{o}C. Goat anti-rabbit immunoglobulin conjugated to Alexa-Fluor 488 (dilution factor, 1:100) and goat anti-mouse immunoglobulin conjugated to Alexa-Fluor 555 (dilution factor) were used as the secondary antibodies. After washing with PBS, the samples were incubated with DAPI (1:5000, in PBS) for 10 min at room temperature. Then, the constructs were washed with PBS and examined with the laser scanning confocal microscope (LSCM, LSM700, Zeiss).

3.2.5 Statistical analysis

Statistical analysis was performed with Graphpad Prism6 program. Differences between group means were analysed with Student's T test. All values were represented as the mean ± standard deviation. Differences were taken to be significant for $p < 0.05$.

4 RESULTS

4.1 Characterization of MeHA Hydrogels

4.1.1 Determination of acetylation degree upon MeHA synthesis (^{1}H-NMR)

The methacrylation reaction of hyaluronic acid showing the methacrylate peaks at 8.3, 6.03, 4.8, 3.5, 1.88, 1.80 and, 1.13 ppm. The results of ^{1}H-NMR spectra of hyaluronic acid and MeHA was given in Figure 16. The indicator peaks of methacrylation reaction of HA were seen in Figure 16b and 16c. The methacrylation reaction of hyaluronic acid was especially determined with the presence of characteristic methyl and methacrylate peaks at 1.88 and 1.80, respectively (Figure 16c). The methacrylation degree of MeHA was found as 40% by calculating from the ratio of the relative peak integrations of the protons of the methacrylate groups in MeHA (peak at 1.80 ppm) to methyl protons (peak at 1.88 ppm).

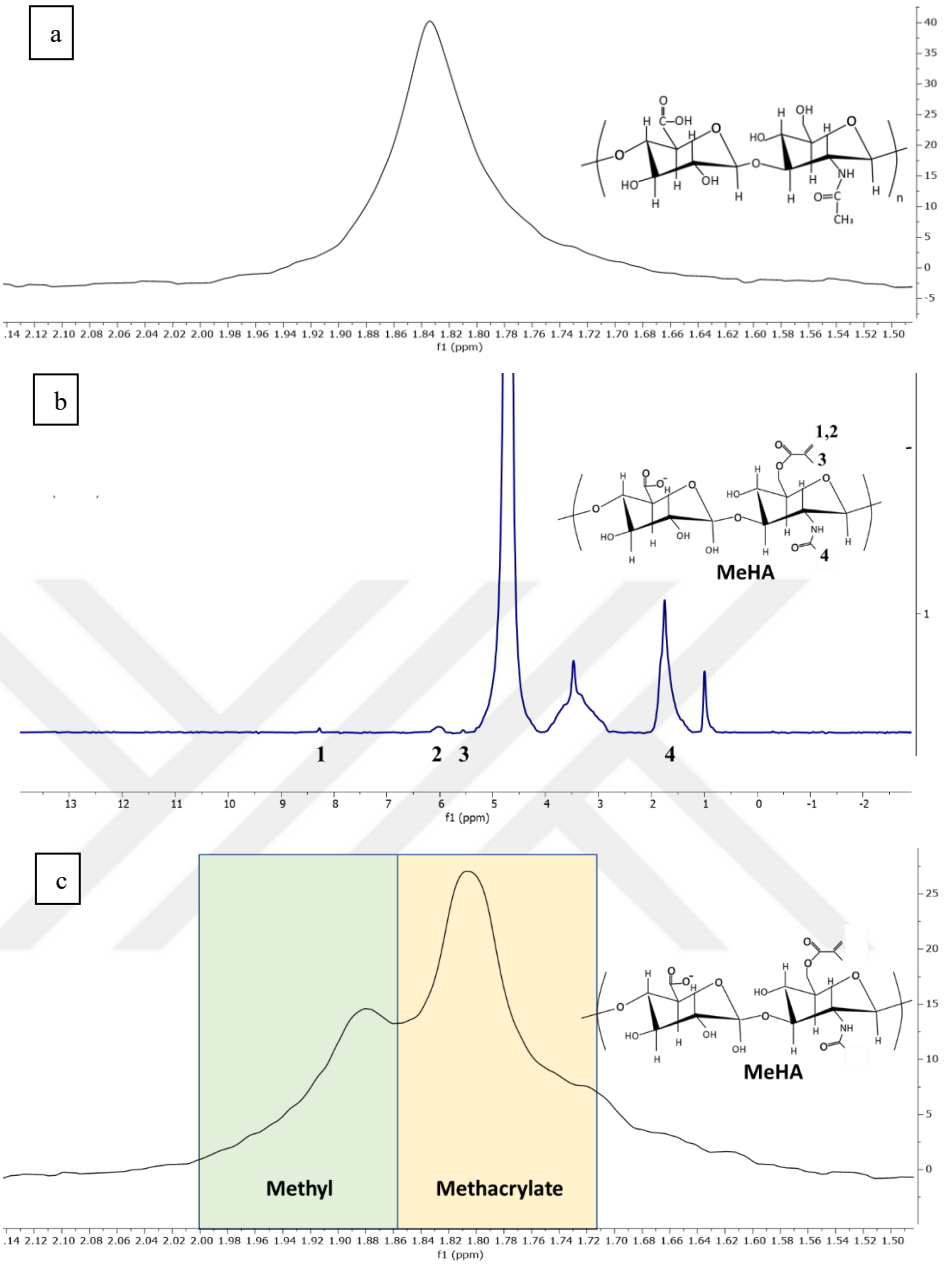

Figure 16. ^{1}H-NMR spectra of (a) hyaluronic acid and (b) MeHA (1% MeHA and 1% Irgacure in PBS), prepared in D_2O at room temperature. (c) The expanded region of MeHA NMR spectrum between 1.5 and 2 ppm was presented showing the methacrylation of hyaluronic acid.

4.1.2 The pH determination of MeHA solution

The pH value of 1% MeHA hydrogel solution in PBS before UV exposure, was controlled by Macherey-Nagel's pH test strips (Figure 17). According to strips colour, the pH of the MeHA hydrogel solution was determined as between pH 7-8.

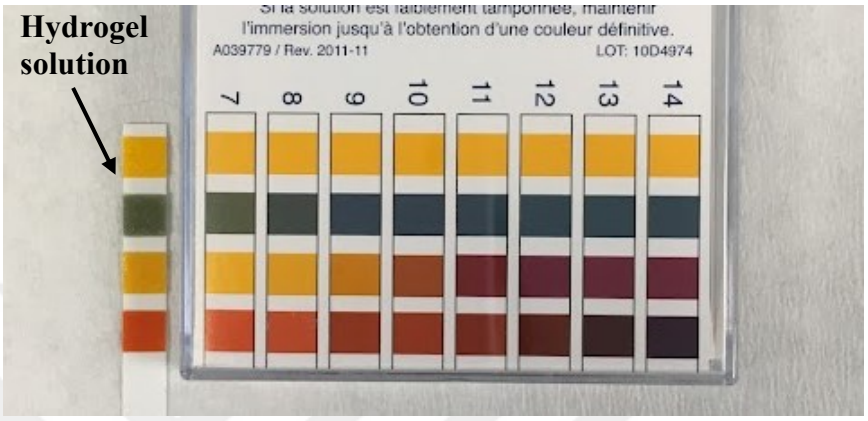

Figure 17. The pH value determination of MeHA solution (1% MeHA and 1% Irgacure in PBS).

4.1.3 Morphology analysis by SEM

The hydrogel scaffold was designed to mimic the stroma and epithelial layer of the cornea. Therefore, the hydrogel had to be porous to allow penetration of nutrients and to provide environment for cell growth within the scaffold. The morphology of MeHA hydrogels prepared in dH_2O and PBS were examined by SEM (Figure 18). Each hydrogel was crosslinked with UV at 365 nm for 13 min. The difference was only the solvent of the hydrogel solution. It was observed that both hydrogels had a porous morphology. However, the hydrogels prepared with PBS as a solvent of hydrogel solution was better than the one prepared in distilled water in terms of having the desired porosity. Therefore, in the further studies the hydrogels were prepared using hydrogel solution dissolved in PBS were used.

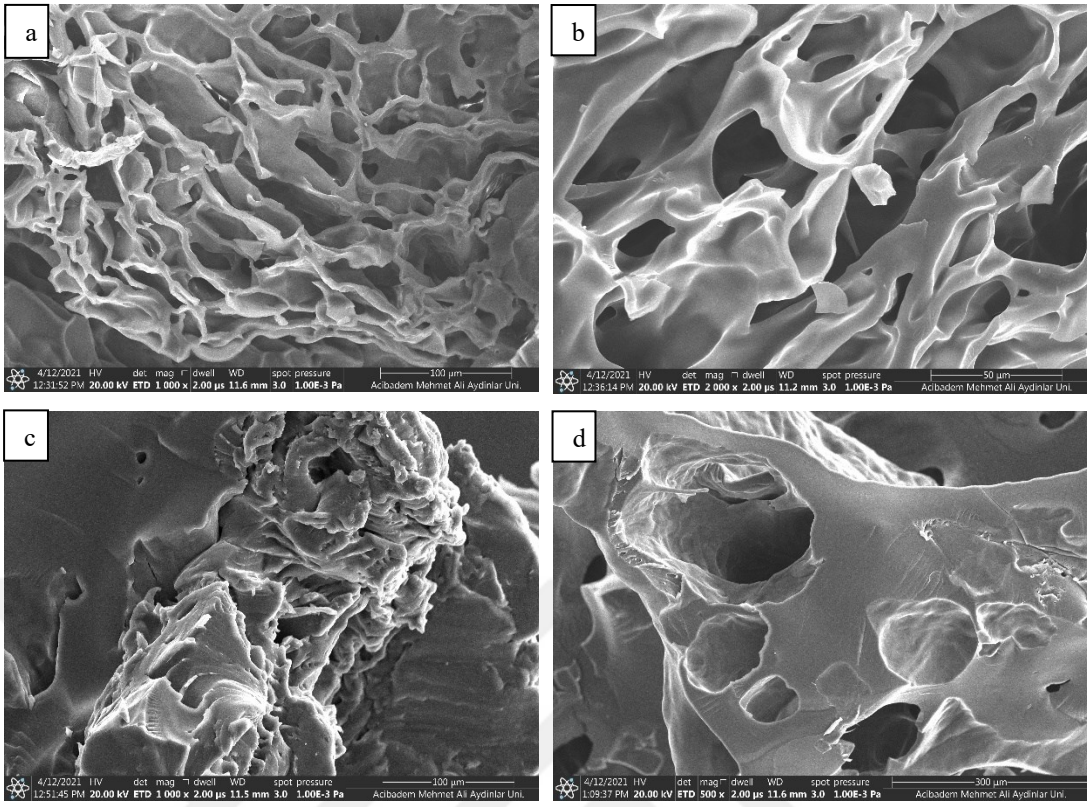

Figure 18. SEM images of MeHA hydrogels prepared with 1% MeHA and 0.5% Irgacure. MeHA hydrogels (a,b) prepared in PBS, and (c,d) in dH_2O. Magnifications: (a,c) X1000, (b) X2000, (d) X500; scale bars: (a,c,d) 100µm, (b) 50µm.

4.1.4 Swelling degree of hydrogels

Swelling test was applied to investigate the ability of hydrophilic hydrogels to swell in the liquid based on the increase in their original mass. The change in weight and swelling degree of hydrogels (n=8) over time were given in Table 7. It was observed that the hydrogels swelled significantly within 15 min, and the water content increased rapidly by 96%. It was observed that after 15 min the degree of swelling remained constant and did not change significantly.

Table 7. Weight and swelling degree of hydrogel samples over time.

Time	Weight (g)	Swelling degree (%)
0 min	0.0005	0
15 min	0.015 ± 0.005	96.38 ± 0.61
30 min	0.015 ± 0.006	96.50 ± 0.65
1 h	0.015 ± 0.004	96.49 ± 0.51
2 h	0.015 ± 0.004	96.56 ± 1.07
4 h	0.025 ± 0.005	97.87 ± 0.67
6 h	0.036 ± 0.012	98.47 ± 0.61
24 h	0.015 ± 0.003	96.46 ± 0.38
48 h	0.015 ± 0.005	96.55 ± 0.49

4.2 Characterization of Electrospun Fibrous Meshes

4.2.1 Morphology analysis by SEM

The Bowman's membrane is a cell-free structure that separate the epithelium from stroma of cornea layers and consisting of random collagen fibers (3). The electrospun random fibrous meshes were fabricated to enhance mechanical properties of the hybrid corneal substitute as well as to mimic Bowman's membrane. In electrospinning, firstly the isolated telocollagen type I was used as a polymer; however, it was not completely dissolved in acetic acid. It was observed that only the solvent reached to the collector, and the collagen was accumulated at the needle tip during electrospinning process. Afterwards, PCL and atelocollagen type were blended in the solvent mixture of formic acid and acetic acid to increase the solubility and to improve electrospinning. In that case, the fibrous mesh was deposited onto the collector, but the fibers were nonuniform and fused, and the mesh was ruptured during removal from the collector (Figure 19). Detachment of the mesh from the collector in intact form was not possible even coating with polyethylene oxide. The fibrous mesh obtained by electrospinning was expected to support the hydrogel scaffold and to provide mechanical support. In addition, the mesh should be transparent for the desired use in the corneal tissue. Therefore, it was

thought that it would be better to fabricate the electrospun meshes using synthetic polymers.

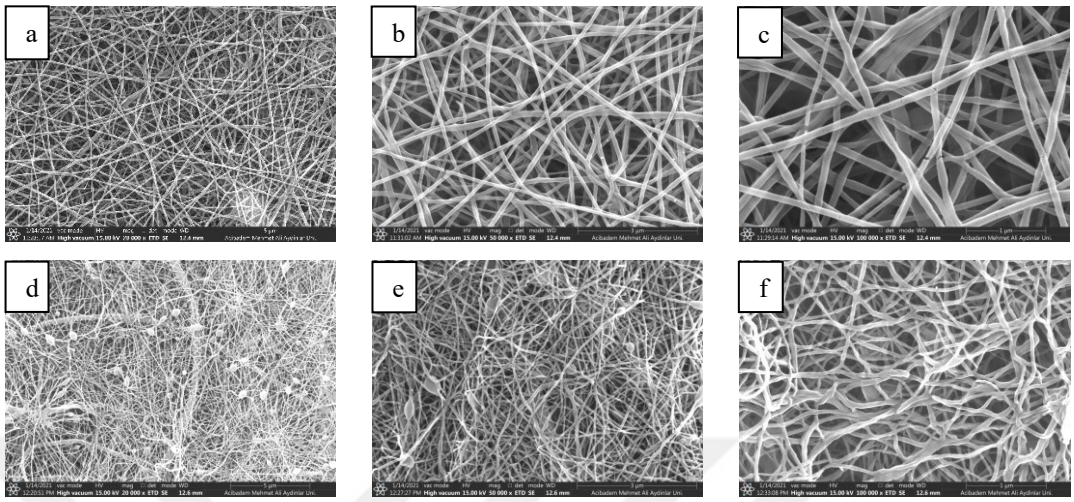

Figure 19. SEM images of PCL-collagen fibers prepared under two different conditions: (a-c) applied voltage 17 kV, distance 17 cm, flow rate 2.5 µL/min; (d-f) applied voltage 15 kV, distance 24 cm, flow rate 1.5 µL/min. Magnifications: (a,d) X20000, (b,e) X50000, (c,f) X100000; scale bars: (a,d) 5 µm, (b,e) 3 µm, (c,f) 1 µm.

The transparent feature sought in the corneal tissue was important. For this reason, it was important to choose a synthetic polymer that could have the desired transparency, and thus it was decided to continue with the blend of tough PLA and PLGA. Firstly, 5% (w/v) of PLA-PLGA (1:1, w:w) polymer solution was prepared in chloroform. However, fibrous mesh could not be collected on the metal plate, only solvent reached the collector. Therefore, it was decided to increase the viscosity and concentration of the polymer solution. Therefore, electrospinning optimization was continued using 20% (w/v) of PLA-PLGA (2:1, w:w) polymer solution under processing conditions; applied voltage 11.5 kV, distance between two poles 15 cm, flow rate 0.1-0.8 mL/h (Figure 20 and 21). It was observed that curly and nonuniform fibers were formed when 0.1 mL/h and 0.4 mL/h flow rates were used. The results showed that the intact fibrous mesh with uniform fibers were fabricated by electrospinning under optimized parameters: applied voltage 11.5 kV, distance between two poles 15 cm, flow rate 0.8 mL/h. In the further studies, the electrospun fibrous meshes produced under optimized conditions were used.

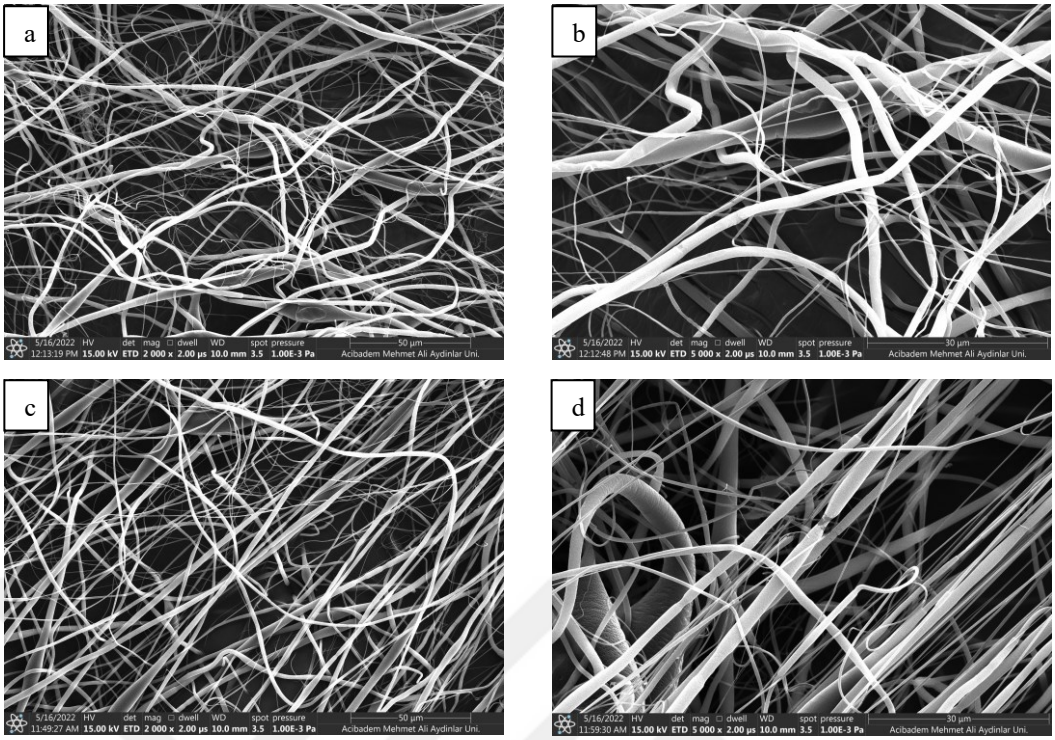

Figure 20. SEM images of PLA-PLGA fibers prepared under two different conditions: (a-b) applied potential 11.5kV, distance 15 cm, flow rate 0.1 mL/h; (c-d) applied potential 11.5 kV, distance 15 cm, flow rate 0.4 mL/h. Magnifications: (a,b) X2000, (c,d) X5000; scale bars: (a,b) 50 µm, (b,c) 30 µm.

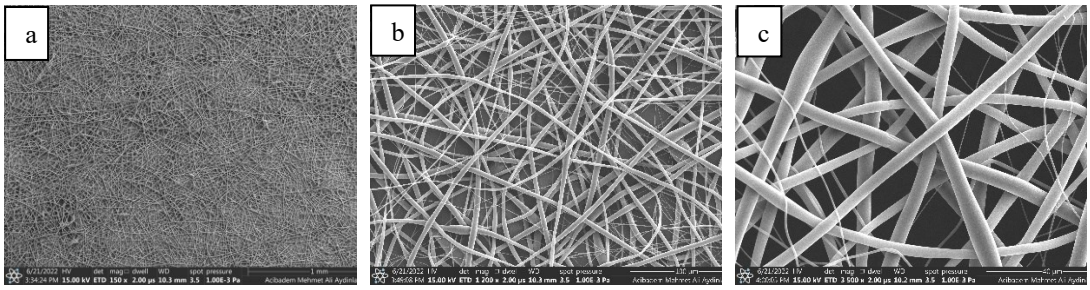

Figure 21. SEM images of PLA-PLGA fibers prepared with optimized parameters: applied potential 11.5 kV, distance15 cm, flow rate 0.8 mL/h. Magnifications: (a) X150, (b) X1200, (c) X3500; scale bars: (a) 1 mm, (b) 100 µm, (c) 40 µm.

4.2.2 Determination of fiber diameter and orientation

The fiber diameter and fiber orientation were quantified with Fibra Quant 1.3 image processing and analysis software. The fiber orientation was based on the

deviation angle of the fibers according to reference direction. These analysis was conducted on the SEM images of the electrospun fibrous mesh that was fabricated using 20% (w/v) of PLA-PLGA (2:1, w:w) polymer solution under optimized conditions: applied voltage 11.5 kV, distance between two poles 15 cm, flow rate 0.8 mL/h as indicated in Section 3.2.1.2. It was observed that the fiber diameter of the PLA-PLGA random fibrous meshes were varied in the range of 0.1 µm to 2 µm in general; however, most of the fibers were in 0.25-1 µm diameter (Figure 22a). In addition, it was seen that most of the fibers deviated at different angles, as it should be in the random fibrous mesh (Figure 22b).

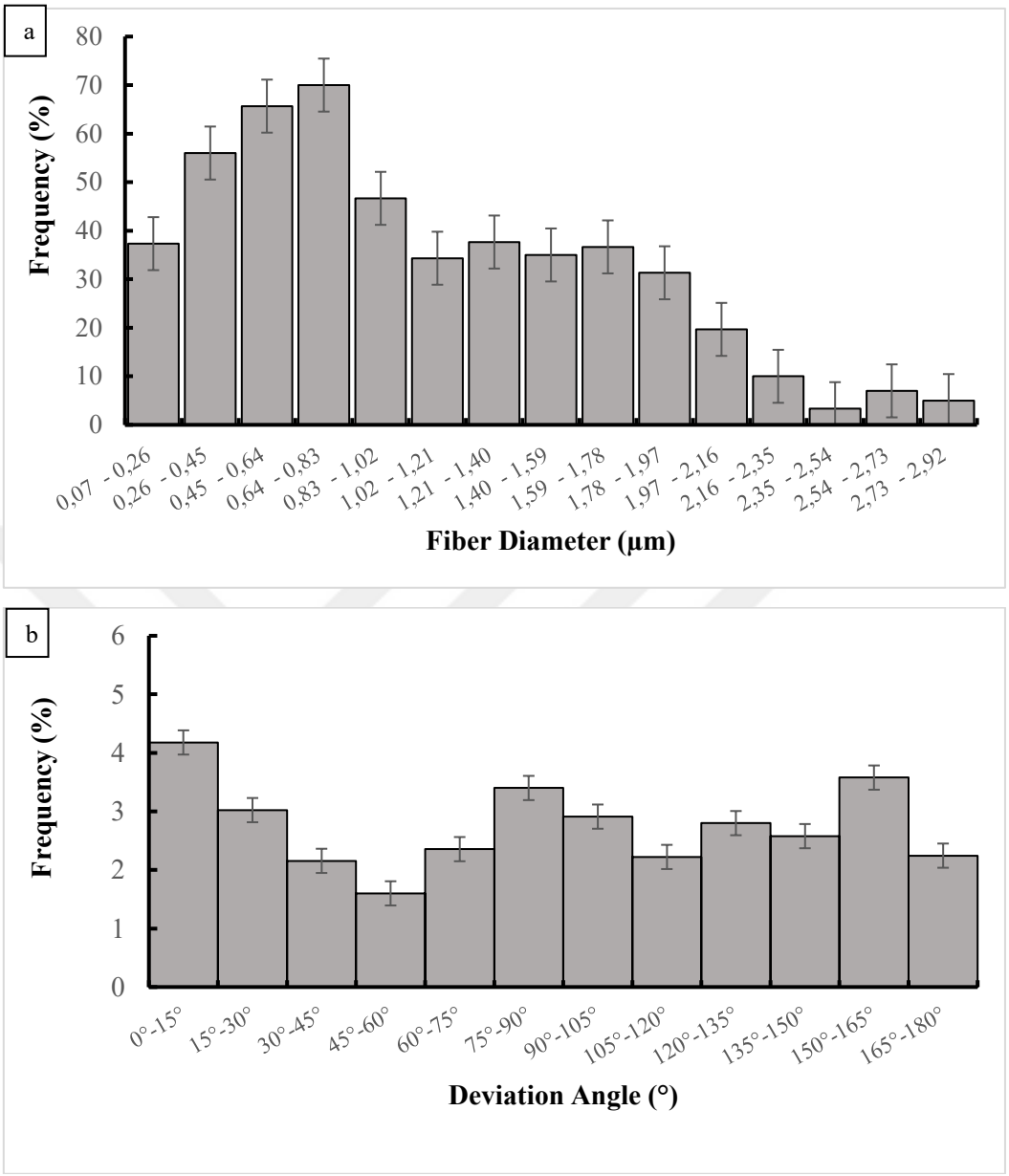

Figure 22. The distribution of (a) fiber diameter and (b) fiber orientation of the electrospun random fibrous mesh fabricated under optimized conditions.

4.2.3 Mechanical analysis

The Bowman's layer is believed to be the stabilizing element of corneal curvature due to its putative mechanical stiffness. Therefore, tensile test was performed to measure the resistance of the electrospun fibrous meshes to a gradually increasing applied force. The mechanical test studies were conducted on the electrospun fibrous

mesh (n=4) that was fabricated using 20% (w/v) of PLA-PLGA (2:1, w:w) polymer solution under optimized conditions: applied voltage 11.5 kV, distance between two poles 15 cm, flow rate 0.8 mL/h as indicated in Section 3.2.1.2. The stress-strain curves were obtained for all samples, and the slope of the stress-strain curve in elastic region refers to Young's Modulus was calculated for each sample. The average Young's Modulus was calculated as 214.08+41.77 MPa.

4.3 Characterization of the Hybrid Scaffolds

4.3.1 Morphology analysis with SEM

The cell-free, three layered scaffold consists of thin MeHA hydrogel, electrospun random fibrous mesh, and thick MeHA hydrogel layer was constructed as described in Section 3.2.1.6 and the morphology of the hybrid scaffold was examined with SEM. The results showed that three layers could be built on top of each other successfully (Figure 23a). It was seen that the fibrous mesh was embedded between thin and thick MeHA hydrogels. In addition, it was observed that that the porosity obtained when the hydrogel is made alone could also be obtained when the hybrid scaffold was formed.

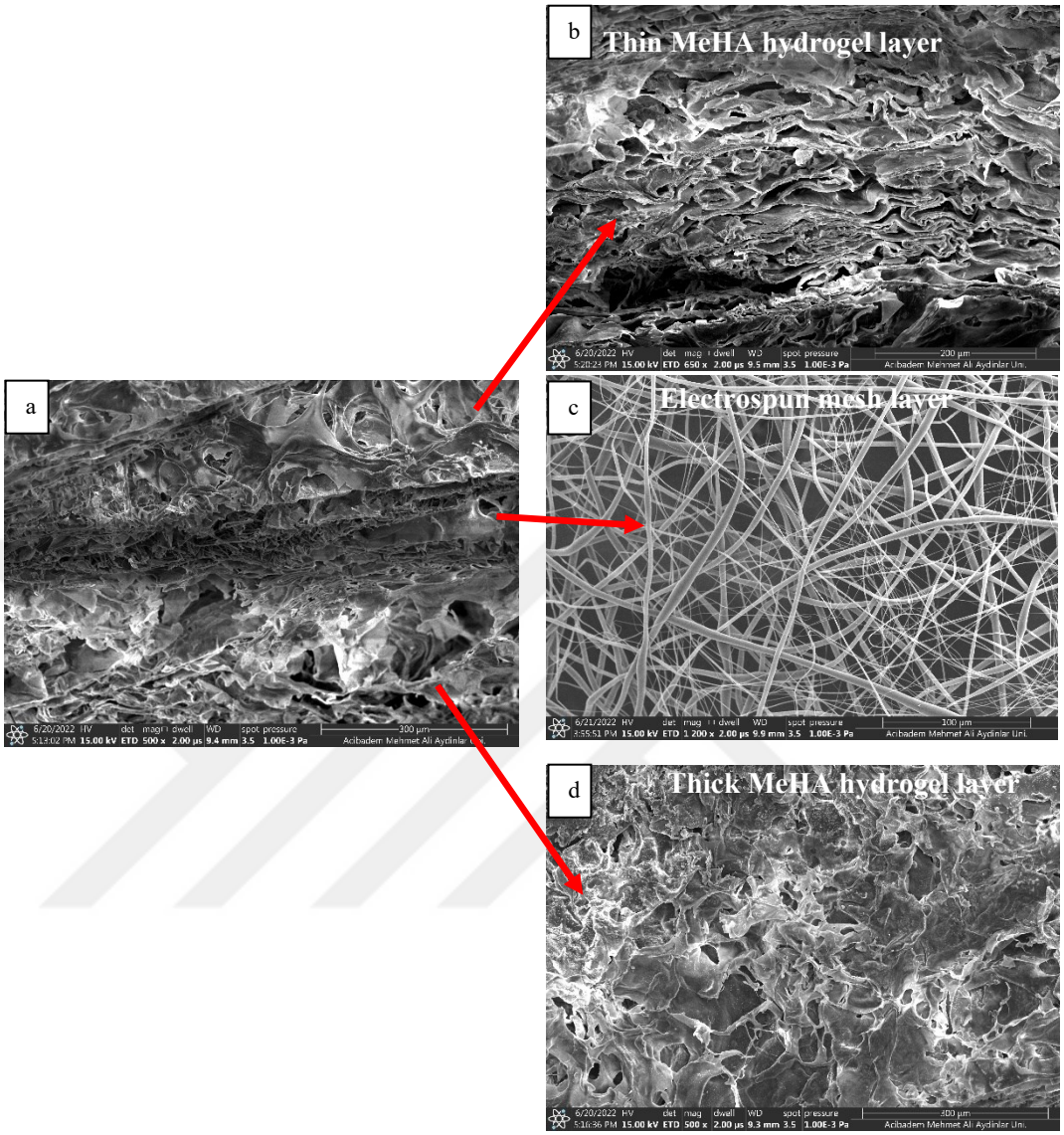

Figure 23. SEM images of the multilayered cell-free corneal scaffold. (a) Longitudinal section of the scaffold, (b) thin MeHA hydrogel layer, (c) random fibrous mesh, (d) thick MeHA hydrogel layer. Magnifications: (a,d) X500, (b) X650, (c) X1200; Scale bars: (a,d) 300 µm, (b) 200 µm, (c) 100 µm.

4.3.2 Mechanical analysis

Mechanical test studies were performed for the final constructs (n=5) using 1% (w/v) cell-free MeHA in PBS under optimized conditions, produced as mentioned in Section 3.2.1.6. Stress-strain curves were obtained for all samples, and the slope of the

stress-strain curve in the elastic region represents the Young's Modulus for each sample. The mean Young's Modulus was calculated as 15.048 + 6.279 kPa.

4.3.3 Transparency of the hybrid scaffolds

Transparency analysis of the final constructs formed with cell-free MeHA (1% MeHA and 1% Irgacure in PBS) hydrogels including PLA-PLGA fibrous mesh was examined by stereomicroscopy (Figure 24). It was observed that the letters could be read over PLA-PLGA fibrous meshes, and this indicated their transparency in terms of light transmission. The hydrogels were also transparent, the letter were clearly seen over the gels. It was observed that in the final hybrid scaffolds, the combination of two layers of hydrogel and fibrous mesh, the transparency was reduced; however, the letters were still readable. This slight decrease in transparency might be due to an increase in the thickness of the final hybrid scaffold.

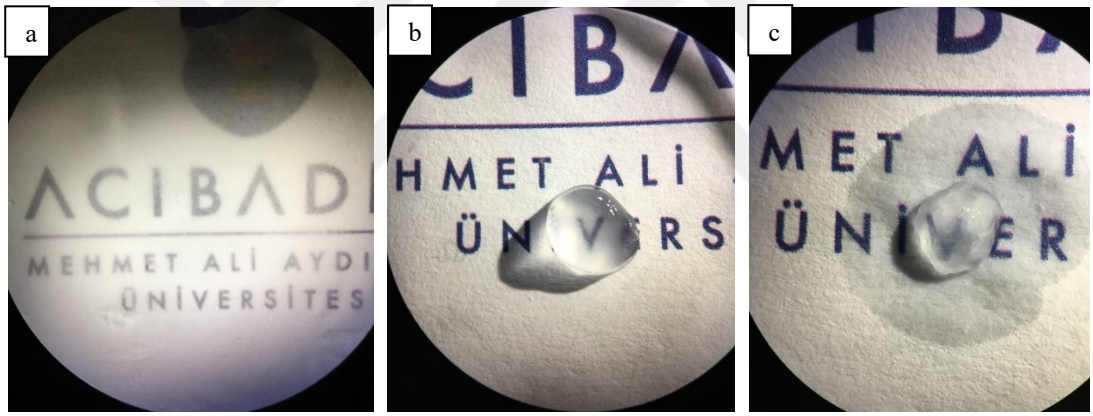

Figure 24**.** Stereomicroscope images taken to evaluate transparency of the layers of the scaffold and the final hybrid scaffold. **(a) PLA-PLGA fibrous mesh, (b) MeHA hydrogel, (c) the final hybrid construct composed of thin layer MeHA hydrogel, fibrous mesh and thick layer MeHA hydrogel. Magnifications: (a) X0.63, (b) X1, (c) X1.25**

4.4 *In Vitro* Studies

4.4.1 Characterization of the isolated WJ MSCs

4.4.1.1 Flow cytometry analysis

In order to confirm that the isolated WJ MSCs (P3) were mesenchymal stem cells, the specific cell surface antigens of the cells were analysed by flow cytometry. The percentage of positivity of antigen expressing cells was calculated considering the isotype control (Figure 25). The surface antigen expressions of the isolated WJ MSCs were given in Table 8. WJ MSCs were strongly positive for the MSC markers CD105, CD90, CD73, CD44 as well as for HLA-ABC (Figure 25 and Table 8). The expression of hematopoietic markers like CD34 and CD45 were negative, as expected. In addition, WJ MSCs were negative for the immunogenic antigen HLA-DR. This means that they would be less prone to immune rejection in allogeneic stem cell transplants. The flow cytometry results showed that isolated WJ MSCs exhibited the characteristic surface antigen expression of MSCs, and the isolated cell culture was pure, free of hematopoietic cells.

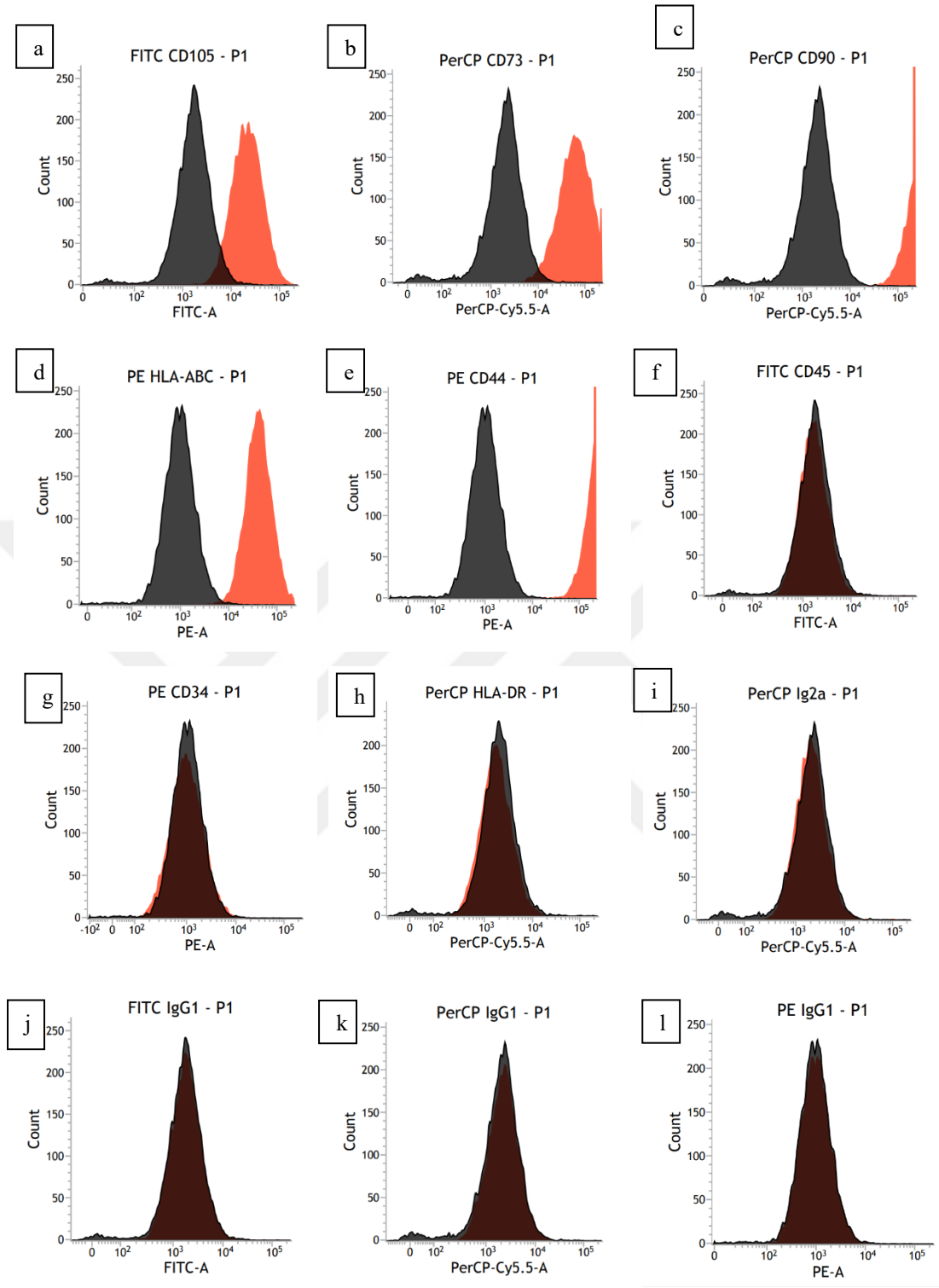

Figure 25. Flow cytometry histograms for different cell surface antigen expression of WJ MSCs isolated from human umbilical cord matrix and histograms of isotype controls.

Table 8. The expression of surface antigens of WJ MSCs (P3) based on isotypes.

Surface Antigen	WJ MSC%*
CD105	97.08 ± 1.11
CD73	96.99 ± 2.70
CD90	99.91 ± 0.04
CD44	99.88 ± 0.13
HLA-ABC	99.26 ± 0.92
CD45	1.18 ± 1.58
CD34	0.21 ± 0.25
HLA-DR	0.01 ± 0.02

*Percentage of the positive cells (Intersection of isotype control and positive sample considered for calculation of absolute positives)

4.4.1.2 Osteogenic differentiation of WJ MSCs

Osteogenic differentiation is one of the characteristic features of mesenchymal stem cells. For that reason, WJ MSCs (P3) were differentiated into osteogenic cells and their differentiation was assessed on 7^{th} and 14^{th} days by ALP activity, which is secreted by osteoblast cells to provide calcification and bone formation. In this study, the undifferentiated WJMSCs were used as controls. The results showed that on day 7 ALP activity of the differentiated cells were similar to that of undifferentiated cells; however, WJ MSCs under osteogenic differentiation exhibited significantly higher ALP activity on day 14 compared to the undifferentiated cells ($p < 0.005$) (Figure 26). Accordingly, the isolated WJ MSCs could differentiate into osteogenic cells after 7 days of osteogenic induction.

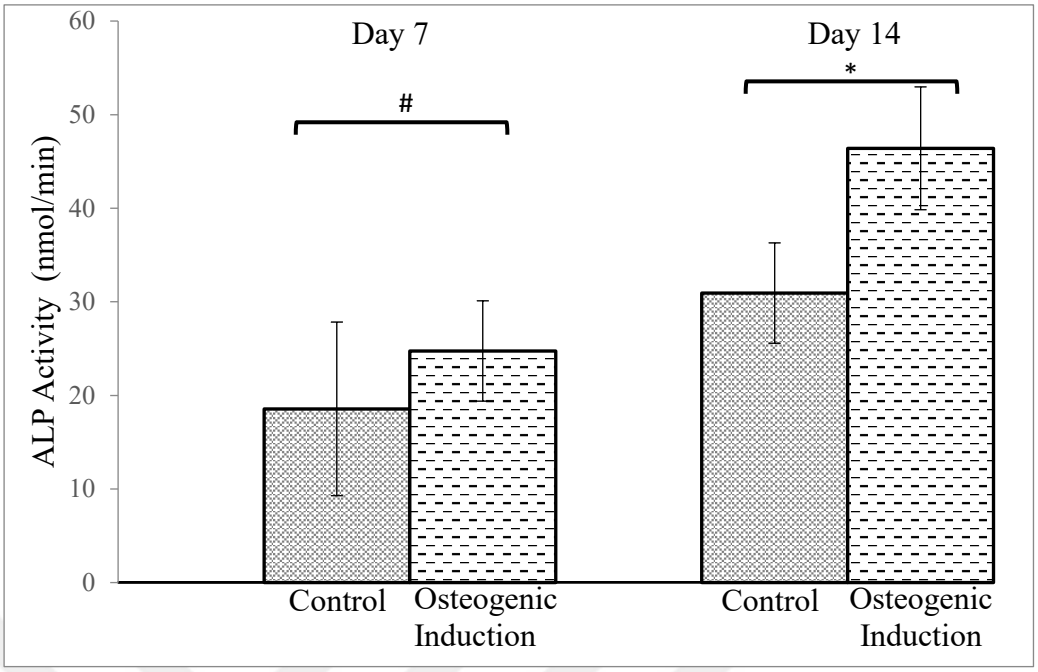

Figure 26. ALP activity of the undifferentiated WJ MSCs (control) and the differentiated cells after 7 and 14 days of osteogenic induction. (#: $p>0.05$, * $p<0.005$)

4.4.1.3 Chondrogenic differentiation of WJ MSCs

Beside osteogenic differentiation, MSCs have also a tendency to differentiate into chondrogenic cells. Therefore, WJ MSCs (P3) were differentiated into chondrogenic cells for 14 and 21 days and this differentiation was evaluated by Alcian blue staining (Figure 27). WJ MSCs were cultured in the absence of stimulants in an undifferentiated state was used as control. According to the results, WJ MSCs subjected to 21 days of chondrogenic induction showed a shift in cell morphological characteristics from a primarily slender, elongated morphology to a relatively spherical cell phenotype. In addition, on both 14 and 21 days WJ MSCs induced with chondrogenic stimulants exhibited intense blue colour after Alcian Blue staining compared to the undifferentiated cells. It showed that chondrogenic induction increased the amount of glycosaminoglycans and proteoglycans, which was expected in chondrogenic differentiation.

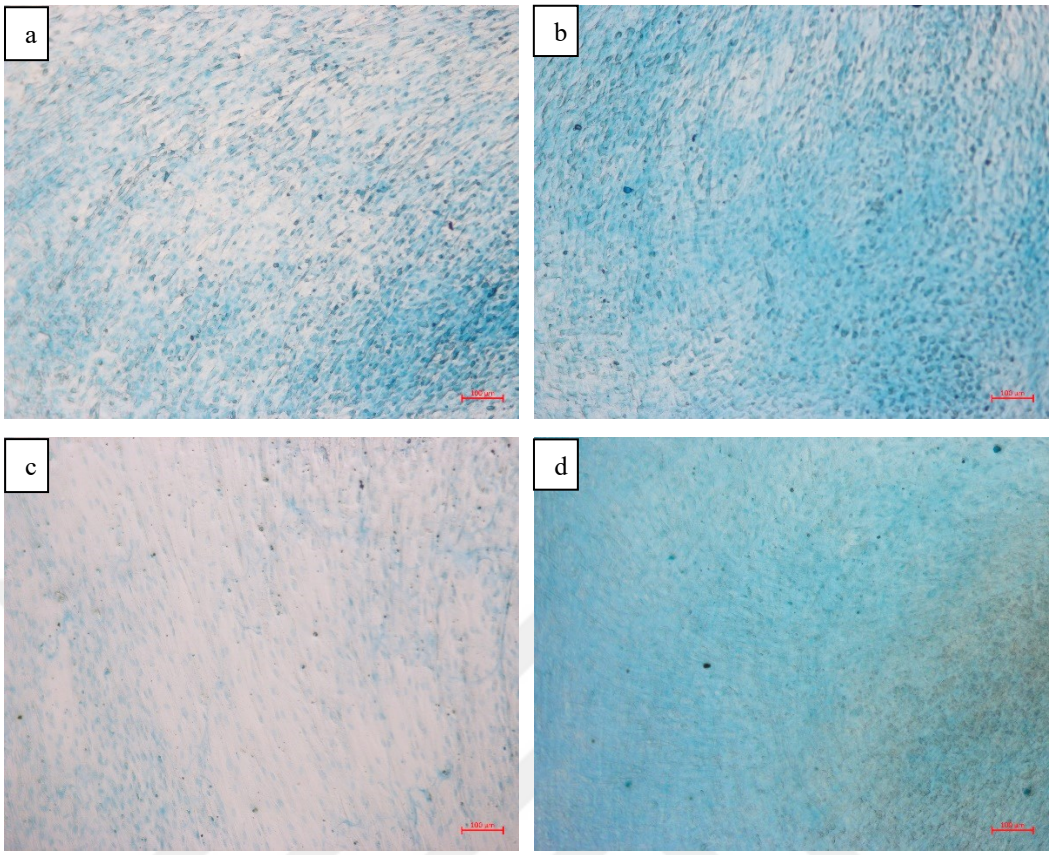

Figure 27. Light microscope images of WJ MSCs after Alcian blue staining; (a) control, and (b) cells subjected to chondrogenic induction for 14 days; (c) control, and (d) cells subjected to chondrogenic induction for 21 days. Scale bars: 100 µm.

4.4.1.4 Growth kinetics of the isolated WJ MSCs

The growth profile of WJ MSCs were analysed by plotting increase in cell number over time (Figure 28). The number of cells was determined by WST-1 assay using the calibration curve (Appendix 1- Figure 40). The growth profile indicated that MSCs reached growth saturation after about 150 h of culture. The doubling time of the used WJ MSCs was determined as 19.6 h from the linear range of the growth curve.

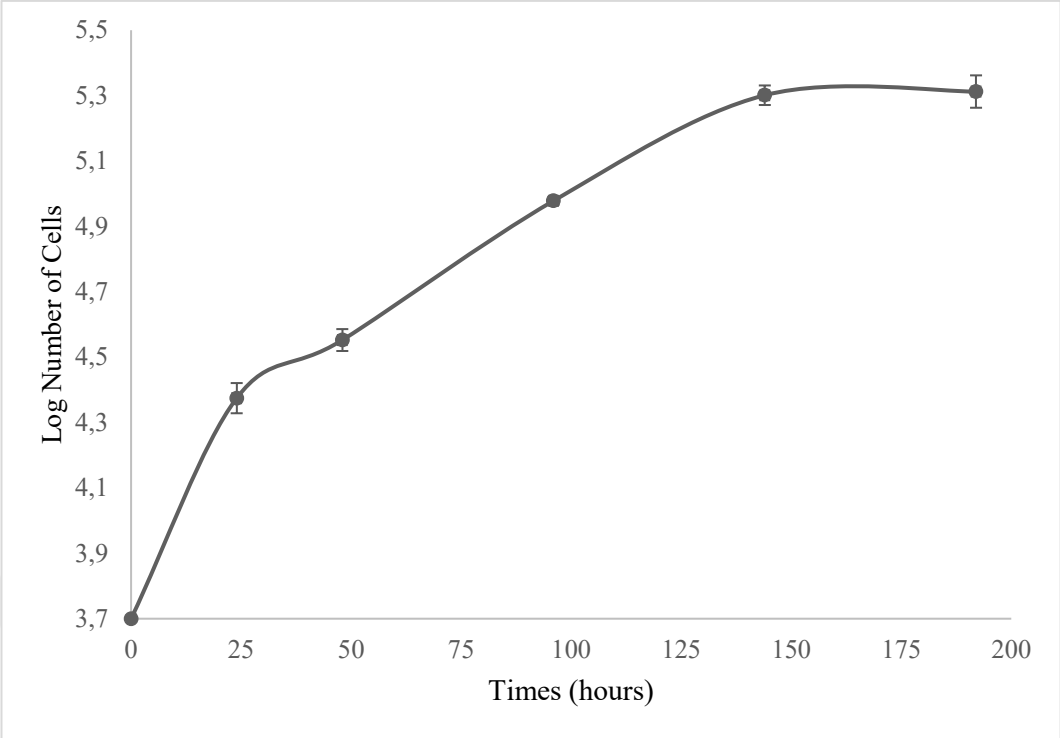

Figure 28. Growth profile of the isolated WJ MSCs.

4.4.2 Differentiation of WJ MSCs into keratocyte cells

4.4.2.1 Protein expression analysis of MSCs by immunostaining upon keratocyte induction

MSCs have the potential to differentiate into mesodermal lineages such as osteoblasts, chondrocytes, and adipocytes under favourable conditions. In addition, there were studies shown that MSCs can differentiate into keratocyte lineages (90, 162). The undifferentiated WJ MSCs are generally elongated, and bipolar-appearing fibroblast morphology cells rigidly attached to a culture dish. Keratocytes are cells with elongated flat cylindrical fibroblast morphology. Keratocytes are rich in specific proteoglycans such as lumican (LUM) (163). Aldehyde dehydrogenase 1A1 (ALDH1A1), defined as corneal crystallin, is ubiquitously expressed in many tissues (164).

In this thesis study, WJ MSCs were differentiated into keratocytes as explained in Section 3.2.3.2 to be used in corneal tissue substitute. The differentiation of WJ MSCs

into keratocytes were evaluated by immunostaining for the expression of ALDH1A1 and LUM at protein level, compared to the undifferentiated WJ MSCs (Figure 29-32). It was observed that WJ MSCs exhibited characteristic keratocyte morphology after 7 and 14 days of keratocyte induction (Figure 29-32). It was seen that WJ MSCs even in the undifferentiated state expressed ALDH1A1 and LUM keratocyte markers, but these expressions were at a very low level. It was observed that on 7th and 14th days of keratocyte induction the differentiated cells significantly expressed ALDH1A1 and LUM markers. There was no meaningful difference in the expression of the differentiated cells on the induction day 7 and 14. However, there was a decrease in cell number on 14 days induction samples that might be due to differentiation. Therefore, it was decided to do keratocyte induction for 7 days in the further studies.

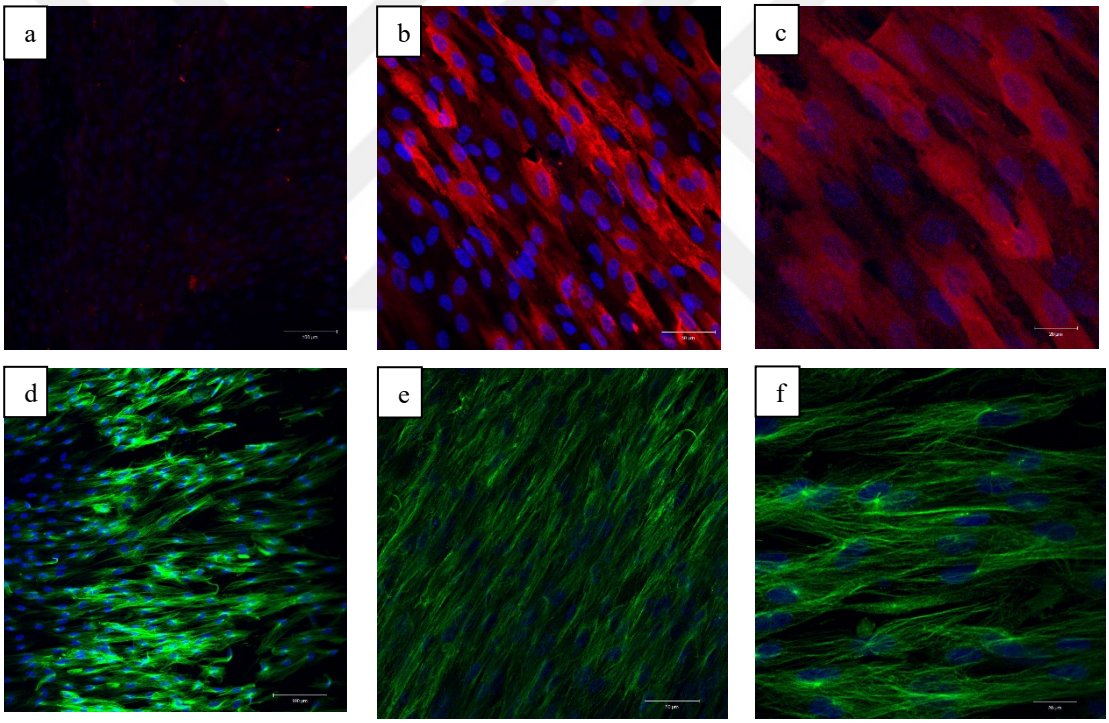

Figure 29. Immunostaining analysis of (a-c) ALDH1A1 (red) and (d-f) LUM (green) expressions of the undifferentiated WJ MSCs at the end of 7 day culture. Magnifications: (a,d) X10, (b,e) X20, (c,f) X40; scale bars: (a,d) 100 µm, (b,e) 50 µm, (c,f) 20 µm.

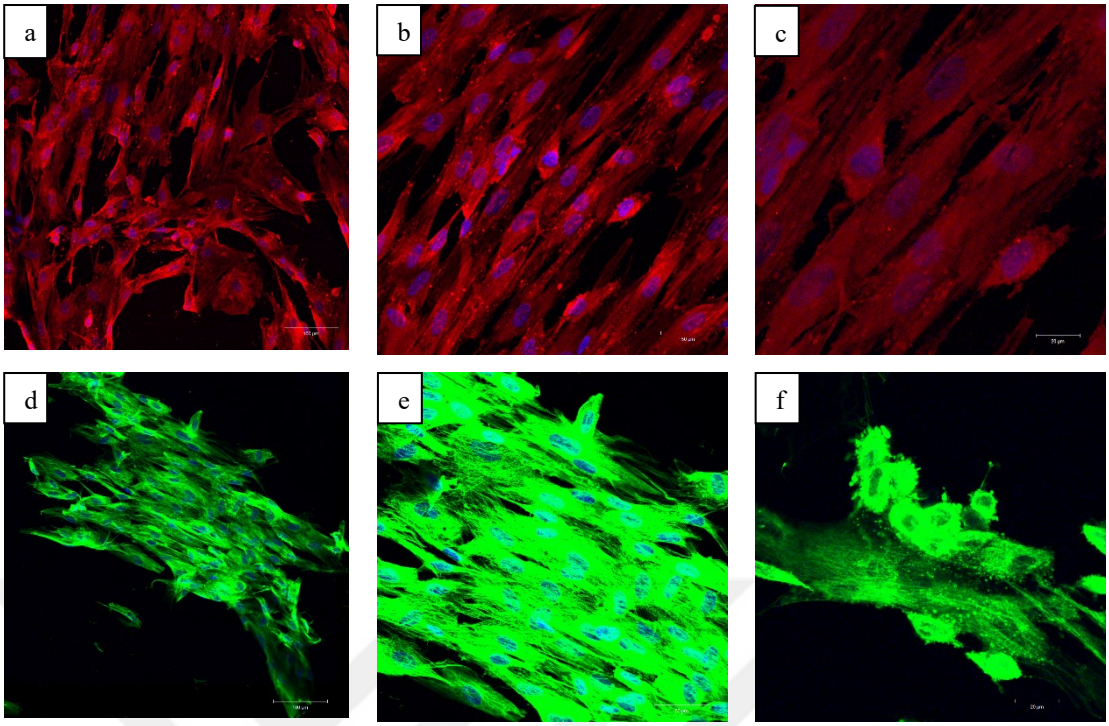

Figure 30. Immunostaining analysis of (a-c) ALDH1A1 (red) and (d-f) LUM (green) expressions of the keratocyte differentiated WJ MSCs at the end of 7 day induction. Magnifications: (a,d) X10, (b,e) X20, (c,f) X40; scale bars: (a,d) 100 µm, (b,e) 50 µm, (c,f) 20 µm.

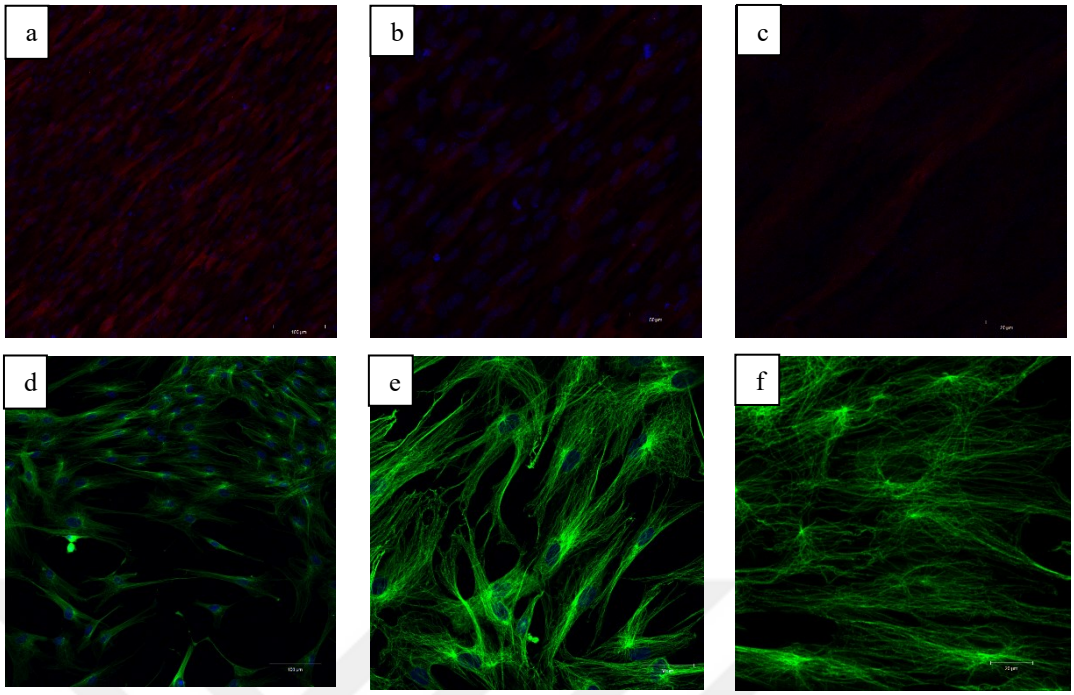

Figure 31. Immunostaining analysis of (a-c) ALDH1A1 (red) and (d-f) LUM (green) expressions of the undifferentiated WJ MSCs at the end of 14 day culture. Magnifications: (a,d) X10, (b,e) X20, (c,f) X40; scale bars: (a,d) 100 µm, (b,e) 50 µm, (c,f) 20 µm.

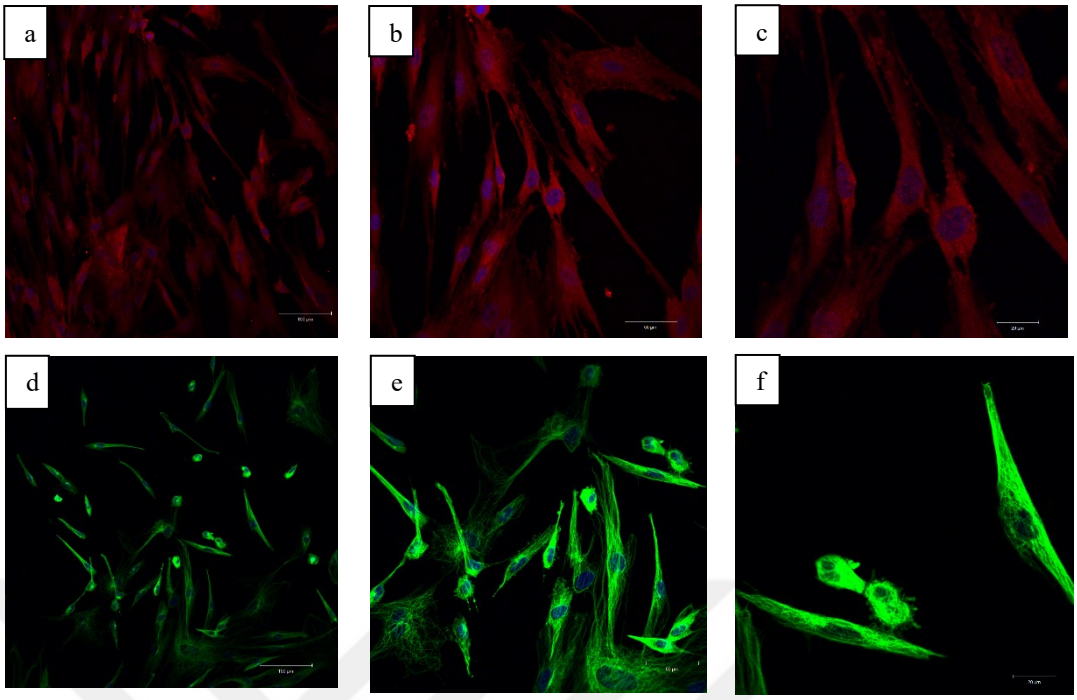

Figure 32. Immunostaining analysis of (a-c) ALDH1A1 (red) and (d-f) LUM (green) expressions of the keratocyte differentiated WJ MSCs at the end of 14 day induction. Magnifications: (a,d) X10, (b,e) X20, (c,f) X40; scale bars: (a,d) 100 µm, (b,e) 50 µm, (c,f) 20 µm.

4.4.3 Cell behaviour in the corneal tissue substitute

A multi-layered cornea tissue equivalent was constructed by combining cell-free thin MeHA hydrogel, PLA-PLGA electrospun fibrous mesh and cells loaded thick MeHA hydrogel to mimic three layers of cornea as epithelium, Bowman layer and stroma, respectively. WJ MSCs were loaded into the thick MeHA hydrogel during formation of the construct, and then these stem cells were induced to differentiate into keratocytes within the 3D hybrid construct. After 1 day of culture without induction and after 7 days of keratocyte induction, the cell viability, proliferation, morphology, and expression of keratocyte markers was investigated.

4.4.3.1 Viability of the cells in the hydrogels

The cell viability within the hybrid hydrogels was examined on day 1 of culture without induction and on 7th of keratocyte induction, by the application of Live-Dead Assay. LSCM images showed that the viable cell seen in green color covered the hydrogel as around 80% and 60% on days 1 and 7, respectively (Figure 34 and 35). In order to form the used MeHA hydrogel, the cell seeded hydrogel scaffold was subjected to photo crosslinking. Therefore, 20% reduction in cell viability could be explained by photo crosslinking and use of PBS during hydrogel formation. However, that much decrease was acceptable considering the literature information that UV exposure at 365 nm was found to be safe in terms of acceptable cell damage (165). In addition, it was observed that WJ MSCs were homogeneously distributed throughout the thick MeHA hydrogel. The increase in red color shown in dead cells also indicated the decrease in cell viability on the 7th day of keratocyte induction. The decrease in cell viability decreases upon differentiation was also seen in the literature (162, 166). The cell-free scaffold was also tested with Live/Dead assay to check autofluorescence of the scaffold and it was shown that there was no signal from scaffolds (Figure 33).

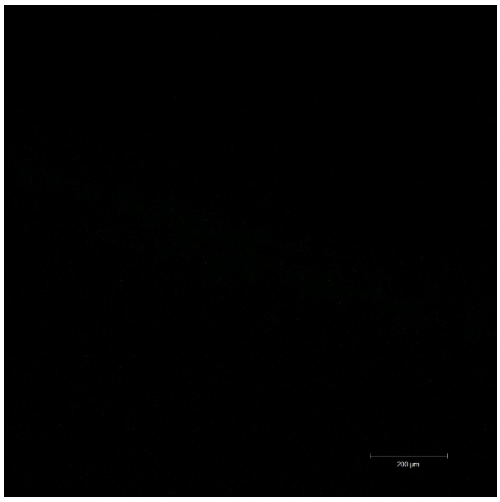

Figure 33. LSCM image of cell-free scaffold after Live-Dead assay application at the end of 7day induction. Magnification X5, scale bar: 200 μm.

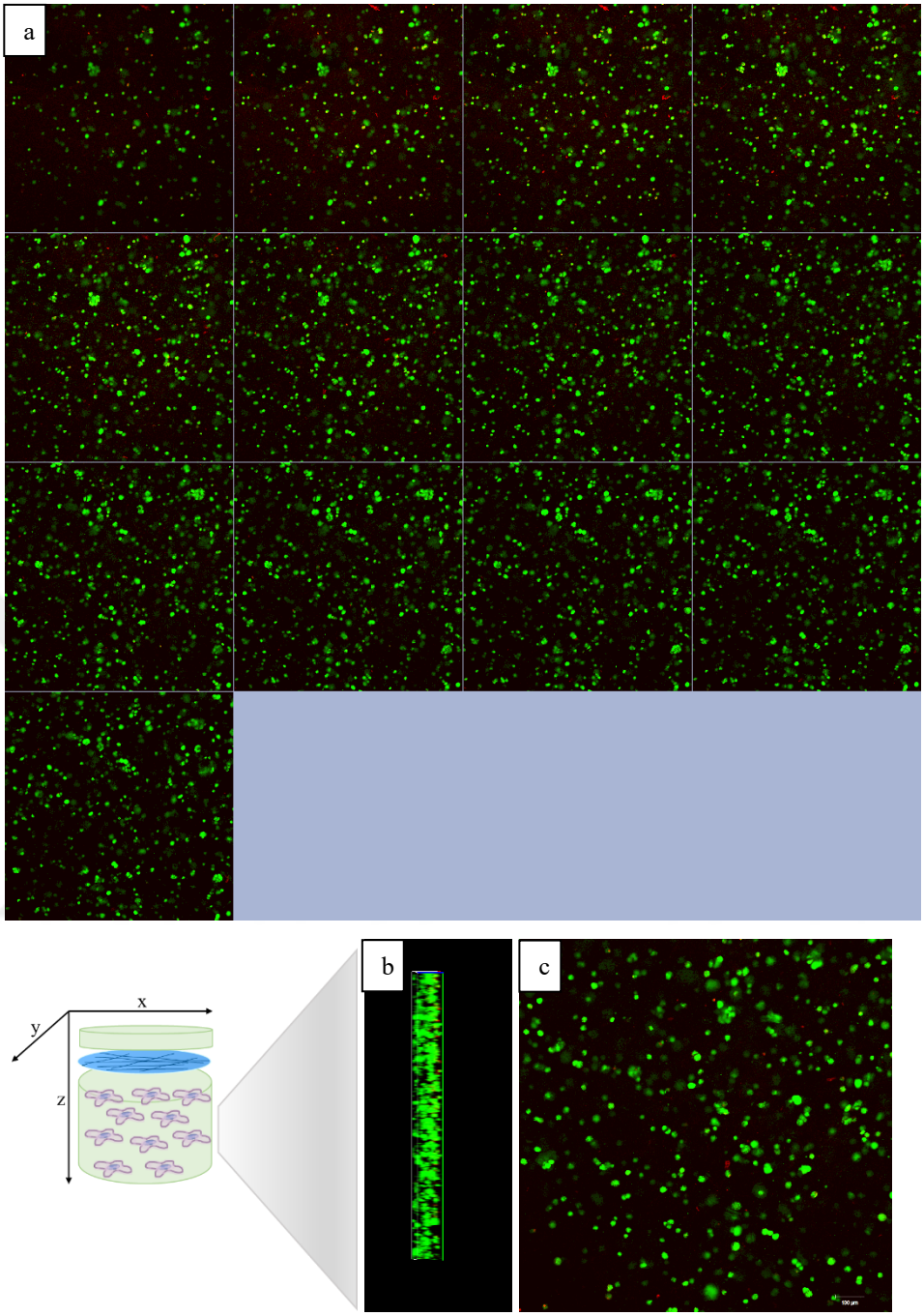

Figure 34. LSCM image of WJ MSCs within the hybrid scaffold after Live-Dead assay application at the end of 1 day culture. The alive cells stained with calcein AM (green) and the dead cells stained with ethidium homodimer-1 (red). (a) The z-stack images (total thickness of the taken image: 112 µm), (b) image taken from longitudinal section (c) 2D image at a certain focal plane. (a-c) Magnification X10, scale bar: 100 µm.

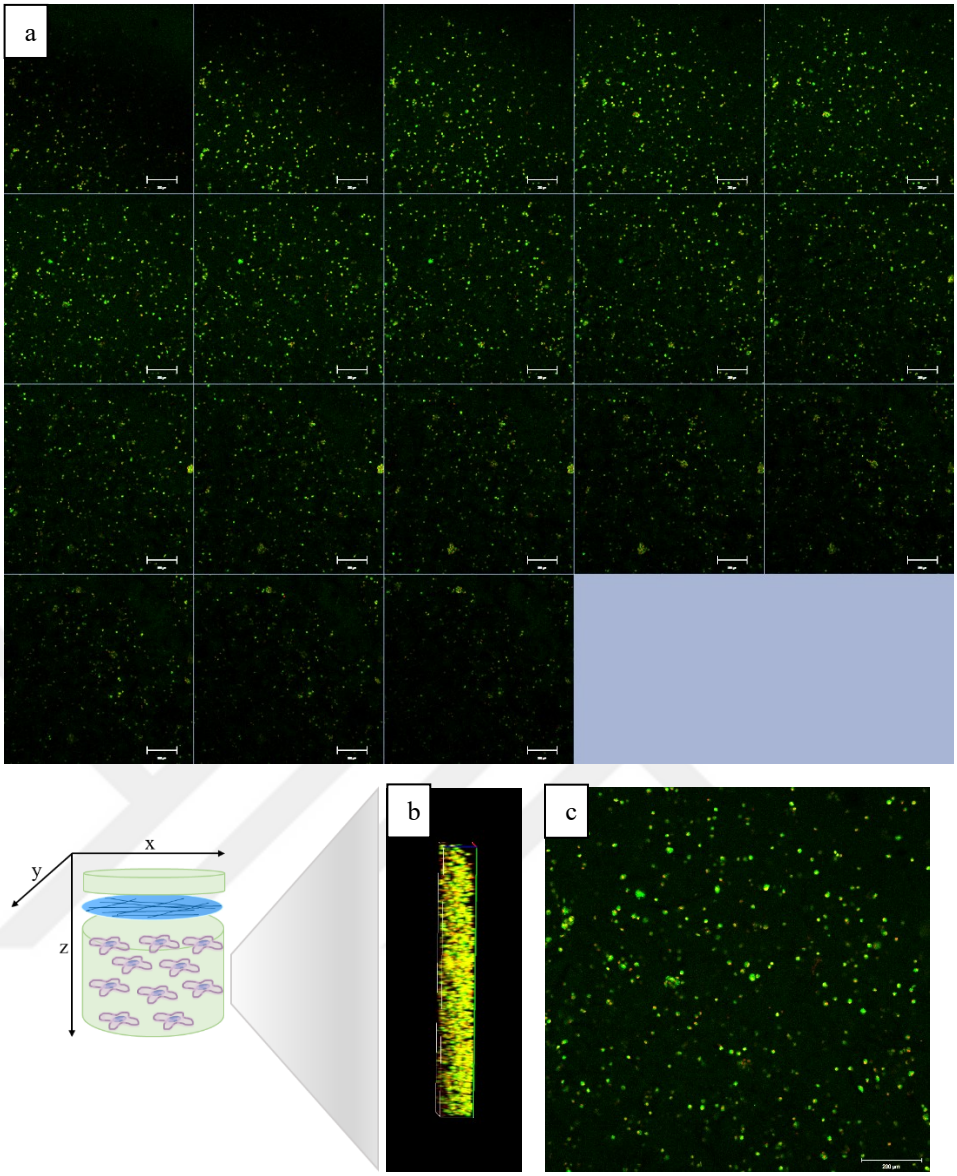

Figure 35. Live-Dead analysis of WJ MSCs in the scaffold at the end of 7-day induction. The cells stained with calcein AM (green) for live and ethidium homodimer-1 (red) for dead cells. (a) The z-stack images (total thickness of the taken image: 167 µm), (b) image taken from longitudinal section (c) 2D image at a certain focal plane. (a-b) Magnification X5, scale bar: 200 µm.

4.4.3.2 Cell proliferation within the hybrid scaffolds

The proliferation of WJ MSCs seeded on the thick hydrogel layer of scaffold were investigated by MTS assay on day 1 of culture without induction and on 7th day of keratocyte induction. WJ MSCs were seeded into the thick hydrogel layer of the

scaffold at a density of $4x10^5$ cells/scaffold. Considering the seeding density, the number of cells on day 1 was slightly low (Figure 36). This reduction in cell number supports the results in Section 4.4.3.1 and was thought to be due to photocrosslinking and the use of PBS during hydrogel formation as mentioned there. However, it was observed that UV exposure did not have much negative effect on cell viability. According to MTS results, there was no sharp, significant decrease in cell number upon keratocyte induction for 7 days ($p>0.05$). The cell number was almost same on day 1 of culture and day 7 of induction. However, it was observed that the proliferation rate was very low, almost no increase in cell number from day 1 to day 7. Since the differentiation was inversely proportional with proliferation this result could be understandable.

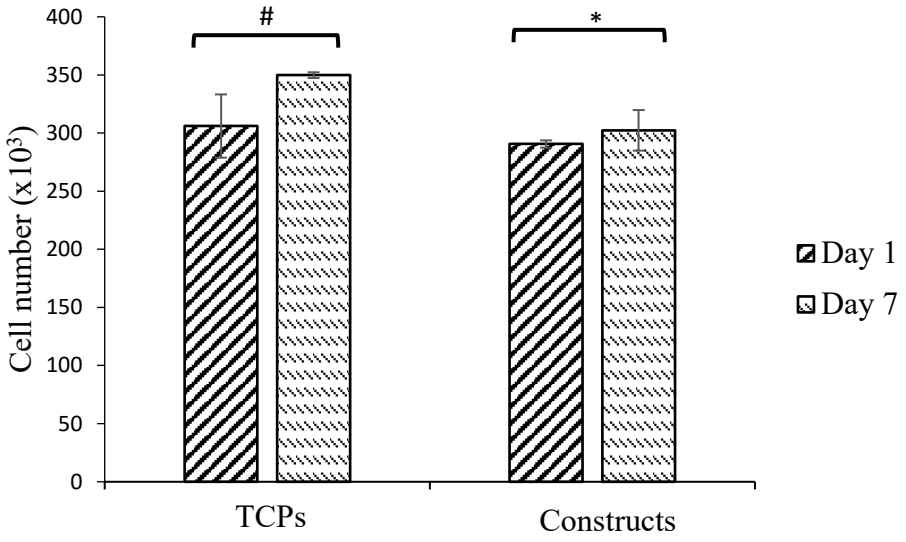

Figure 36. Proliferation of WJ MSCs cultured on TCPs and the final constructs on day 1 and day 7. (# $p>0.05$, * $p>0.05$)

4.4.3.3 Cell morphology in the scaffolds

The morphology of the cells within the hybrid scaffolds was examined by SEM after 7 day of keratocyte differentiation (Figure 37). The corneal tissue substitute was composed of thin layer of MeHA hydrogel to mimic the corneal epithelium layer, electrospun random fibrous mesh to provide mechanical support to the tissue and

imitate Bowman's membrane, and cell-loaded thick MeHA hydrogel layer to mimic the stroma, the thickest layer of the cornea. All layers were demonstrated in SEM images given in Figure 37. In corneal substitute, cells were observed to have a size of approximately 10.84±2.47 µm and adhere to MeHA hydrogel pores. Thin hydrogel layer thickness of the construct, random fibrous mesh thickness and cell-loaded thick hydrogel layer thickness was determined as 63.96±3.41 µm, 41.76±4.65 µm and 451.57±144.87 µm, respectively, according to SEM images. It was known from the literature that the epithelial layer was approximately 50-90 µm, the Bowman's membrane was approximately 8-10 µm, and the stroma layer was approximately 450 µm. When evaluated in this context, it was revealed that the developed corneal substitute was constructed at approximately thicknesses of the natural cornea ECM.

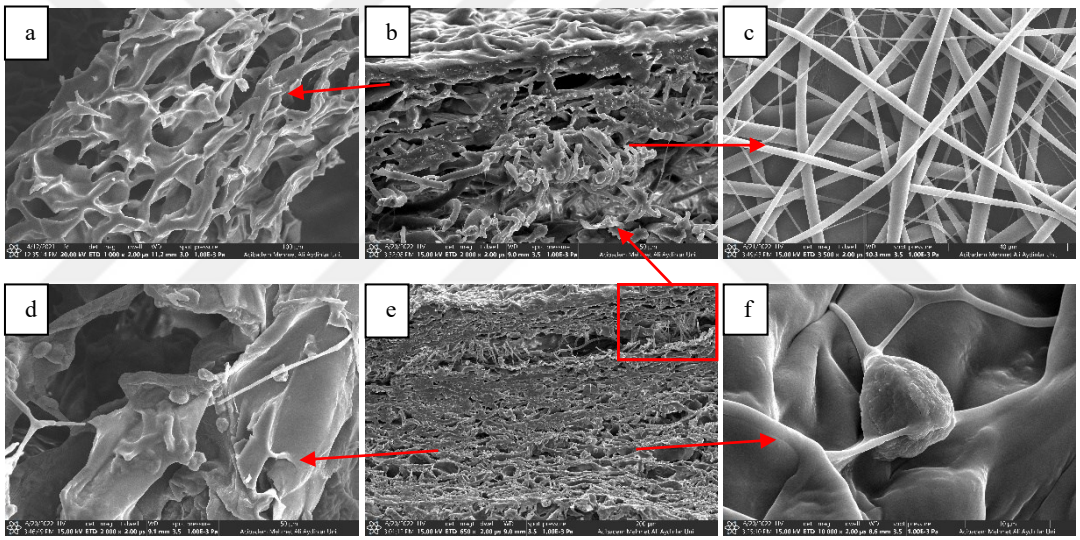

Figure 37. SEM images of the cell-loaded corneal tissue substitute. (a) Thin MeHA hydrogel layer, (b) top two layers of scaffold including thin MeHA hydrogel and electrospun random fibrous mesh, (c) electrospun random fibrous mesh, (d) cell-loaded thick MeHA hydrogel, (e) longitudinal section of hybrid scaffold, (f) cell within the thick hydrogel. Magnifications: (a,f) X1000, (b,d) X2000, (c) X3500; (e) X650; Scale bars: (a) 100 µm, (b,d) 50 µm, (c) 40 µm, (d) 200 µm, (e) 10 µm.

4.4.3.4 Immunostaining of MSC-derived keratocytes in the scaffolds

The expression of keratocyte specific markers ALDH1A1 (Figure 38) and LUM (Figure 39) of the cells within corneal tissue substitute was investigated by immunostaining after 7 days of induction. Cell-free scaffolds were prepared as a control group to check autofluorescence of the scaffolds. It was observed under same imaging parameters there was no signal from scaffolds. In corneal tissue substitutes, it was seen that the differentiated cells exhibited keratocyte morphology and they showed both ALDH1A1 and LUM expression at the end of 7 days of induction within hydrogel-based 3D construct. The results indicated that the cells differentiated within the hybrid scaffolds and conserved their expression pattern within these constructs.

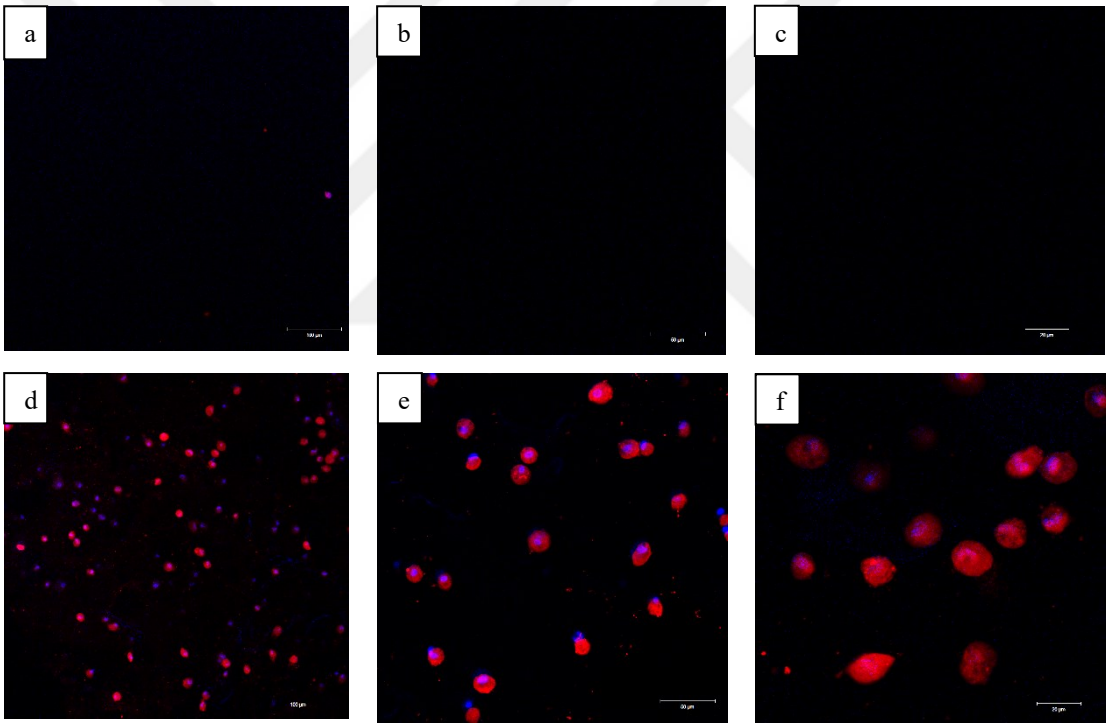

Figure 38. Immunostaining analysis of samples. (a-c) cell-free scaffolds used as control; (d-f) the expression of ALDH1A1 (red) of cells on the tissue substitute at the end of 7 day induction. Magnifications: (a,d) X10, (b,e) X20, (c,f) X40; Scale bars: (a,d) 50 µm, (b,e) 20 µm, (c,f) 100 µm.

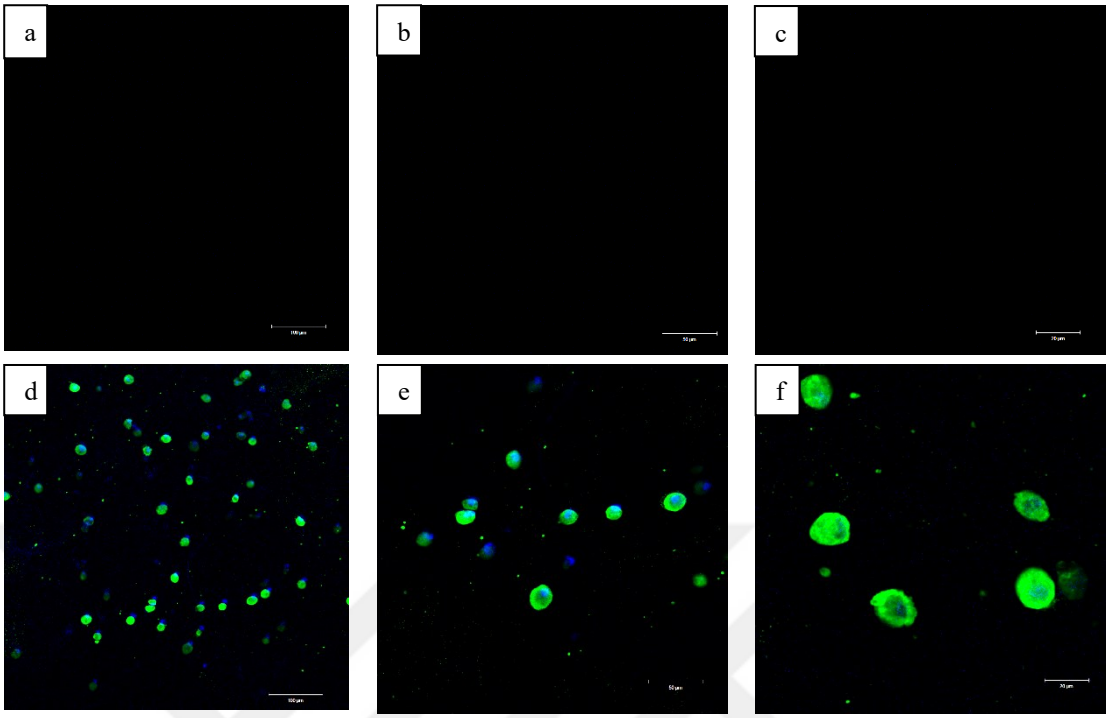

Figure 39. Immunostaining analysis of samples. (a-c) cell-free scaffolds used as control; (d-f) the expression of LUM (green) of cells on the tissue substitute at the end of 7 day induction. Magnifications: (a,d) X10, (b,e) X20, (c,f) X40; Scale bars: (a,d) 50 µm, (b,e) 20 µm, (c,f) 100 µm.

5 DISCUSSION

The cornea is a convex tissue and consists of five layers (18). The outermost corneal epithelium is a stratified squamous epithelial tissue (19). Bowman's membrane, which supports the basal cells in the epithelial tissue, consists of collagen fibers in an irregular organization. The thickest layer of the cornea, the stroma layer in the middle is composed of connective tissue containing collagen and proteoglycan. (3). The organization of collagen fibers in a certain order gives transparency to the cornea. Descemet's membrane, a thick basement membrane, supports single-layer flat endothelial cells in the innermost layer. In this thesis study, it was aimed to develop a stem cell loaded, hydrogel based, 3D, hybrid corneal tissue substitute under *in vitro* conditions via tissue engineering approach. The hybrid scaffold was planned to be constructed by combining thin MeHA hydrogel, electrospun random fibrous mesh, and thick MeHA hydrogel to imitate corneal epithelium, Bowman's membrane, and corneal stroma, respectively.

The thin and thick MeHA hydrogel parts were designed to mimic the epithelial and the stroma layers of the cornea, respectively. They had to be permeable and porous to nutrients and to allow cell growth within the structure. The results showed that hydrogels were porous, and the cells could survive within these pores throughout the gel. The swelling degree of the hydrogel was above 95% which could provide nutrient diffusion within the hydrogel for the survival of cells. Cornea has a curved structure and mechanical stiffness of the Bowman layer plays a role in stabilizing the curvature of the cornea (167). In this thesis study, the other component of the hybrid scaffold was electrospun fibrous mesh to improve the mechanical properties of the hydrogel-based construct as well as to mimic the Bowman's membrane of the cornea. According to the literature, it is known that the elastic modulus of PLA is between 2.7-16 GPa (154) and that of PLGA between 0.1-0.5 MPa (168). In this thesis study, according to the mechanical test results, the elastic modulus of the fibrous mesh was calculated as 214.08+41.77 MPa. Considering that 20% concentration of PLA and PLGA are used in 2:1 ratio, the obtained elastic modulus was between the elastic modulus of PLA and PLGA which could be acceptable. It was observed that it was durable enough to support the hydrogel and but not too flexible as the native Bowman's membrane.

However, there were studies in which Young's Modulus was reported around this value for on fish scale collagen and silk based corneal substitutes (169). In the hybrid structure, the elastic modulus was found to be 15.048 ± 6.279 kPa. In conclusion, the fibrous mesh acted as a support for two hydrogel parts and could improve the mechanical properties of the hybrid scaffold. The results also showed that individual parts of the scaffold were transparent and also this transparency was conserved in the hybrid scaffold even its thickness.

The results demonstrated that all three layers can be successfully constructed in cell-loaded scaffolds and cell-free scaffolds. The fibrous mesh was properly integrated between two hydrogel layers. Since MSCs are adherent cells, adhesion of cells to the surface was important as it would induce cell proliferation and differentiation (166). SEM results showed that cells were placed within the pores of the thick MeHA hydrogel part of the scaffolds. It was thought that the pH of the MeHA hydrogel being in the range of 7-8 also facilitated the adaptation of the cell to its environment. Also in the literature, it was seen that cell attachment could occur in cell-loaded HA-based hydrogel scaffolds (11, 150, 170).

Studies have shown that WJ MSCs can differentiate into keratocyte lineages (90). When the morphological structure of WJ MSCs is examined, it is observed that they generally have a long and bipolar fibroblast cell structure. Keratocytes, on the other hand, appear as cells with long flat cylindrical fibroblast morphology. Keratocytes are rich in specific proteoglycans such as lumican (163). Aldehyde dehydrogenase 1A1 (ALDH1A1), defined as corneal crystal, is ubiquitously expressed in many tissues (164). Liu et al. (171) have been shown that collagen lamellae are rearranged in the corneal stroma by using WJ MSCs in the cornea treatment of lumican null mice. This information demonstrated that WJ MSCs could be used in cornea tissue engineering by upregulating keratocan and aldehyde dehydrogenase gene expressions, which are specific to keratocyte cells, by differentiating them into keratocytes. Coulson-Thomas et al. (172) showed that WJ MSCs had the ability to become established stromal cells by differentiating into keratocyte cells in *in vivo* cornea studies. WJ MSCs were capable taking and recycling glycosaminoglycans and glycosaminoglycan degradation products in stroma. Thus, they had proven with this study that they prevented the progression of the disease by decreasing the size of the treated cornea. In a study by

Garzon et al. (173), WJ MSCs and corneal epithelial cells were compared comparatively. Accordingly, compared to the corneal tissues produced by WJ MSCs and corneal epithelial cells, more cell layers were observed in tissues produced by WJ MSCs and showed more similarity to natural cornea. In addition, although the level of proteoglycans and well-structured mature collagen fibers in tissues produced with WJ MSCs yielded approximately the same level as the control group, it gave better results than tissues produced with corneal epithelial cells. In the light of these studies, in this thesis study isolated human WJ MSCs were used to differentiate into keratocytes. It was observed that the differentiated cells expressed the keratocyte markers LUM and ALDH1A1.

Cell viability assay in the hybrid hydrogels showed that on day 1 of culture without induction and at day 7 of keratocyte induction, the viable cells covered the hydrogel by 80% and 60%, respectively. Hydrogels are known to limit cell proliferation as they trap cells and prevent the transport of oxygen and nutrients to the center of structures (151). In the study of Bahçecioğlu G. et al., the low vitality of 60% on gels containing MeHA is acceptable and supports our results.

WJ MSCs were loaded with hydrogel and during this process the cells were exposed to UV irradiation and incubated in PBS for a certain time. Considering the seeding density, it was observed that the number of cells on day 1 was slightly lower. However, it was reported by Bencherif SA. et al. that both photoinitiator and 10 min UV exposure caused a statistically significant decrease in cell viability (174). The reducing effect of PBS on cell viability was also shown in the study of Sersonova D. et al. (175). However, in our study, it was observed that UV exposure did not have much negative effect on cell viability. According to MTS results, after keratocyte induction for 7 days, there was no sharp, significant decrease in cell number, but the proliferation rate was low. This result was understandable as differentiation was inversely proportional to proliferation (176).

After it was determined that WJ MSCs differentiated into keratocytes, their differentiation in the scaffolds was also examined. Since PLA, PLGA and hyaluronic acid used in scaffolds are non-toxic biocompatible materials for cells, it was expected that the cells would adapt to their environment and differentiate into keratocytes under

appropriate stimulants. At the end of 7 days of differentiation, it was observed that the cells adhered to the scaffolds and expressed high levels of ALDH1A1 and LUM keratocyte markers. These results showed that the developed scaffolds could be attractive candidate for the corneal tissue. Looking at the literature, Chameettachal S. et.al. study showed that when cells were seeded or encapsulated in a gel, keratocytes could successfully preserve their morphology and function (177). Garagorri N. et.al. has shown that hydrogels encourage viable keratocyte populations to support and stabilize their phenotypes (178).

6 CONCLUSION

In this thesis study, a stem cell-loaded, hydrogel based, 3D, hybrid corneal tissue substitute was developed under *in vitro* conditions via tissue engineering approach. The hybrid scaffold was constructed by combining thin MeHA hydrogel, electrospun random fibrous mesh, and thick MeHA hydrogel to imitate corneal epithelium, Bowman's membrane and corneal stroma, respectively. The hybrid scaffold having transparency, appropriate swelling degree and intended architecture was obtained. The potential stem cell source, human WJ MSCs were loaded in the thick hydrogel part and then differentiated into keratocytes under optimized induction conditions. It was observed that the cell viability was 60% as a result of differentiation, and this viability was supported by the literature to be acceptable. After 7 days of induction of cell-loaded scaffolds in differentiation medium, the cell expressed the keratocyte markers Lumican and ALDH1A1 which indicated their differentiation even within the scaffolds.

It was expected that the corneal tissue substitute developed in this thesis study would contribute to the studies in the field of biomaterials and tissue engineering. It was thought that this corneal tissue substitute consisting of human mesenchymal stem cells and biodegradable scaffolds could be tested in *in vivo* studies and might be a potential regenerative treatment approach in the future.

7 REFERENCES

1. Mariotti S, Pascolini DJGDoVI. Visual Impairment, Vision Loss and Blindness 2010 global estimates, and VI and blindness causes. 2010.
2. Panda A, Vanathi M, Kumar A, Dash Y, Priya SJSoo. Corneal graft rejection. 2007;52(4):375-96.
3. Langer R, Vacanti JJS. Tissue engineering, 1993. 1993;260(5110).
4. Ionescu A-M, Alaminos M, de la Cruz Cardona J, Durán JdDG-L, González-Andrades M, Ghinea R, et al. Investigating a novel nanostructured fibrin–agarose biomaterial for human cornea tissue engineering: Rheological properties. 2011;4(8):1963-73.
5. Wray LS, Orwin EJJTEPA. Recreating the microenvironment of the native cornea for tissue engineering applications. 2009;15(7):1463-72.
6. Bektas CK, Hasirci VJBs. Cell loaded 3D bioprinted GelMA hydrogels for corneal stroma engineering. 2020;8(1):438-49.
7. Chirila TVJB. An overview of the development of artificial corneas with porous skirts and the use of PHEMA for such an application. 2001;22(24):3311-7.
8. Acun A, Hasirci VJJoBS, Polymer Edition. Construction of a collagen-based, split-thickness cornea substitute. 2014;25(11):1110-32.
9. Kilic Bektas C, Burcu A, Gedikoglu G, Telek HH, Ornek F, Hasirci VJJoBS, Polymer Edition. Methacrylated gelatin hydrogels as corneal stroma substitutes: in vivo study. 2019;30(18):1803-21.
10. Kilic Bektas C, Hasirci VJJoMSMiM. Cell Loaded GelMA: HEMA IPN hydrogels for corneal stroma engineering. 2020;31(1):1-15.
11. Kilic Bektas C, Hasirci VJJote, medicine r. Mimicking corneal stroma using keratocyte-loaded photopolymerizable methacrylated gelatin hydrogels. 2018;12(4):e1899-e910.
12. Vrana NE, Builles N, Justin V, Bednarz J, Pellegrini G, Ferrari B, et al. Development of a reconstructed cornea from collagen–chondroitin sulfate foams and human cell cultures. 2008;49(12):5325-31.
13. Zorlutuna P, Builles N, Damour O, Elsheikh A, Hasirci VJB. Influence of keratocytes and retinal pigment epithelial cells on the mechanical properties of polyester-based tissue engineering micropatterned films. 2007;28(24):3489-96.
14. Zorlutuna P, Tezcaner A, Kıyat I, Aydınlı A, Hasırcı VJJoBMRPAAOJoTSfB, The Japanese Society for Biomaterials,, Biomaterials TASf, et al. Cornea engineering on polyester carriers. 2006;79(1):104-13.
15. Ross M, Pawlina WJC, Williams MBteBL, Wilkins. Histology: A Test and Atlas with Correlated. 2015.
16. DelMonte DW, Kim TJJoC, Surgery R. Anatomy and physiology of the cornea. 2011;37(3):588-98.
17. Kim K, Doi A, Wen B, Ng K, Zhao R, Cahan P, et al. Epigenetic memory in induced pluripotent stem cells. 2010;467(7313):285-90.
18. Marfurt CF, Cox J, Deek S, Dvorscak LJEer. Anatomy of the human corneal innervation. 2010;90(4):478-92.
19. Dua HS, Azuara-Blanco AJSoo. Limbal stem cells of the corneal epithelium. 2000;44(5):415-25.
20. Wu J, Du Y, Watkins SC, Funderburgh JL, Wagner WRJB. The engineering of organized human corneal tissue through the spatial guidance of corneal stromal stem cells. 2012;33(5):1343-52.
21. Tonsomboon K, Strange D, Oyen M, editors. Gelatin nanofiber-reinforced alginate gel scaffolds for corneal tissue engineering. 2013 35th Annual International Conference of the IEEE Engineering in Medicine and Biology Society (EMBC); 2013: IEEE.
22. Ghezzi CE, Rnjak-Kovacina J, Kaplan DLJTEPBR. Corneal tissue engineering: recent advances and future perspectives. 2015;21(3):278-87.
23. Wang L, Lu C, Liu H, Lin S, Nan K, Chen H, et al. A double network strategy to improve epithelization of a poly (2-hydroxyethyl methacrylate) hydrogel for corneal repair application. 2016;6(2):1194-202.
24. Mi S, Chen B, Wright B, Connon CJJTepA. Ex vivo construction of an artificial ocular surface by combination of corneal limbal epithelial cells and a compressed collagen scaffold containing keratocytes. 2010;16(6):2091-100.

25. Cejka C, Holan V, Trosan P, Zajicova A, Javorkova E, Cejkova JJOm, et al. The favorable effect of mesenchymal stem cell treatment on the antioxidant protective mechanism in the corneal epithelium and renewal of corneal optical properties changed after alkali burns. 2016;2016.
26. Yamashita K, Inagaki E, Hatou S, Higa K, Ogawa A, Miyashita H, et al. Corneal endothelial regeneration using mesenchymal stem cells derived from human umbilical cord. 2018;27(16):1097-108.
27. Monteiro BG, Loureiro RR, Cristovam PC, Covre JL, Gomes JÁP, Kerkis IJAbdo. Amniotic membrane as a biological scaffold for dental pulp stem cell transplantation in ocular surface reconstruction. 2019;82(1):32-7.
28. Nishida T. Cornea. Krachmer JH, Mannis MJ, Holland EJ (Eds.). Cornea. Philadelphia, Elsevier lnc; 2005.
29. Martola E-L, Baum JLJAoO. Central and peripheral corneal thickness: a clinical study. 1968;79(1):28-30.
30. Rüfer F, Schröder A, Erb CJC. White-to-white corneal diameter: normal values in healthy humans obtained with the Orbscan II topography system. 2005;24(3):259-61.
31. Böhnke M, Masters BRJPir, research e. Confocal microscopy of the cornea. 1999;18(5):553-628.
32. Yanoff M, Duker J. Ophthalmology. Edinburgh: Mosby. Elsevier; 2009.
33. Eghrari AO, Riazuddin SA, Gottsch JDJPimb, science t. Overview of the cornea: structure, function, and development. 2015;134:7-23.
34. Yanoff M, Duker J. Ophthalmology.: Elsevier Inc. 2014.
35. Santhanam A, Torricelli AA, Wu J, Marino GK, Wilson SEJMv. Differential expression of epithelial basement membrane components nidogens and perlecan in corneal stromal cells in vitro. 2015;21:1318.
36. Funderburgh JL, Hevelone ND, Roth MR, Funderburgh ML, Rodrigues MR, Nirankari VS, et al. Decorin and biglycan of normal and pathologic human corneas. 1998;39(10):1957-64.
37. Dawson DG, Ubels JL, Edelhauser HFJAsPotE. Cornea and sclera. 2011;11:71-130.
38. Chen Z, You J, Liu X, Cooper S, Hodge C, Sutton G, et al. Biomaterials for corneal bioengineering. 2018;13(3):032002.
39. Kabosova A, Azar DT, Bannikov GA, Campbell KP, Durbeej M, Ghohestani RF, et al. Compositional differences between infant and adult human corneal basement membranes. 2007;48(11):4989-99.
40. Ruberti JW, Zieske JDJPir, research e. Prelude to corneal tissue engineering–gaining control of collagen organization. 2008;27(5):549-77.
41. Cursiefen C, Chen L, Dana MR, Streilein JWJC. Corneal lymphangiogenesis: evidence, mechanisms, and implications for corneal transplant immunology. 2003;22(3):273-81.
42. Watsky MA, McDermott ML, Edelhauser HFJEer. In vitro corneal endothelial permeability in rabbit and human: the effects of age, cataract surgery and diabetes. 1989;49(5):751-67.
43. Bonanno JA. Molecular mechanisms underlying the corneal endothelial pump. Experimental eye research. 2012;95(1):2-7.
44. Waring GO, Go W. Clinical and pathologic alterations of Descemet's membrane: with emphasis on endothelial metaplasia. 1974.
45. Lubeck D, Greene JS, editors. Corneal injuries. Seminars in ophthalmology; 1990: Taylor & Francis.
46. Loskutova E, Nolan J, Howard A, Beatty SJN. Macular pigment and its contribution to vision. 2013;5(6):1962-9.
47. Reinhard T, Larkin F. Essentials in Ophthalmology: Cornea and External Eye Disease: Springer; 2006.
48. Waring III GO, Rodrigues MM, Laibson PRJSoo. Corneal dystrophies. II. Endothelial dystrophies. 1978;23(3):147-68.
49. Thomas PA, Geraldine PJCoiid. Infectious keratitis. 2007;20(2):129-41.
50. Leonardi A, Motterle L, Bortolotti MJC, Immunology E. Allergy and the eye. 2008;153:17-21.
51. Amescua G, Miller D, Alfonso EJE. What is causing the corneal ulcer? Management strategies for unresponsive corneal ulceration. 2012;26(2):228-36.
52. Soiberman U, Foster JW, Jun AS, Chakravarti SJTooj. Suppl-1, M9: Pathophysiology of Keratoconus: What Do We Know Today. 2017;11:252.
53. Pascolini D, Mariotti SPJBJoO. Global estimates of visual impairment: 2010. 2012;96(5):614-8.

54. Cursiefen C, Kruse FE. New aspects of angiogenesis in the cornea. Cornea and External Eye Disease: Springer; 2006. p. 83-99.
55. Klausner EA, Peer D, Chapman RL, Multack RF, Andurkar SVJJoCR. Corneal gene therapy. 2007;124(3):107-33.
56. Chirila TV, Hicks CR, Dalton PD, Vijayasekaran S, Lou X, Hong Y, et al. Artificial cornea. 1998;23(3):447-73.
57. Griffith M, Osborne R, Munger R, Xiong X, Doillon CJ, Laycock NL, et al. Functional human corneal equivalents constructed from cell lines. 1999;286(5447):2169-72.
58. Griffith M, Jackson W, Lagali N, Merrett K, Li F, Fagerholm PJE. Artificial corneas: a regenerative medicine approach. 2009;23(10):1985-9.
59. Stoiber J, Fernandez V, Lamar PD, Kaminski S, Acosta AC, Dubovy S, et al. Biocompatibility of a nonpenetrating synthetic cornea in vascularized rabbit corneas. 2005;24(4):467-73.
60. Lee S-D, Hsiue G-H, Kao C-Y, Chang PC-TJB. Artificial cornea: surface modification of silicone rubber membrane by graft polymerization of pHEMA via glow discharge. 1996;17(6):587-95.
61. Grayson WL, Martens TP, Eng GM, Radisic M, Vunjak-Novakovic G, editors. Biomimetic approach to tissue engineering. Seminars in cell & developmental biology; 2009: Elsevier.
62. O'brien FJJMt. Biomaterials & scaffolds for tissue engineering. 2011;14(3):88-95.
63. Hicks C, Crawford G, Chirila T, Wiffen S, Vijayasekaran S, Lou X, et al. Development and clinical assessment of an artificial cornea. 2000;19(2):149-70.
64. Arabpour Z, Baradaran-Rafii A, Bakhshaiesh NL, Ai J, Ebrahimi-Barough S, Esmaeili Malekabadi H, et al. Design and characterization of biodegradable multi layered electrospun nanofibers for corneal tissue engineering applications. 2019;107(10):2340-9.
65. Bakhshandeh H, Soleimani M, Hosseini SS, Hashemi H, Shabani I, Shafiee A, et al. Poly (ε-caprolactone) nanofibrous ring surrounding a polyvinyl alcohol hydrogel for the development of a biocompatible two-part artificial cornea. 2011;6:1509.
66. Xue M, Jackson CJJAiwc. Extracellular matrix reorganization during wound healing and its impact on abnormal scarring. 2015;4(3):119-36.
67. Yue BJJog. Biology of the extracellular matrix: an overview. 2014:S20.
68. Rama P, Matuska S, Paganoni G, Spinelli A, De Luca M, Pellegrini GJNEjom. Limbal stem-cell therapy and long-term corneal regeneration. 2010;363(2):147-55.
69. Yam GHF, Teo EPW, Setiawan M, Lovatt MJ, Yusoff NZBM, Fuest M, et al. Postnatal periodontal ligament as a novel adult stem cell source for regenerative corneal cell therapy. 2018;22(6):3119-32.
70. Arnalich-Montiel F, Pastor S, Blazquez-Martinez A, Fernandez-Delgado J, Nistal M, Alio JL, et al. Adipose-derived stem cells are a source for cell therapy of the corneal stroma. 2008;26(2):570-9.
71. Karaşahin T. Embriyonik kök hücreler. Erciyes Üniversitesi Veteriner Fakültesi Dergisi. 2012;9(1):65-71.
72. Hasirci N, Hasirci V. Biomaterials: From Molecules to Engineered Tissue: Springer Science & Business Media; 2010.
73. Phadke A, Chang C-W, Varghese S. Functional biomaterials for controlling stem cell differentiation. Biomaterials as stem cell niche: Springer; 2010. p. 19-44.
74. Kalra K, Tomar PJAJoP, Therapeutics C. Stem cell: basics, classification and applications. 2014;2(7):919-30.
75. Sylvester KG, Longaker MTJAos. Stem cells: review and update. 2004;139(1):93-9.
76. Takahashi K, Yamanaka SJc. Induction of pluripotent stem cells from mouse embryonic and adult fibroblast cultures by defined factors. 2006;126(4):663-76.
77. Takahashi K, Okita K, Nakagawa M, Yamanaka SJNp. Induction of pluripotent stem cells from fibroblast cultures. 2007;2(12):3081.
78. Hayashi R, Ishikawa Y, Ito M, Kageyama T, Takashiba K, Fujioka T, et al. Generation of corneal epithelial cells from induced pluripotent stem cells derived from human dermal fibroblast and corneal limbal epithelium. 2012;7(9):e45435.
79. Hamrah P, Sahin AJOSDC, Conjunctiva, Film T. Limbus and corneal epithelium. 2013:29-33.
80. Selver ÖB, Yağcı A, Eğrilmez S, Gürdal M, Palamar M, Çavuşoğlu T, et al. Limbal stem cell deficiency and treatment with stem cell transplantation. 2017;47(5):285.
81. Prockop DJJS. Marrow stromal cells as stem cells for nonhematopoietic tissues. 1997;276(5309):71-4.
82. da Silva Meirelles L, Chagastelles PC, Nardi NBJJocs. Mesenchymal stem cells reside in virtually all post-natal organs and tissues. 2006;119(11):2204-13.

83. Hasirci V, Hasirci N. Fundamentals of biomaterials: Springer; 2018.
84. Ziaei M, Zhang J, Patel DV, McGhee CNJSoo. Umbilical cord stem cells in the treatment of corneal disease. 2017;62(6):803-15.
85. Goodison S, Urquidi V, Tarin DJMp. CD44 cell adhesion molecules. 1999;52(4):189.
86. Dominici M, Le Blanc K, Mueller I, Slaper-Cortenbach I, Marini F, Krause D, et al. Minimal criteria for defining multipotent mesenchymal stromal cells. The International Society for Cellular Therapy position statement. 2006;8(4):315-7.
87. Zuk PA, Zhu M, Mizuno H, Huang J, Futrell JW, Katz AJ, et al. Multilineage cells from human adipose tissue: implications for cell-based therapies. 2001;7(2):211-28.
88. Karamichos D, Hutcheon A, Zieske JJJote, medicine r. Transforming growth factor-β3 regulates assembly of a non-fibrotic matrix in a 3D corneal model. 2011;5(8):e228-e38.
89. Villaron EM, Almeida J, López-Holgado N, Alcoceba M, Sánchez-Abarca LI, Sanchez-Guijo FM, et al. Mesenchymal stem cells are present in peripheral blood and can engraft after allogeneic hematopoietic stem cell transplantation. 2004;89(12):1421-7.
90. Syed-Picard FN, Du Y, Lathrop KL, Mann MM, Funderburgh ML, Funderburgh JLJSctm. Dental pulp stem cells: a new cellular resource for corneal stromal regeneration. 2015;4(3):276-85.
91. Weiss ML, Troyer DLJScr. Stem cells in the umbilical cord. 2006;2(2):155-62.
92. Zavala G, Prieto CP, Villanueva AA, Palma VJScr, therapy. Sonic hedgehog (SHH) signaling improves the angiogenic potential of Wharton's jelly-derived mesenchymal stem cells (WJ-MSC). 2017;8(1):1-17.
93. Markov V, Kusumi K, Tadesse MG, William DA, Hall DM, Lounev V, et al. Identification of cord blood-derived mesenchymal stem/stromal cell populations with distinct growth kinetics, differentiation potentials, and gene expression profiles. 2007;16(1):53-74.
94. Mitchell KE, Weiss ML, Mitchell BM, Martin P, Davis D, Morales L, et al. Matrix cells from Wharton's jelly form neurons and glia. 2003;21(1):50-60.
95. Wang HS, Hung SC, Peng ST, Huang CC, Wei HM, Guo YJ, et al. Mesenchymal stem cells in the Wharton's jelly of the human umbilical cord. 2004;22(7):1330-7.
96. Wang CC, Rogers MSJBAIJoO, Gynaecology. Lipid peroxidation in cord blood: the effects of umbilical nuchal cord. 1997;104(2):251-5.
97. Minguell JJ. Umbilical Cord-Derived Mesenchymal Stem Cells. Regenerative Medicine Using Pregnancy-Specific Biological Substances: Springer; 2011. p. 249-53.
98. Wang JC, Doedens M, Dick JEJB, The Journal of the American Society of Hematology. Primitive human hematopoietic cells are enriched in cord blood compared with adult bone marrow or mobilized peripheral blood as measured by the quantitative in vivo SCID-repopulating cell assay. 1997;89(11):3919-24.
99. Pittenger MF, Mackay AM, Beck SC, Jaiswal RK, Douglas R, Mosca JD, et al. Multilineage potential of adult human mesenchymal stem cells. 1999;284(5411):143-7.
100. Zhang L, Coulson-Thomas VJ, Ferreira TG, Kao WWJBo. Mesenchymal stem cells for treating ocular surface diseases. 2015;15(1):55-65.
101. Zhang Q, Fang Z, Cao Y, Du H, Wu H, Beuerman R, et al. High refractive index inorganic–organic interpenetrating polymer network (IPN) hydrogel nanocomposite toward artificial cornea implants. 2012;1(7):876-81.
102. Miyashita H, Shimmura S, Kobayashi H, Taguchi T, Asano-Kato N, Uchino Y, et al. Collagen-immobilized poly (vinyl alcohol) as an artificial cornea scaffold that supports a stratified corneal epithelium. 2006;76(1):56-63.
103. Uchino Y, Shimmura S, Miyashita H, Taguchi T, Kobayashi H, Shimazaki J, et al. Amniotic membrane immobilized poly (vinyl alcohol) hybrid polymer as an artificial cornea scaffold that supports a stratified and differentiated corneal epithelium. 2007;81(1):201-6.
104. Chen D, Qu Y, Hua X, Zhang L, Liu Z, Pflugfelder S, et al. A hyaluronan hydrogel scaffold-based xeno-free culture system for ex vivo expansion of human corneal epithelial stem cells. 2017;31(6):962-71.
105. Orwin EJ, Borene ML, Hubel AJJBE. Biomechanical and optical characteristics of a corneal stromal equivalent. 2003;125(4):439-44.
106. Watanabe R, Hayashi R, Kimura Y, Tanaka Y, Kageyama T, Hara S, et al. A novel gelatin hydrogel carrier sheet for corneal endothelial transplantation. 2011;17(17-18):2213-9.
107. Alaminos M, Sánchez-Quevedo MDC, Munoz-Ávila JI, Serrano D, Medialdea S, Carreras I, et al. Construction of a complete rabbit cornea substitute using a fibrin-agarose scaffold. 2006;47(8):3311-7.

108. Rafat M, Li F, Fagerholm P, Lagali NS, Watsky MA, Munger R, et al. PEG-stabilized carbodiimide crosslinked collagen–chitosan hydrogels for corneal tissue engineering. 2008;29(29):3960-72.
109. Zhang W, Chen J, Backman LJ, Malm AD, Danielson PJAhm. Surface topography and mechanical strain promote keratocyte phenotype and extracellular matrix formation in a biomimetic 3D corneal model. 2017;6(5):1601238.
110. Brigham MD, Bick A, Lo E, Bendali A, Burdick JA, Khademhosseini AJTEPA. Mechanically robust and bioadhesive collagen and photocrosslinkable hyaluronic acid semi-interpenetrating networks. 2009;15(7):1645-53.
111. Wright B, Mi S, Connon CJJDdt. Towards the use of hydrogels in the treatment of limbal stem cell deficiency. 2013;18(1-2):79-86.
112. Zhou H, Wang Z, Cao H, Hu H, Luo Z, Yang X, et al. Genipin-crosslinked polyvinyl alcohol/silk fibroin/nano-hydroxyapatite hydrogel for fabrication of artificial cornea scaffolds—a novel approach to corneal tissue engineering. 2019;30(17):1604-19.
113. Ozcelik B, Brown KD, Blencowe A, Daniell M, Stevens GW, Qiao GGJAb. Ultrathin chitosan–poly (ethylene glycol) hydrogel films for corneal tissue engineering. 2013;9(5):6594-605.
114. Teng W, Long TJ, Zhang Q, Yao K, Shen TT, Ratner BDJB. A tough, precision-porous hydrogel scaffold: ophthalmologic applications. 2014;35(32):8916-26.
115. Baradaran-Rafii A, Biazar E, Heidari-Keshel SJCer. Cellular response of limbal stem cells on polycaprolactone nanofibrous scaffolds for ocular epithelial regeneration. 2016;41(3):326-33.
116. Hong S, Yun JH, Kim E-S, Kim JS, Tchah H, Hwang CJIo, et al. Human conjunctival epithelial sheets grown on poly (lactic-co-glycolic) acid membranes and cocultured with human tenon's fibroblasts for corneal repair. 2018;59(3):1475-85.
117. Wilson SL, Wimpenny I, Ahearne M, Rauz S, El Haj AJ, Yang YJAFM. Chemical and topographical effects on cell differentiation and matrix elasticity in a corneal stromal layer model. 2012;22(17):3641-9.
118. Crabb RA, Chau EP, Decoteau DM, Hubel AJAobe. Microstructural characteristics of extracellular matrix produced by stromal fibroblasts. 2006;34(10):1615-27.
119. Sommer AC, Blumenthal EZJGsAfC, Ophthalmology E. Implementations of 3D printing in ophthalmology. 2019;257(9):1815-22.
120. Isaacson A, Swioklo S, Connon CJJEer. 3D bioprinting of a corneal stroma equivalent. 2018;173:188-93.
121. Zhang C, Du L, Sun P, Shen L, Zhu J, Pang K, et al. Construction of tissue-engineered full-thickness cornea substitute using limbal epithelial cell-like and corneal endothelial cell-like cells derived from human embryonic stem cells. 2017;124:180-94.
122. Wang S, Ghezzi CE, Gomes R, Pollard RE, Funderburgh JL, Kaplan DLJB. In vitro 3D corneal tissue model with epithelium, stroma, and innervation. 2017;112:1-9.
123. Ulag S, Ilhan E, Sahin A, Yilmaz BK, Ekren N, Kilic O, et al. 3D printed artificial cornea for corneal stromal transplantation. 2020;133:109744.
124. Ghezzi CE, Marelli B, Omenetto FG, Funderburgh JL, Kaplan DLJPo. 3D functional corneal stromal tissue equivalent based on corneal stromal stem cells and multi-layered silk film architecture. 2017;12(1):e0169504.
125. Vrana NE, Elsheikh A, Builles N, Damour O, Hasirci VJB. Effect of human corneal keratocytes and retinal pigment epithelial cells on the mechanical properties of micropatterned collagen films. 2007;28(29):4303-10.
126. Liang Y, Liu W, Han B, Yang C, Ma Q, Zhao W, et al. Fabrication and characters of a corneal endothelial cells scaffold based on chitosan. 2011;22(1):175-83.
127. Tsai I-L, Hsu C-C, Hung K-H, Chang C-W, Cheng Y-HJJotCMA. Applications of biomaterials in corneal wound healing. 2015;78(4):212-7.
128. Wang S, Ghezzi CE, White JD, Kaplan DLJJoBMRPA. Coculture of dorsal root ganglion neurons and differentiated human corneal stromal stem cells on silk-based scaffolds. 2015;103(10):3339-48.
129. Duan X, Sheardown HJB. Dendrimer crosslinked collagen as a corneal tissue engineering scaffold: mechanical properties and corneal epithelial cell interactions. 2006;27(26):4608-17.
130. Strange DG, Tonsomboon K, Oyen MLJMOPL. Electrospun fiber-Hydrogel composites for nucleus pulposus tissue engineering. 2012;1417.

131. Sharma S, Gupta D, Mohanty S, Jassal M, Agrawal AK, Tandon RJIo, et al. Surface-modified electrospun poly (ε-caprolactone) scaffold with improved optical transparency and bioactivity for damaged ocular surface reconstruction. 2014;55(2):899-907.
132. Long Y-Z, Yan X, Wang X-X, Zhang J, Yu M. Electrospinning: the setup and procedure. Electrospinning: nanofabrication and applications: Elsevier; 2019. p. 21-52.
133. Ye J, Shi X, Chen X, Xie J, Wang C, Yao K, et al. Chitosan-modified, collagen-based biomimetic nanofibrous membranes as selective cell adhering wound dressings in the treatment of chemically burned corneas. 2014;2(27):4226-36.
134. Chen J, Yan C, Zhu M, Yao Q, Shao C, Lu W, et al. Electrospun nanofibrous SF/P (LLA-CL) membrane: a potential substratum for endothelial keratoplasty. 2015;10:3337.
135. Yan J, Qiang L, Gao Y, Cui X, Zhou H, Zhong S, et al. Effect of fiber alignment in electrospun scaffolds on keratocytes and corneal epithelial cells behavior. 2012;100(2):527-35.
136. McLaughlin CR, Tsai R, Latorre MA, Griffith MJFB. Bioengineered corneas for transplantation and in vitro toxicology. 2009;14:3326-37.
137. Pourjabbar B, Biazar E, Heidari Keshel S, Ahani-Nahayati M, Baradaran-Rafii A, Roozafzoon R, et al. Bio-polymeric hydrogels for regeneration of corneal epithelial tissue. 2021:1-18.
138. Lima LH, Morales Y, Cabral TJJoo. Ocular biocompatibility of poly-N-isopropylacrylamide (pNIPAM). 2016;2016.
139. Somaiah C, Kumar A, Mawrie D, Sharma A, Patil SD, Bhattacharyya J, et al. Collagen promotes higher adhesion, survival and proliferation of mesenchymal stem cells. 2015;10(12):e0145068.
140. Matthyssen S, Van den Bogerd B, Dhubhghaill SN, Koppen C, Zakaria NJAb. Corneal regeneration: A review of stromal replacements. 2018;69:31-41.
141. Yang H, Shu ZJJoc, research p. The extraction of collagen protein from pigskin. 2014;6(2):683-7.
142. Shoulders MD, Raines RTJArob. Collagen structure and stability. 2009;78:929-58.
143. Matthews JA, Wnek GE, Simpson DG, Bowlin GLJB. Electrospinning of collagen nanofibers. 2002;3(2):232-8.
144. Lodish H, Berk A, Zipursky SL, Matsudaira P, Baltimore D, Darnell JJMcb. Collagen: the fibrous proteins of the matrix. 2000;4.
145. Ricard-Blum SJCSHpib. The collagen family. 2011;3(1):a004978.
146. Bayer ISJM. Hyaluronic acid and controlled release: A review. 2020;25(11):2649.
147. Burdick JA, Prestwich GDJAm. Hyaluronic acid hydrogels for biomedical applications. 2011;23(12):H41-H56.
148. Necas J, Bartosikova L, Brauner P, Kolar JJVm. Hyaluronic acid (hyaluronan): a review. 2008;53(8):397-411.
149. Balazs EA, Laurent T. Chemistry, biology and medical applications of hyaluronan and its derivatives: Portland; 1998.
150. Eke G, Mangir N, Hasirci N, MacNeil S, Hasirci VJB. Development of a UV crosslinked biodegradable hydrogel containing adipose derived stem cells to promote vascularization for skin wounds and tissue engineering. 2017;129:188-98.
151. Bahcecioglu G, Hasirci N, Bilgen B, Hasirci VJIjobm. Hydrogels of agarose, and methacrylated gelatin and hyaluronic acid are more supportive for in vitro meniscus regeneration than three dimensional printed polycaprolactone scaffolds. 2019;122:1152-62.
152. Armentano I, Bitinis N, Fortunati E, Mattioli S, Rescignano N, Verdejo R, et al. Multifunctional nanostructured PLA materials for packaging and tissue engineering. 2013;38(10-11):1720-47.
153. Teixeira S, Eblagon KM, Miranda F, R. Pereira MF, Figueiredo JLJC. Towards controlled degradation of poly (lactic) acid in technical applications. 2021;7(2):42.
154. Middleton JC, Tipton AJJB. Synthetic biodegradable polymers as orthopedic devices. 2000;21(23):2335-46.
155. Hu Y, Daoud WA, Cheuk KKL, Lin CSKJM. Newly developed techniques on polycondensation, ring-opening polymerization and polymer modification: Focus on poly (lactic acid). 2016;9(3):133.
156. Razak SIA, Dahli FN, Wahab IF, Abdul Kadir MR, Muhamad II, Yusof AHM, et al. A Conductive polylactic acid/polyaniline porous scaffold via freeze extraction for potential biomedical applications. 2016;14(2):78-86.

157. Martins C, Sousa F, Araujo F, Sarmento BJAhm. Functionalizing PLGA and PLGA derivatives for drug delivery and tissue regeneration applications. 2018;7(1):1701035.
158. Danhier F, Ansorena E, Silva JM, Coco R, Le Breton A, Préat VJJocr. PLGA-based nanoparticles: an overview of biomedical applications. 2012;161(2):505-22.
159. Zolnik BS, Burgess DJJJoCR. Effect of acidic pH on PLGA microsphere degradation and release. 2007;122(3):338-44.
160. Endogan Tanir T, Hasirci V, Hasirci NJPC. Preparation and characterization of Chitosan and PLGA-based scaffolds for tissue engineering applications. 2015;36(10):1917-30.
161. Bahcecioglu G, Hasirci N, Hasirci VJIjobm. Cell behavior on the alginate-coated PLLA/PLGA scaffolds. 2019;124:444-50.
162. Dos Santos A, Balayan A, Funderburgh ML, Ngo J, Funderburgh JL, Deng SXJIo, et al. Differentiation capacity of human mesenchymal stem cells into keratocyte lineage. 2019;60(8):3013-23.
163. Funderburgh JL, Mann MM, Funderburgh MLJJoBC. Keratocyte phenotype mediates proteoglycan structure: a role for fibroblasts in corneal fibrosis. 2003;278(46):45629-37.
164. Lassen N, Black WJ, Estey T, Vasiliou V, editors. The role of corneal crystallins in the cellular defense mechanisms against oxidative stress. Seminars in cell & developmental biology; 2008: Elsevier.
165. Klotz BJ, Gawlitta D, Rosenberg AJ, Malda J, Melchels FPJTib. Gelatin-methacryloyl hydrogels: towards biofabrication-based tissue repair. 2016;34(5):394-407.
166. Sidney LE, Hopkinson AJJote, medicine r. Corneal keratocyte transition to mesenchymal stem cell phenotype and reversal using serum-free medium supplemented with fibroblast growth factor-2, transforming growth factor-β3 and retinoic acid. 2018;12(1):e203-e15.
167. Seiler T, Matallana M, Sendler S, Bende TJJoRS. Does Bowman's layer determine the biomechanical properties of the cornea? : SLACK Incorporated Thorofare, NJ; 1992. p. 139-42.
168. Guo M, Chu Z, Yao J, Feng W, Wang Y, Wang L, et al. The effects of tensile stress on degradation of biodegradable PLGA membranes: A quantitative study. 2016;124:95-100.
169. Bollu TK, Parimi DS, Bhatt CS, Suresh AKJAM. Fish-scale waste to portable bioactive discs: a sustainable platform for sensitive and reliable blood group analysis. 2022.
170. Kilic Bektas CrnHV. Cell incorporated methacrylated gelatin (GelMA) hydrogels for corneal stroma tissue engineering. Frontiers in Bioengineering and Biotechnology.
171. Liu H, Zhang J, Liu C-Y, Wang I-J, Sieber M, Chang J, et al. Cell therapy of congenital corneal diseases with umbilical mesenchymal stem cells: lumican null mice. 2010;5(5):e10707.
172. Coulson-Thomas VJ, Caterson B, Kao WWYJSC. Transplantation of human umbilical mesenchymal stem cells cures the corneal defects of mucopolysaccharidosis VII mice. 2013;31(10):2116-26.
173. Garzón I, Martín-Piedra MA, Alfonso-Rodríguez C, González-Andrades M, Carriel V, Martínez-Gómez C, et al. Generation of a biomimetic human artificial cornea model using Wharton's jelly mesenchymal stem cells. 2014;55(7):4073-83.
174. Bencherif SA, Srinivasan A, Horkay F, Hollinger JO, Matyjaszewski K, Washburn NRJB. Influence of the degree of methacrylation on hyaluronic acid hydrogels properties. 2008;29(12):1739-49.
175. Sersenová D, Machala Z, Repiská V, Gbelcová H. The effect of plasma activated medium and PBS on human melanoma cells compared with other cancer and normal cells. 2021.
176. Fajas LJAom. Adipogenesis: a cross-talk between cell proliferation and cell differentiation. 2003;35(2):79-85.
177. Chameettachal S, Prasad D, Parekh Y, Basu S, Singh V, Bokara KK, et al. Prevention of corneal myofibroblastic differentiation in vitro using a biomimetic ECM hydrogel for corneal tissue regeneration. 2020;4(1):533-44.
178. Garagorri N, Fermanian S, Thibault R, Ambrose WM, Schein OD, Chakravarti S, et al. Keratocyte behavior in three-dimensional photopolymerizable poly (ethylene glycol) hydrogels. 2008;4(5):1139-47.

8 APPENDIX

APPENDIX 1. Calibration Curves for Cell Number Determination of WJ MSCs

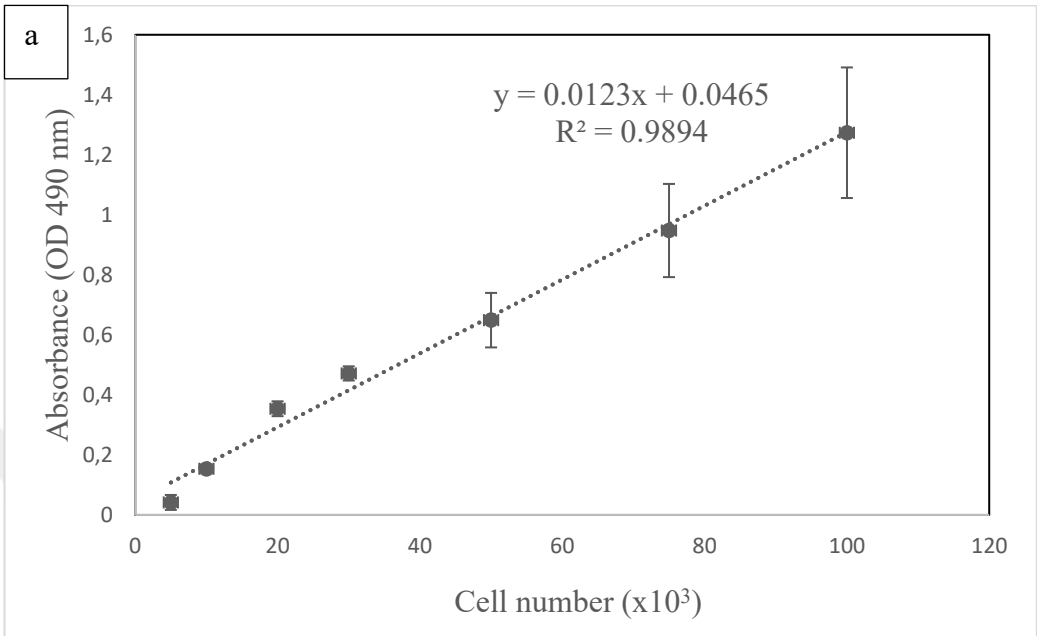

Figure 40. The calibration curve obtained by WST-1 assay using WJ MSCs.

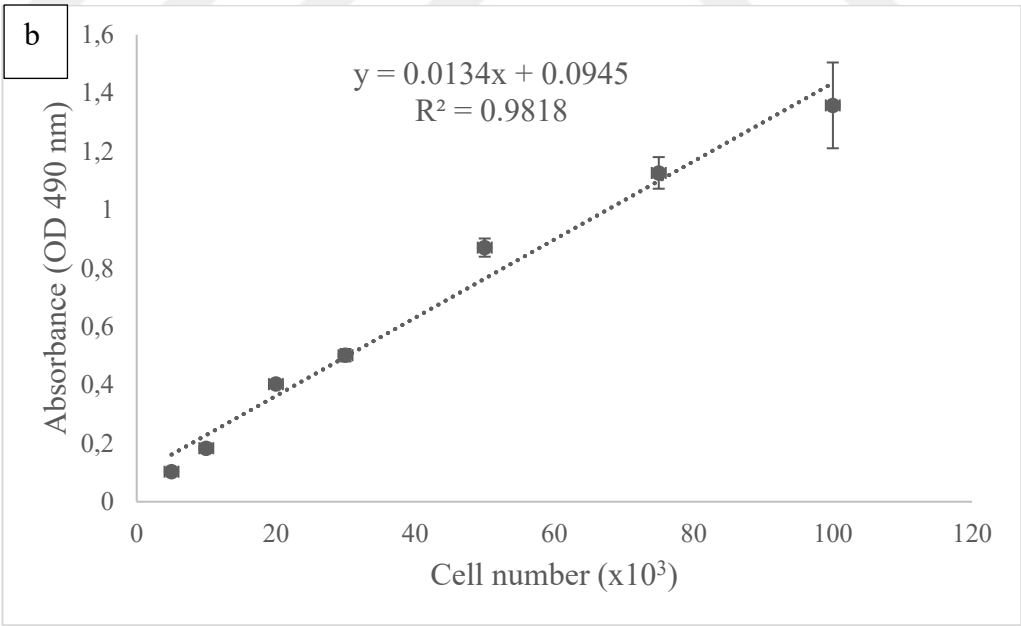

Figure 41. The calibration curve obtained by MTS assay using WJ MSCs.

APPENDIX 2. Calibration Curves for ALP Activity

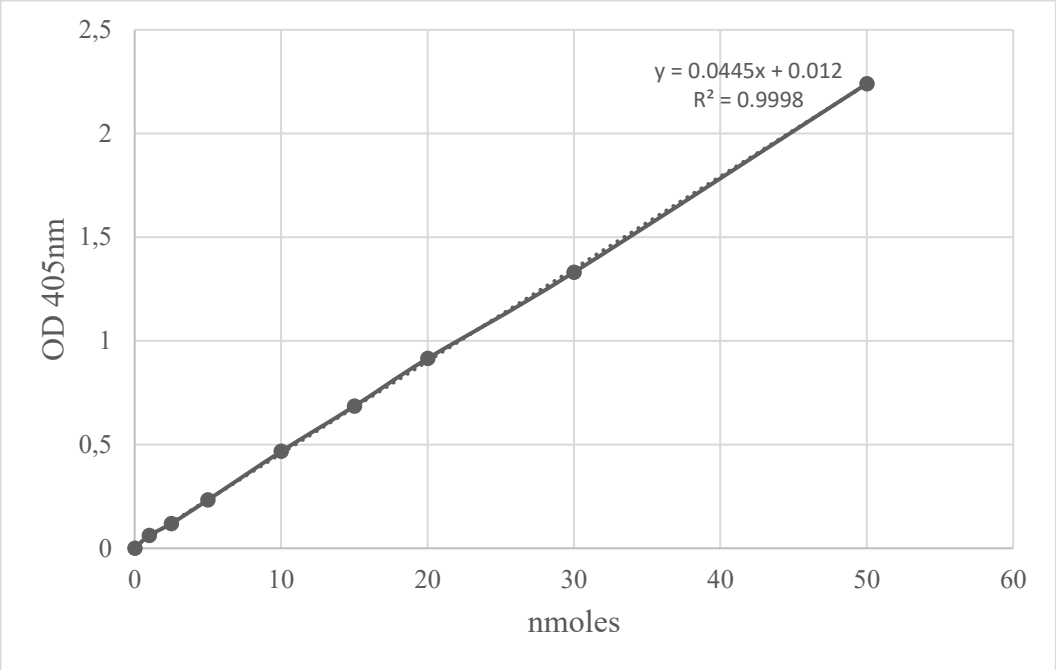

Figure 42. The calibration curve for ALP activity prepared by p-nitrophenol at different concentrations.

9 CURRICULUM VITAE